Numerical simulation of the coupled hydro-mechanical response of the Leendert de Boerspolder dyke

By

Matthaios Theodoridis

4416872

Master of Science

Faculty of Civil Engineering and Geosciecnes
MSc Geo-Engineering
Delft University of Technology

TU Delft

Numerical simulation of the coupled hydro-mechanical response of the Leendert de Boerspolder dyke

A Thesis presented for the degree of
Master of Science in Geo - Engineering

by

M. Theodoridis

Student number: 4416872

Thesis committee:	Prof. dr. ir. C. Jommi,	TU Delft, supervisor (chair)
	Dr. ir. R. B. J. Brinkgreve,	TU Delft, supervisor
	Ir. K. Reinders,	TU Delft, supervisor
	Ir. S. Muraro,	TU Delft, daily supervisor

TU Delft Delft University of Technology

Faculty of Civil Engineering and Geosciences
Department of Geoscience and Engineering
Delft University of Technology
December, 2017

Acknowledgements

The research presented in this thesis would not have been accomplished without the support, contribution and encouragement of several people.

First of all, I would like to express my gratitude to my thesis advisor Prof. Dr. C. Jommi for her expert guidance and support during all the steps of my research.

Secondly, I would like to thank Dr. Ir. R. Brinkgreve and Ir. K. Reinders for their participation and valuable inputs improving the quality of my work.

I would like to thank my daily supervisor Ir. S. Muraro for his continuous support. His willingness to listen and discuss my questions and thoughts was a tremendous help to me.

I am very grateful to my colleagues at Plaxis bv that helped me deepen my knowledge with regards to Plaxis software capabilities as well as their contribution to carrying out my thesis smoothly.

Last but not least, I am immensely grateful to my family for providing me with continuous support and encouragement throughout my years of study. Without them this accomplishment would not have been possible.

M. Theodoridis
Delft, the Netherlands
December, 2017

Abstract

This study was conducted in the framework of the Leendert de Boerspolder stress test. It focuses on the investigation the performance of the available constitutive models in describing the coupled hydro-mechanical response of peats and organic clays as observed during the stress test. The soil models that are considered are the Mohr-Coulomb model, the Soft Soil model and the Hardening Soil model as are implemented in PLAXIS, a standard commercial finite element code.

The evaluation of the models is performed in two steps. First, the performance of the constitutive models is evaluated by simulating the laboratory tests as single soil element tests with PLAXIS SoilTest facility. Based on the comparison of the numerical results with the laboratory data it is concluded that the HS performs the best compared to the SS and the MC model. In order to achieve good fit it is found that it is necessary to drastically reduce the failure stress ratio, Rf to an average value of 0.15 in contrast to what is mentioned in literature for soft soils. In terms of one-dimensional compression stress path both the HS and SS model are deemed to perform similarly. The MC model is found to reproduce poorly the laboratory tests due to the assumption of linear elasticity - perfect plasticity.

Subsequently, soil models are evaluated through a fully coupled hydro-mechanical simulation of the Leendert de Boerspolder stress test in PLAXIS 2D. The evaluation is done through the comparison of the measured to computed displacements and pore water pressure. It is found that the prediction of the HS model is "soft" for peat while the stiffness degradation in the organic clay results in excessive lateral displacements. Response of the SS is found to be better considering both displacements and pore water pressure. The best description of the stress test was found to be possibly by using the SS for the organic clay and the HS for peat. The performance of the MC model is quantitatively good however qualitatively is deemed to be poor. Furthermore, the influence of (a) the soil anisotropy and (b) the interface between organic clay and peat layers are pointed out as factors influencing the outcome of the simulation.

Based on this study, it is concluded that in general the Soft Soil model, at this stage, is recommended for use for both soils. The Hardening Soil model should be used for peat but with caution and mainly when the deviatoric strains are deemed to be important. In this

case the calibration should be done focusing on triaxial tests, therefore compromising the oedometric response. Moreover, a high secant stiffness should be considered to describe peat. That might be justifiable due to presence of fibers which under tensioning provide additional stiffness. Moreover, results suggest that the use of the HS model for the organic clay is not justifiable. Finally, the Mohr-Coulomb model should be used only as a rough approximation.

Table of Contents

List of Figures

List of Tables

Chapter 1

Introduction

1-1 Motivation

The Netherlands is a country where more than 50% of the land is located below the high-water level of the rivers and the sea. To protect these areas from flooding a large number of earth structures, i.e. dykes, have been constructed since the middle ages. The dyke system stretches for a length of 17000 kilometers across the country (Den Haan and Feddema, 2012), where 3200 km of the total length of dykes are primary dykes, located along the rivers and the sea, and the rest are regional dykes (van Baars, 2005). The assessment of the stability of the dykes has to be carried out regularly every 5 years.

The majority of these dykes are located over soft soils such as clays and peats. In general, it is difficult to predict and evaluate the response of these soils, especially for peats, due to some peculiar characteristics such as water content, organic content, previous stress-strain history, high friction angle, time dependent behaviour etc. Even though Dutchs have a great experience, over the years few dykes have failed causing social and economic losses. For example, in 2003 the Wilnis dyke, a secondary dyke located south-east of Amsterdam, failed causing considerable economic damage (van Baars, 2005).

These failures demonstrated the necessity to further investigate the behaviour of earth structures on soft soils. Therefore, many research projects were run over the last few years, aiming to enrich knowledge and provide answers to various questions related to dyke and embankment stability on soft soils. Worth mentioning is the full-scale failure test in Booneschans, Groningen in 2010 (den Haan et al., 2012) and the field test in Uitdam, near Amsterdam, that took place in 2011 (Zwanenburg & Jardine, 2015). The latest full-scale experiment that took place in the Netherlands was the induced failure of the Leendert de Boerspolder regional dyke in 2015.

This thesis project represents part of the extensive research activities within the project of Leendert de Boerspolder stress test. Its objectives are presented in detail in the following section.

1-2 Research objectives

The main objective of this research can be summarized in the following research question:

> Which of the available constitutive models in the commercial finite element code PLAXIS performs better in modeling the coupled hydro-mechanical behaviour (consolidation) of peat and organic clay as observed during the Leendert de Boerspolder stress test?

The above-stated research question is divided in two parts: (a) evaluation of the selected soil models through the simulation of laboratory tests and (b) conducting a fully coupled hydro-mechanical analysis of the stress test in PLAXIS 2D. Hence, the performance of constitutive models can be evaluated and compared against actual hydraulic head and displacement measurements as well as the laboratory measurements. The constitutive models considered in this research are the Mohr-Coulomb model, the Hardening Soil model and the Soft Soil model.

In more detail the main research question can be further divided into the following sub-questions:

- Which one of the considered constitutive models can simulate better the behaviour of peat and organic clay in triaxial and oedometric laboratory testing?
- How do these soil models perform in the simulation of a real embankment with complex hydraulic and stress conditions as is case of the Leendert de Boerspolder stress test?
- Which soil model is currently recommended for the simulation of these soils?

1-3 Methodology

The aforementioned research questions outline the research approach that was followed.

The first step was to study the available literature on peat and the constitutive models implemented in PLAXIS to establish the necessary knowledge for the realization of the thesis project. The mechanical characteristics of peat were examined in order to establish its behavior as well as the main aspects and constitutive equations of the Hardening Soil, the Soft Soil and the Mohr-Coulomb model.

The next step was to analyze the available field data and measurements (displacements and pore water pressures). The analysis of these data provided the necessary understanding of the in situ geotechnical conditions and an initial evaluation of the hydro-mechanical response of the system.

Subsequently, the laboratory tests were analyzed and preliminary parameters were estimated for each one of the considered soil models. Then, these parameters were calibrated in order to reflect the mechanical behaviour of material, using the SoilTest facility in PLAXIS for the exact purpose. This process also allowed for a first assessment of the capabilities of the constitutive models to describe peat and organic clay as observed in the laboratory.

Finally, a fully-coupled flow-deformation numerical simulation of the stress test was carried out, where results for the different constitutive models were compared against measured data and against each other in order to unveil their strengths and limitations.

1-4 Limitations

To be able to fulfill the research goals some limitations are set to create a framework in which the research is done. These limitations are as follows:

- PLAXIS finite element code is used to conduct the analysis. The specific commercial program is selected as it represents a standard finite element code used in engineering practise offering high quality, reliable results. Subsequently, in this research only models available in PLAXIS are considered.
- Time dependent deformation characterizes organic soils. However, within the context of this research creep is not considered. The decision is considered reasonable due to the short duration of the stress test.
- Soil anisotropy is not considered in the present work.
- Being mostly interested in the pre-failure behavior of the system, the response of the dyke at failure in not analyzed in this study.

1-5 Thesis outline

The present report consists of six chapters in total.

Chapter 1 introduces the research motivation and objectives of the present thesis project.

The focus of Chapter 2 is the establishment of in situ geotechnical conditions and the analysis of displacement and pore water pressure data recorded during the stress test by inclinometers, extensometers and piezometers.

Chapter 3 provides an overview of the most important characteristics of peat. Moreover, the Hardening Soil, the Soft Soil and the Mohr-Coulomb constitutive models are described.

Chapter 4 elaborates on the determination of parameters and the consequent calibration of parameters with PLAXIS SoilTest facility. Additionally, difficulties encountered during the calibration of the parameters and possible limitations of the models are elaborated.

Chapter 5 addresses the simulation of the dyke in PLAXIS 2D. Furthermore, the results of the simulation are discussed and conclusions are drawn.

Finally, Chapter 6 concludes the findings of this thesis study and proposes further relevant research.

Chapter 2

Geotechnical conditions and field measurements

The scope of this chapter is to present an overview of the Leendert de Boerspolder stress test in terms of in situ geotechnical conditions and measurements. Particular attention has been given to the response of the piezometers and the vertical and horizontal displacements that were recorded during the stress test. Finally, the role of permeability on the observed hydraulic response is discussed.

2-1 Project overview

The Leendert de Boerspolder dyke is located on a small island north-eastern of Leiden at the Harlemmermeer polder. Figure 2-1 shows an aerial photograph of the island and the location of the dyke. Dykes surrounding the island date back to 17^{th} century, providing a unique chance to study the behaviour of a real dyke.

Figure 2-1: Aerial photograph of the Leendert de Boerspolder. The location of the dyke which was tested is highlighted in red

The stress test started on 21^{st} September 2015 and ended on 14^{th} October early in the morning, when the Central and South sections of the dyke collapsed. The dyke was brought to failure by a staged excavation at the toe and by altering the water level in the trench i.e. lowering water level by one meter and refilling back to the initial level. Table 2-1 presents the different phases of the stress test and their duration. In Figure 2-2 the geometry of the three excavations in relation to the dyke is depicted.

Table 2-1: Phases of the stress test

Step	Duration (days)
Wetting	6.75
Excavation I	0.29
Consolidation	1.71
Drawdown I	0.11
Consolidation	1
Filling I	0.05
Consolidation	3.75
Excavation II	0.39
Consolidation	1.64
Drawdown II	0.17
Consolidation	0.77
Filling II	0.08
Consolidation	3.88
Excavation III	0.39
Consolidation	1.32
Drawdown III	0.21

2-2 Geotechnical conditions

The ground surface at the polder side is located at an elevation of -1.7 m to -1.9 m NAP. The dyke's crest is at -0.4 m NAP, i.e. about 1.5 m above the polder level. The water level in the canal is at -0.7 m NAP, while the groundwater surface in the polder is about 0.3 m below the surface. Both are artificially controlled with small variations during the year.

An extended site investigation program, comprised of sampling boreholes and a large number of CPTs, was executed during the year before the initiation of the stress test. From the data collected 3 soil layers were identified below the dyke Rodriguez Barragan (2015): (a) a peat layer, (b) an organic clay layer and (c) a deep silty clay layer (Figure 2-2).

The dyke material is characterized by a relative high unit weight of 18 kN/m^3; its composition is highly heterogeneous. The unit weight of peat is equal to 10 kN/m^3, which is typical for that type of soil. A distinction was made between the upper and lower part of peat, as the upper part was found to be more fibrous. The void ratio ranges from 6.5 below the dyke, where peat is compressed, to 7.5 at the polder. Moreover, the water content ranges between 600% and 900%. The unit weight of organic clay was reported to be 14 kN/m^3, while the water content and void ratio are around 60% and 0.8, respectively.

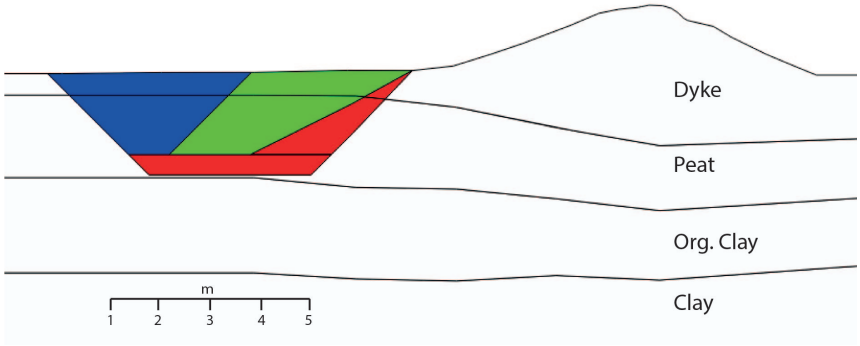

Figure 2-2: Cross-section of central section of the dyke. In color Excavation I, Excavation II and Excavation III are depicted

An average friction angle of 35° and 31° for peat and organic clay, respectively, was calculated from the available undrained triaxial tests, while the apparent effective cohesion, c' was found to be on average 2 and 4 kPa, respectively. K_0-CRS test on peat indicate a coefficient of lateral earth pressure at rest at normally consolidated state (K_0^{nc}) equal to $\sim$ 0.3, a value that is in agreement with the literature (e.g. Mayne & Kulhawy, 1982). The value of K_0^{nc} of the organic clay was reported to be around 0.4. Compression index, C_C was calculated to be in the range of 3.7 to 4.5 and 0.75 to 0.85 for peat and organic clay, respectively, while swelling index, C_s for peat and organic clay was determined to be around 0.7 and 0.05, respectively.

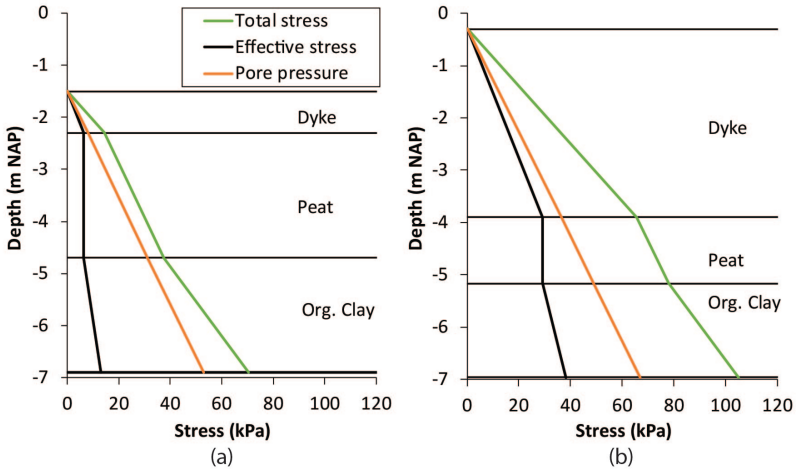

Figure 2-3: Soil stresses at location of inclinometers (a) StC and (b) ScC

Figure 2-3 shows the distribution of stresses at the toe and below dyke, at the location of inclinometers StC and ScC (see Figure 2-4), assuming hydro-static condition of the pore water pressure distribution. Considering the preconsolidation stress reported from laboratory tests and the in situ effective stresses, the peat and organic clay at the toe and polder are characterized by an over-consolidation ratio, OCR of 3 and 2.5 respectively. With regards to the definition of OCR the reader is referred to Equation 3-18 and Figure 3-12. Below the dyke peat appeared to be normally consolidated in contrast to organic clay that is slightly overconsolidated (OCR $\approx$ 2.5). Hence, using the empirical Equation 2-1 (Knappett & Craig,

2012), the coefficient of lateral earth pressure for overconsolidation, K_0^{oc} in the polder was estimated to be equal to 0.51 for the peat and 0.63 for the organic clay.

$$K_0^{oc} = K_0^{nc}\sqrt{OCR} \tag{2-1}$$

2-3 Monitoring data analysis

An extensive monitoring system was installed in order to record displacements and pore water pressures throughout the test. The monitoring equipment consisted of: (a) 25 piezometers, (b) 5 inclinometers and (c) 16 extensometers. The equipment was distributed in three sections: (a) North, (b) South and (c) Central. The Central section was the most heavily monitored. The location of different sensors in the central section is shown in Figure 2-4. The monitoring equipment in the other two sections is located in similar positions [1]; cross-sections are provided in the Appendix.

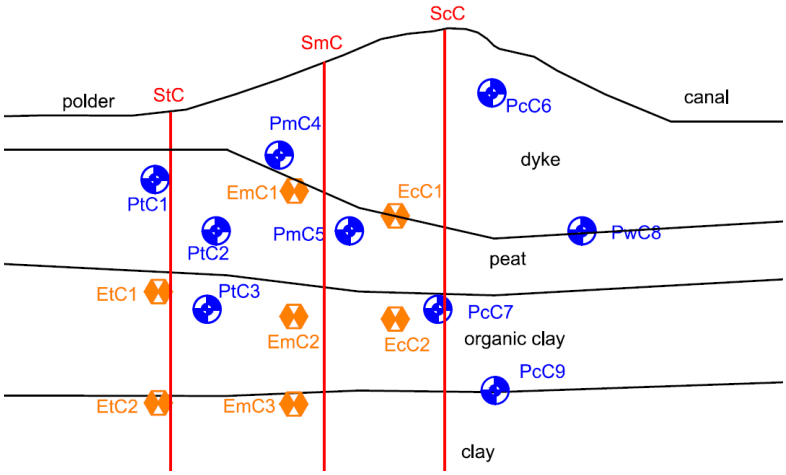

Figure 2-4: Location of sensors (inclinometers, piezometers and extensometers) in central section. Location of sensors in North and South section is similar

2-3-1 Pore pressure response during the stress test

The pore water pressure was monitored through 25 piezometers in total, 8 piezometers were placed in each section of the dyke, while one extra sensor was placed in the central section at the interface of organic clay and silty clay. The piezometer located at the top of the dyke (piezometer PcC6 in Figure 2-4) is not considered as the measurements were affected by the adjacent water body of the canal. Moreover, sensor PcC9, depicted in the same Figure, is omitted as only one was placed at the central section of the dyke, therefore no comparison can be made between the different sections.

[1] Three letters are used to denote each sensor: the first letter indicates the types of sensor, the second letter indicates the location of sensor relative to toe and crest, the third letter designates the section where the sensor is located.

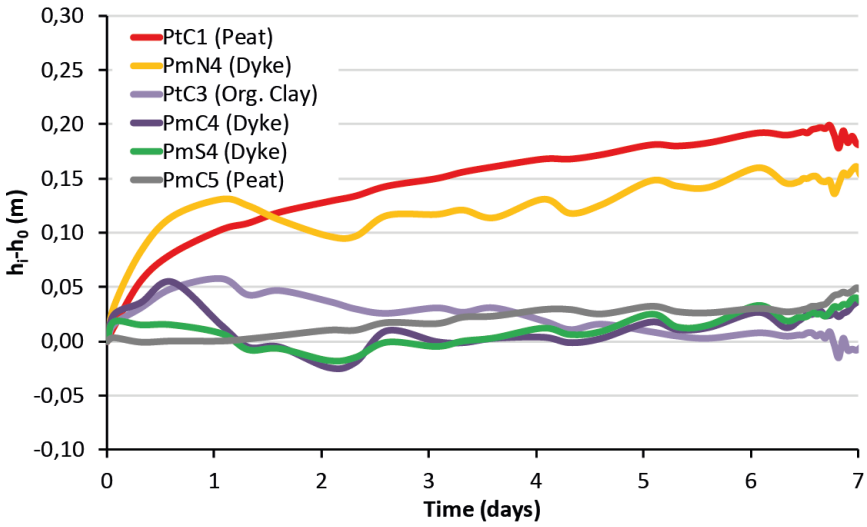

Figure 2-5: Changes in the hydraulic head against time during the Wetting stage for selected piezometers

The analysis of pore water pressure measurements is divided into three parts, (a) Wetting, (b) Stage I, where the measurements during the first excavation, drawdown and filling are discussed and (c) Stage II, where the measurements from the second excavation to the third excavation are presented. The distinction in these three stages is kept throughout the report. Moreover, in order to make a meaningful comparison, data presented in Figures 2-6 and 2-7 are offset to 0 considering as reference time the beginning of wetting. h_0 refers to the hydraulic head during at moment the wetting started.

Wetting stage

About seven days prior to the initiation of the stress test, in order to assure complete saturation of the system, a pipe was placed at the top of dyke, allowing flow of water. The inflow of water was kept constant through out the stress test.

In Figure 2-5 the response of selected piezometers during this phase is shown. The response of these piezometers is considered indicative of the response of soil layers at the toe and below the dyke.

Piezometers located in the dyke in Central and Southern section recorded no change in pore water pressure, while an increase of 0.15m was recorded in the Northern section. Considering peat an increase was observed at the piezometers located at the toe of the dyke. The increase in hydraulic head is an indication that the top layers at the toe, i.e. dyke material and peat, were not fully saturated. Piezometers located below the dyke recorded no change as the hydraulic head was regulated mainly by the hydraulic head in the canal. A similar neutral behaviour is observed for piezometers located in the organic clay.

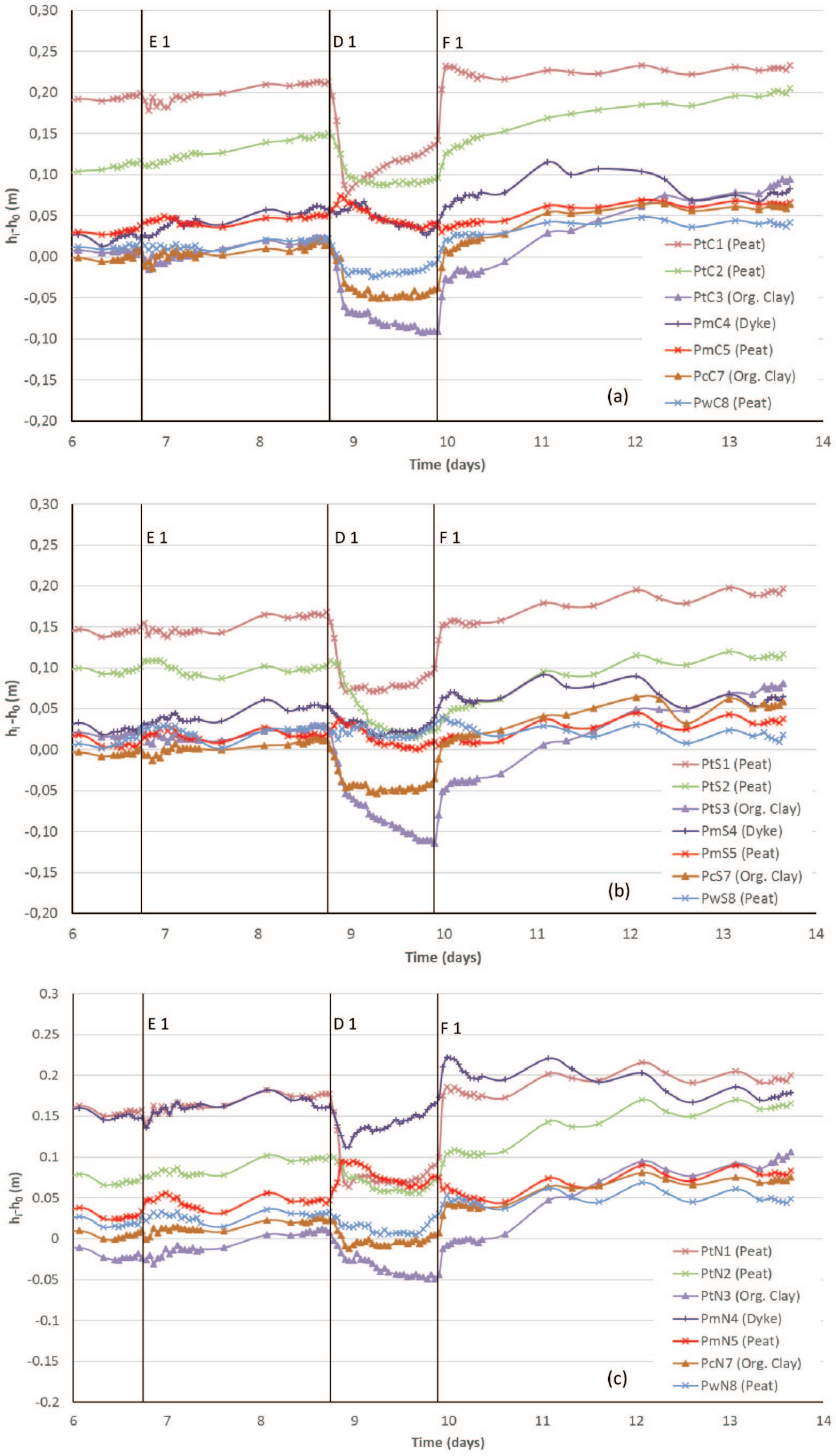

Figure 2-6: Changes in hydraulic head over time during the 1^{st} stage in (a) Central section, (b) South section and (c) North section. Black lines indicate different steps, i.e. excavation (E), drawdown (D) and filling (F). y-axis is offset to 0. Time origin is the beginning of wetting. h_0 denotes the value of the hydraulic head at the beginning of wetting

Stage I

After the first excavation some minor fluctuations in hydraulic head were recorded (Figure 2-6) but in general hydraulic head remained constant. A contributing factor to that was the continuous inflow of water at the top of the dyke but also the distance between the excavation and the dyke toe.

Following a period of about two days the water level in the trench was lowered by one meter in a short period of time of about 3 hours. As shown in Figure 2-6, between the different sections piezometers located in the same position, for example piezometer 2, recorded a similar response with some exceptions. All piezometers recorded a gradual change in groundwater head, except piezometers 4 in Central and South section where groundwater head remained constant. A likely explanation for that behaviour is lower permeability due to local soil variability. Another contributing factor could be the presence of an impermeable layer at the interface of the dyke and peat acting as a hydraulic seal. The equivalent [2] piezometer in North section recorded a drop suggesting that the impermeable layer is not present.

Furthermore, in contrast to most sensors, piezometer 5 initially recorded an increase. Possibly, that can be explained by an increase in horizontal displacements recorded by some inclinometers during the drawdown, as discussed in Section 2-3-2. Therefore, the increase could be shear induced.

Stage II

In Figure 2-7 the change in hydraulic head during the second stage is presented. Immediately after the second excavation piezometers 1 and 2, in all sections, recorded a decrease of the hydraulic head by about 0.1 m. That is explained by the proximity of the excavation face to the toe compared to Excavation I. During the second drawdown, similar to Stage I, all piezometers recorded a decrease in hydraulic head except piezometer 5 that initially recorded an increase. Between drawdown and filling, piezometers reached a plateau, indicating steady state condition. However, piezometer 4 deviates. Likely explanation is that the increase was shear induced. Considering the third excavation, it is worth mentioning that even though it was the closest to the dyke toe no change in pore pressure was recorded.

It is important to mention that changes in the hydraulic head can be partially explained not only through shearing as indicated by inclinometers but also the extensometers, i.e. the volumetric response on soils. That is addressed in the following section.

2-3-2 Displacement response during the stress test

The displacements recorded by the inclinometers and extensometers are presented in Figures 2-8 and 2-9, respectively. Positive measurements in inclinometers and extensometers indicated movement towards the polder or heave, respectively.

As shown in Figure 2-8 during the first two steps, i.e. wetting and excavation I, no major displacements were recorded. An increase in horizontal displacements occurred during the

[2] In this section, when the term "equivalent piezometer" is mentioned, it refers to piezometers with the same number, e.g. PtC**1**, PtS**1**, PtN**1**.

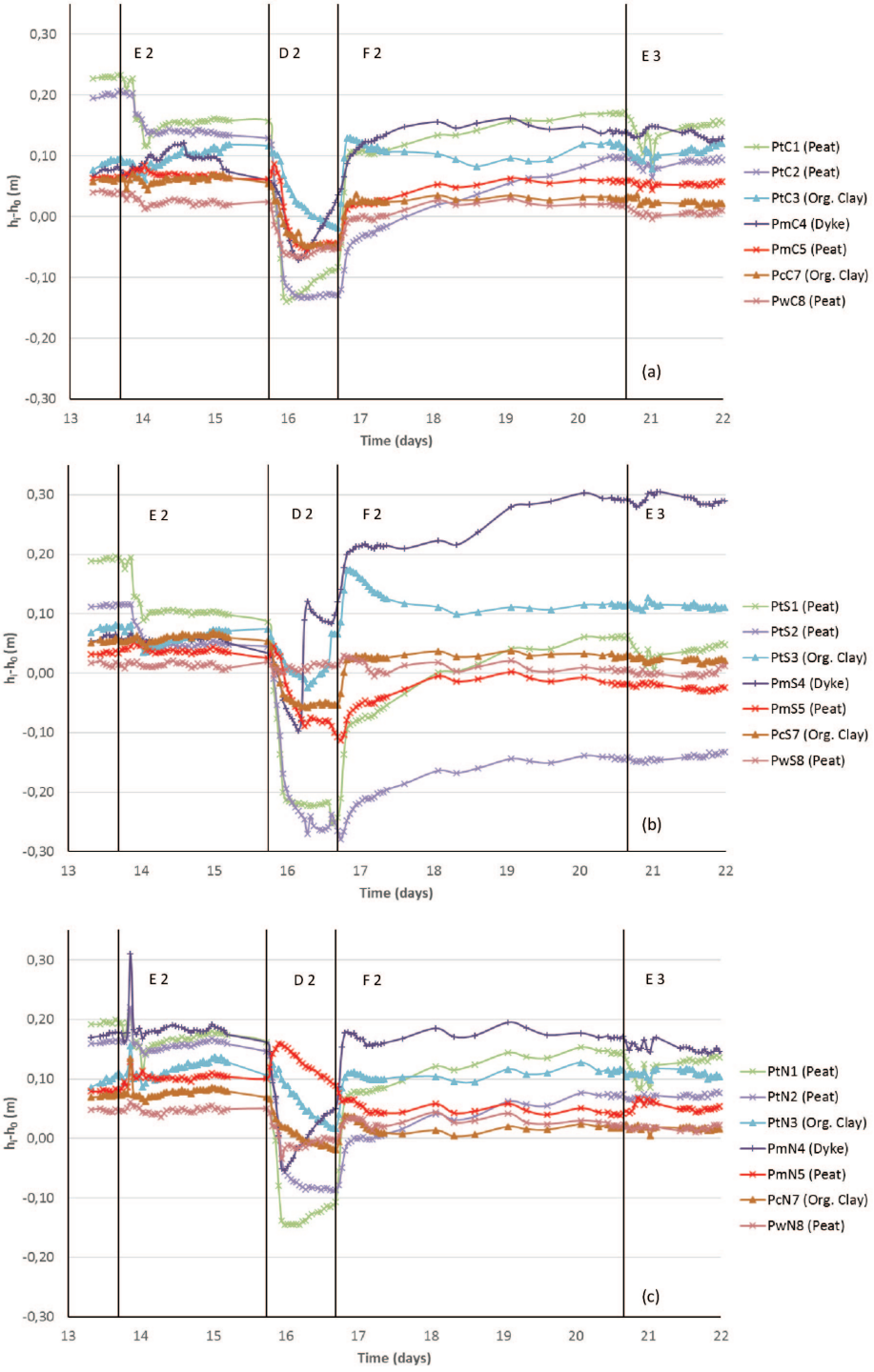

Figure 2-7: Change in hydraulic head over time during the 2^{nd} stage in (a) Central section, (b) South section and (c) North section. Black lines indicate different steps, i.e. excavation (E), drawdown (D) and filling (F). y-axis is offset to 0. Time origin is the beginning of wetting. h_0 denotes the value of the hydraulic head at the beginning of wetting

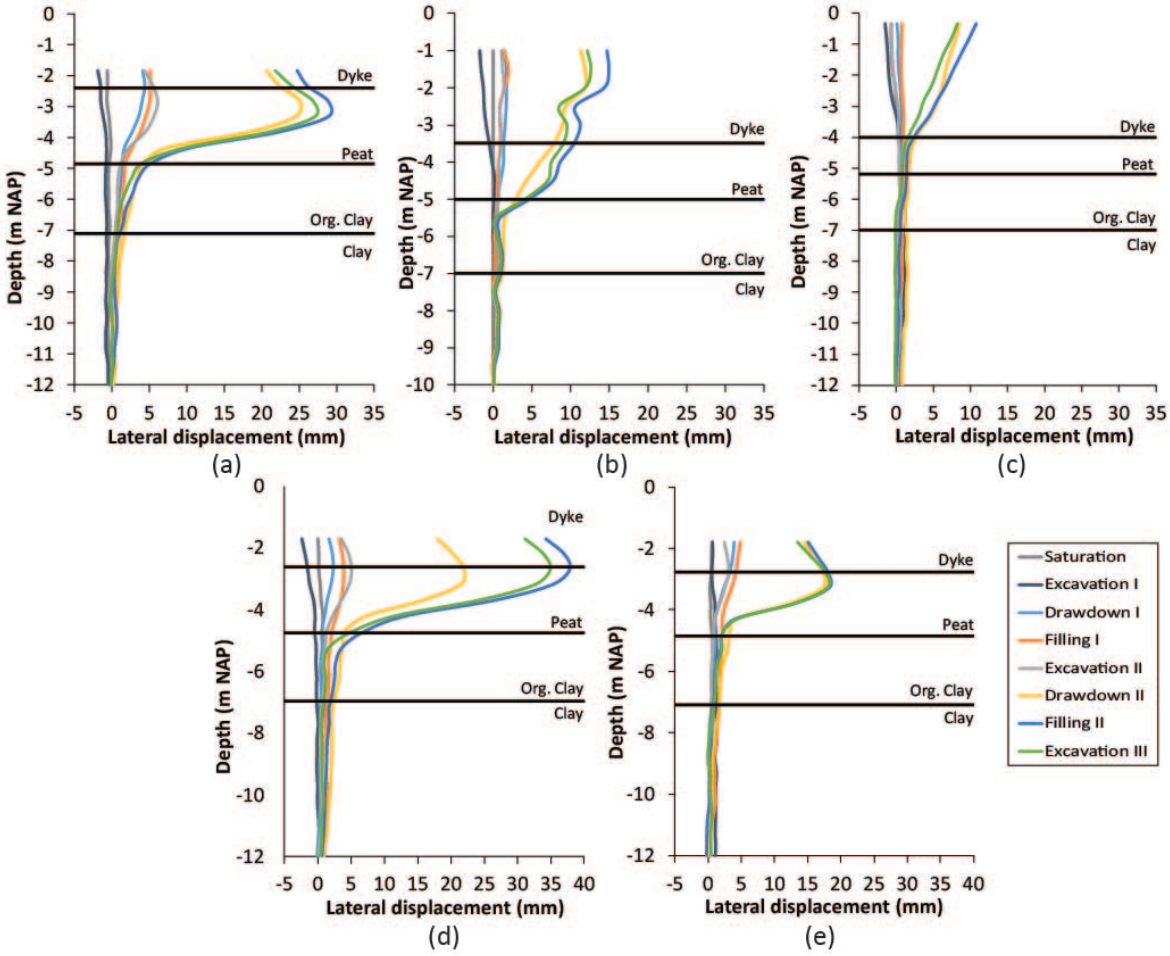

Figure 2-8: Horizontal displacement measurements for inclinometers (a) StC, (b) SmC, (c) ScC, (d) StS and (e) StN. Positive displacement indicates movement towards the polder

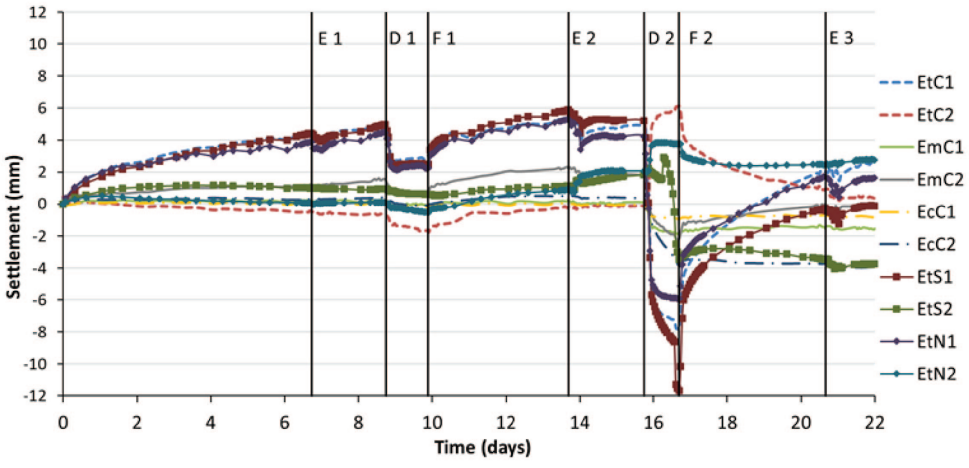

Figure 2-9: Vertical displacement measurements for extensomaters located in peat and organic clay. Time origin is the beginning of wetting. Positive displacement indicates heave. Black lines indicate different steps, i.e. excavation (E), drawdown (D) and filling (F). Values > 0 indicate heave while negative values indicate settlement

first drawdown. Similar behaviour was recorded during the second drawdown. That increase in displacement during drawdown is related to the increase in hydraulic head recorded by some piezometers, i.e. shear induced pore water pressure, as discussed in section 2-3-1. An interesting observation is the probability of presence of two shear zones; one shear zone located at the lower part of peat and a second shallower zone at the bottom of the dyke, as measurements of sensor SmC indicate.

Vertical displacement measurements (Figure 2-9) indicate a response similar to what was observed with the pore water measurements. In general, an increase in pore water pressure translated into a decrease in effective stress and heave, while a decrease in pore water pressure indicated increase of effective stresses and settlement. During the initial wetting Sensors EtC1, EtN1 and EtS1 recorded a positive displacement of 5mm whereas the other sensors recorded a negligible increase <1mm. An exception is the sensor which indicated settlement of -1mm. During the first drawdown and filling the majority of sensors recorded a small settlement and heave, respectively as expected. Noteworthy is the response after the second drawdown as different sensors indicate the opposite response. For example, during the drawdown EtC1 recorded settlement while EtC2 recorded heave. Similar was the response of equivalent sensors in the other two sections. The exact reason for that behavior is not absolutely clear to the author. In combination with the inclinometer data which indicate an important increase in the horizontal displacements, it is speculated that water was "squeezed" from the peat to the underlying organic clay resulting in an increase of pore water pressure, and subsequently heave, at the are zone of the interface between the organic and silty clay.

2-3-3 Evaluation of hydraulic head variation during drawdown

Analyzing the change in hydraulic head during the drawdown, meaningful conclusions can be drown about the permeability and the drainage response of peat and organic clay. In Figures 2-10 and 2-11 the normalized change in hydraulic head during the drawdown against the change of water level in the trench, for Stages I and II, respectively, is presented. In both graphs positive change indicates a decrease in hydraulic head.

The change in both stages and between equivalent piezometers is similar. Focusing on peat there is a clear differentiation between piezometers 1 and 2. The latter responded slower than the former. That is explained by the fact that even though both piezometers are located at the toe, piezometer 1 was at the upper part of the peat layer, while piezometer 2 was at the lower part. Considering that the upper part was more fibrous, a variation in permeability between the sub-layers may explain the lower rate of change in piezometer 2. The increase recorded by piezometer 5 is shear induced, as discussed earlier, while piezometer 8, located below the dyke, where peat is compressed and partially affected by the water level in the canal recorded a small change.

Finally, combining the measurements presented in Figures 2-6 and 2-10, North section appears to be less pervious than the other two sections as both the change in hydraulic head during the drawdown and the maximum value that was recorded after the end of the drawdown, are smaller compared to the other sections.

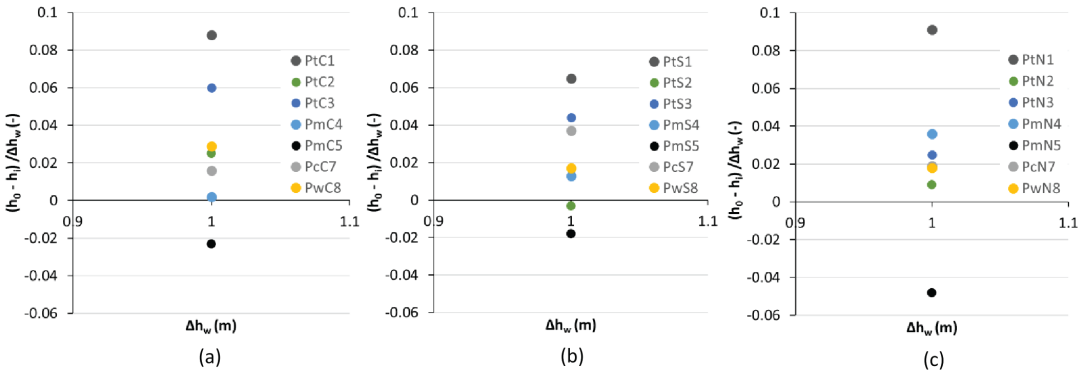

Figure 2-10: Normalized change in groundwater head versus change of water level in the trench (Δh_w) during the 1^{st} drawdown in: (a) Central section, (b) South section and (c) North section. The water level was lowered by 1 meter in 3 hours. h_0 denotes the value of the hydraulic head at the beginning of the first drawdown

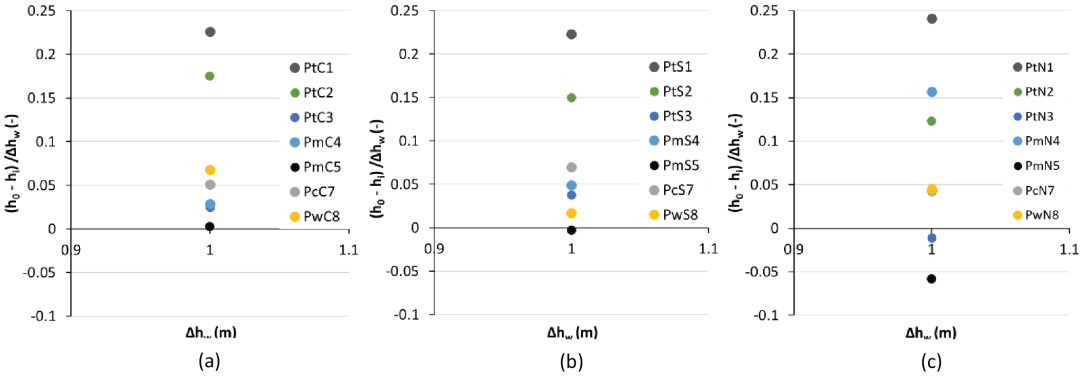

Figure 2-11: Normalized change in groundwater head versus change of water level in the trench (Δh_w) during the 2^{nd} drawdown in: (a) Central section, (b) South section and (c) North section. The water level was lowered by 1 meter in 4 hours. h_0 denotes the value of the hydraulic head at the beginning of the second drawdown

Chapter 3

Literature Review

This chapter presents an overview of the necessary principles and theory that is needed for the realization of this thesis project. In the first part, the geomechanical characteristics of peat are introduced. In the second part, the main characteristics and constitutive relations of Mohr-Coulomb, Hardening Soil and Soft Soil model are presented.

3-1 Peat

Peat is a soil that is formed from partially decomposed and fragmented remains of plant that have accumulated under water, which helps in the preservation of the organic remains (Radforth, 1969; Farrell, 2012). The source of organic matter is mainly dead plants that are gradually accumulated and decomposed. The organic matter combined with a percentage of inorganic matter is forming peat soil. According to Dutch standards, a soil should consist of at least 20% to 30% and higher of organic matter in order to be characterized as peat.

In general, it is difficult to characterize the behaviour of such material due to specific characteristics that greatly affect and differentiate its behaviour from inorganic soils. These key characteristics are: (a) fiber content (fibrosity), (b) high compressibility, (c) high water content, (d) anisotropy, (e) low compressive strength but relatively high tensile strength and frictional resistance, (f) high initial permeability and void ratio, which decreases rapidly under loading due to high compressibility, and (g) time dependent behaviour (creep). Some of these characteristics are discussed further in this section.

3-1-1 Classification

Over the years many classification systems have been proposed (see Landva et al., 1983; Hobbs, 1986). However, none of them is generally accepted. Hence, here the classification of the Dutch norm NEN5104 (1989) is presented.

The classification is based on the two triangle charts presented in Figure 3-1. Peat is found in the left triangle, where using the percentage of organic matter, determined by the Loss on

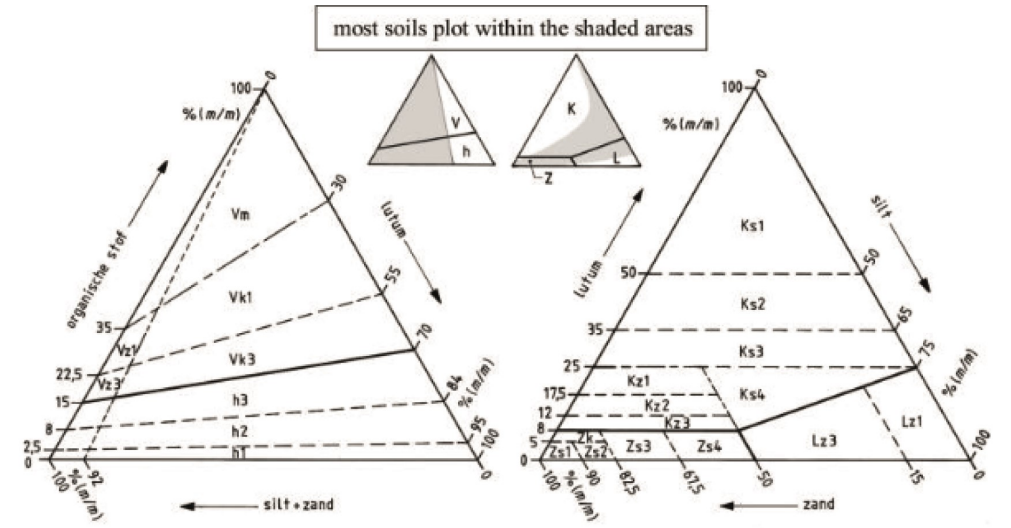

			Bulk density ρ (t/m^3)	
Designation	Description	nr	Mean	Range
Vm	Peat, poor in mineral matter	98	1.06	0.95–1.13
Vk1	Slightly clayey peat	21	1.11	1.02–1.17
Vk3	Very clayey peat	16	1.18	1.09–1.25
Kh3	Highly organic clay	13	1.27	1.20–1.35
Kh2	Mod. organic clay	30	1.37	1.26–1.51
Kh1	Slightly organic clay	60	1.45	1.30–1.60
Ks	Slightly to highly silty clay	89	1.51	1.40–1.60

Figure 3-1: Classification diagrams for soft soils (top) and indicative bulk density of Dutch soft soils (bottom) (NEN5104, 1989)

Ignition test (LOI), fines, silt and sand a soil sample can be characterized. According to the norm, a soil with an organic content higher than 15% is characterized as peat mixed with clay, while an organic content higher than 30% characterizes a soil as pure peat.

Additionally, bulk density or unit weight can be used to characterize organic soils. A saturated soil with a unit weight less than 12 kN/m^3 is characterized as peat, while a soil with a unit weight higher than 14 kN/m^3 is described as clay. In Figure 3-1 the classification based on bulk density is presented.

Another characteristic that is important for a complete classification of peat is the degree of humification or decomposition of peat. For further information reader is referred to ASTM D5715-00 (2006).

3-1-2 Index properties

Water content is defined as the ratio of the mass of water to the mass of solids. Depending on the type of peat, water content can vary from a few hundred per cent to values greater than 2000% (O'Kelly, 2015b). That range of water content corresponds to in situ void ratio

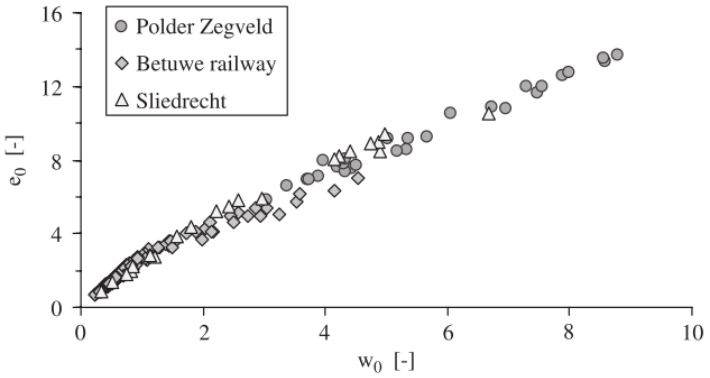

Figure 3-2: Correlation of natural water content (w_0) and void ratio (e_0) for Dutch peat (den Haan & Kruse, 2007)

of 7.5 to 30, respectively (Mesri & Ajlouni, 2007). For Dutch peat the correlation of water content and void ratio is shown in Figure 3-2.

As shown in Figure 3-3, the water in peat is found in different forms that can be categorized as (Hayward & Clymo, 1982):

- Free water contained internally in cells
- Inter-particle water held in cavities
- Water absorbed and held by the fibers

The majority of the water is in states (A) and (B) (Landva & Pheeney, 1980) and can be expelled easily by compression. Absorbed water can only be removed by drying.

Water content affects many properties of peat and therefore has a profound effect on its mechanical characteristics, e.g. compressibility and strength. It is therefore safe to say that together with bulk density is the most important index property (den Haan et al., 2012).

Other useful index properties of peat are the organic content, determined by the bulk weight and the loss on ignition, and bulk density. Regarding Atterberg limits O'Kelly (2015a) suggested that they are not appropriate for fibrous peat soils. Scale effects and fiber reinforcement as well as the sample preparation method play an important role in measured LL and PL values. Subsequently, Atterberg limit testing does not produce meaningful results.

3-1-3 Permeability

Permeability is a soil characteristics that is related to void ratio and the size and shape of flow channels. As discussed in section 3-1-2, peat exhibits a high initial void ratio. Many researchers have attributed (e.g. Landva & Pheeney, 1980) high void ratio to the fact that fibrous peat has a large pore size allowing easy flow of water. That, combined with the fact that usually peat deposits are surficial and therefore have experienced very low effective overburden pressure, the initial permeability of peat can be as high as 10^{-5} m/s (Mesri &

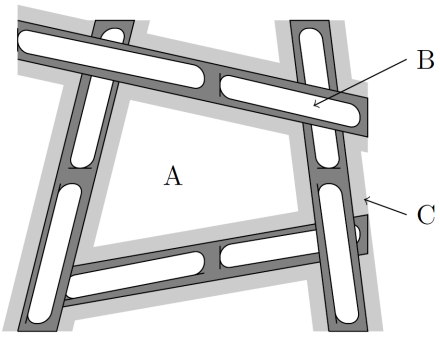

Figure 3-3: Forms of water content in peat, (A) free water, (B) inter-particle water and (C) absorbed water (de Jong, 2007)

Ajlouni, 2007). Figure 3-4 shows data on vertical permeability and void ratio for different peats from the literature. As a frame for reference, permeability data of other soils such as clay mineral montmorillonite and sand are included.

As a parameter, permeability of peat is very sensitive to scale effects, as in field preferential drainage paths can develop because of the large heterogeneity of peat and non uniformity of pore-size distribution (Dhowian & Edil, 1980; Yamaguchi et al., 1985). Scale effects also explain the fact that peat permeability determined from oedometer tests is usually greatly underestimated compared to in situ values (e.g. Hobbs, 1986; Hayashi et al., 2012). Furthermore, because of the high heterogeneity and the fibrous nature, peat exhibits anisotropy in terms of permeability (see Section 3-1-6).

Under load the permeability of fibrous peat decrease dramatically as a result of the large change in void ratio. Hobbs (1986) reported a decrease of permeability by three orders of magnitude upon a decrease in void ratio of only half an order. A great part of that fast reduction of void ratio and permeability is attributed in the closing of macropores.

A way to quantify the change of permeability with change in void ratio is through the permeability change index, C_k. It is defined as $C_k = \Delta e / \Delta \log k_v$. It should be noted that C_k is not a direct indicator of permeability change. When C_k is small, then the decrease of permeability for a given decrease of void ratio is large, whereas a large C_k translates into a small change in permeability. Mesri & Ajlouni (2007) proposed the following empirical correlation between C_k and in situ void ratio, e_0:

$$C_k / e_0 = 0.25 \tag{3-1}$$

Figure 3-5 shows that data for fibrous peat are described satisfactory by that empirical correlation. In the same Figure it is shown that the equivalent empirical correlation for clays and silts is $C_k/e_0 = 0.5$ (see Tavenas et al., 1983).

3-1-4 Compression and consolidation

A distinctive characteristic of peat is its extreme compressibility. The large compression that can occur in virgin peat is clearly illustrated in Figure 3-6. For a relative small increase in

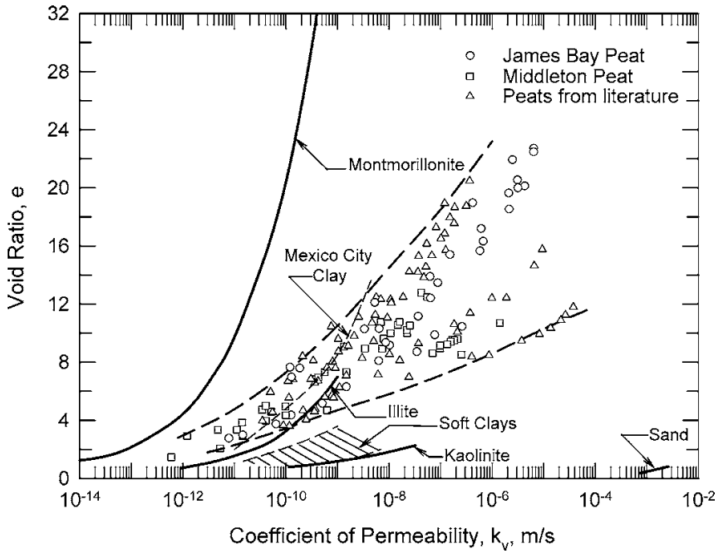

Figure 3-4: Correlation between void ratio (e) and logarithmic coefficient of permeability ($\log k_v$) for fibrous peat within frame of reference of permeability data of other soils (Mesri & Ajlouni, 2007)

the effective stress, at the order of 50 kPa, a peat stratum can reduce in thickness by more than 50%.

That behaviour is directly related to the high water content of peat. Initially when loaded there is expulsion of water, eased by initial high permeability, combined by simultaneous rearrangement of particles and structure of peat. That process continues until the dissipation of pore water pressure. The end of this phase denotes the end of primary consolidation. Primary consolidation is usually completed within a few weeks or months (Mesri & Ajlouni, 2007). After pore water pressures have dissipated soil skeleton deformations continue for a long period, due to the viscous nature of organic matter. The duration of secondary compression of peat is measured in years. Moreover, the magnitude and the rate of secondary compression is higher than primary compression (e.g. Landva & Pheeney, 1980). Because of these characteristics, secondary compression accounts for the majority of settlement. It is therefore the dominant consolidation process in peat.

3-1-5 Shear strength and stiffness

Strength and stiffness of peat are controlled by the presence of fibers and their properties, as fibers act as a reinforcing component providing tensile strength.

The measured strength depends on the test method. In triaxial testing measured friction angles usually exceed the 30-35° reaching values up to 90° (den Haan & Feddema, 2012). On the other hand direct shear testing result in lower friction angle with values ranging between 20 to 40° (Farrell, 2012). That difference between friction angle values is attributed to the entangled fibers which provide reinforcement. The orientation of fibers in peat has been noted to be predominantly horizontal. Therefore, in direct shear testing the reinforcement effect is not active, while in triaxial testing fibers are "activated". It is important to note that the

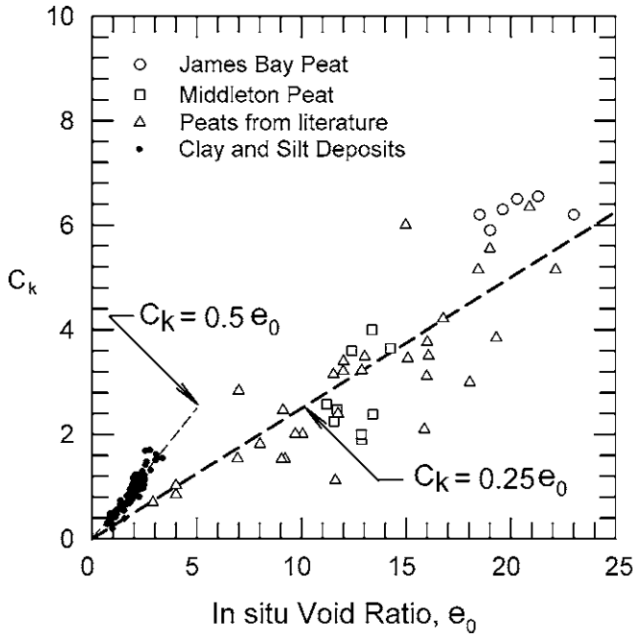

Figure 3-5: Relationship between C_k and in situ void ratio (e_0) for fibrous peat and soft clay (Mesri & Ajlouni, 2007)

shear deformations required to mobilize the maximum frictional resistance are 5 to 10 times higher than those required for soft clays (Mesri & Ajlouni, 2007).

Another effect of the fiber reinforcement in peat is that peat manifests a high tensile strength compared to inorganic soils due to tension mobilized by the fibers. For the same reason the coefficient of earth pressure at rest for fibrous peat is usually around 0.3 (Mesri & Ajlouni, 2007). In amorphous peat, where fibers do not have a predominant effect as in fibrous peat, a much higher value of 0.5 has been reported (Edil & Wang, 2000). Another typical phenomenon that arise from fiber reinforcement is that under triaxial testing the stress path usually reaches the zero radial effective stress condition, i.e. the "tension cut-off" making the failure of peat specimens ill-defined (den Haan et al., 2012; Cola & Cortellazzo, 2005; Yamaguchi et al., 1985).

The stiffness of peat, expressed as an elastic Young's modulus is generally low and highly variable. Reported values in literature range from 400 to 7000 kPa (Hendry et al., 2014; Cola & Cortellazzo, 2005). Horizontal stiffness has also been found to be higher than vertical stiffness (Hendry et al., 2012).

3-1-6 Anisotropy

The discussion in previous sections make evident the fact that peat is a highly anisotropic material in terms of stiffness, strength and permeability.

Yamaguchi et al. (1985) studied the strength of peat specimens in triaxial testing for different orientation, i.e. vertically and horizontally loaded specimens. For vertically-oriented peat specimens Yamaguchi et al. reported a value ϕ' between 51° and 55°, while a significantly lower value of 35° is reported for horizontally-oriented specimens.

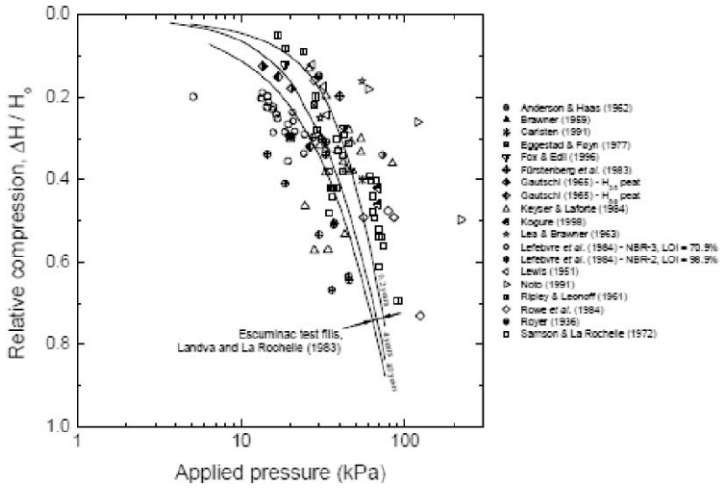

Figure 3-6: Relative compression versus logarithmic applied pressure (Farrell, 2012)

In the same study Yamaguchi showed that fibers provide an elastic cross-anisotropic stiffness, a result that has confirmed by other researchers (e.g. Zwanenburg, 2005). Furthermore, in literature is also mentioned that the horizontal secant stiffness of peat can be up to 50% higher than the vertical secant modulus (Hendry, 2012). However, the cross-anirotropy of stiffness is only apparent when fibers are in tension.

Anisotropy in peat was further studied by Zwanenburg (2005). A distinction between structural and induced anisotropy was made. The former depends solely on the structure of peat, i.e. presence of fibers, while the latter is stress-induced anisotropy related to load history, i.e. pre-consolidation pressure.

Permeability anisotropy is another important aspect of peat. Mesri & Ajlouni (2007) mention that in literature, reported values for ratio k_h/k_v range from 3 to 10. O'Kelly (2007) found that when peat is surficial, ratio k_h/k_v can be as low as 1 or even lower than one in some cases. However, with a small increase in effective stress, permeability ratio increases. That is also confirmed by Beckwith et al. (2003) who investigated permeability anisotropy and heterogeneity, variation with depth. Worth mentioning that Beckwith et al. (2003) found evidence that peat with relatively high permeability values can also be found at relative high depth.

3-2 Constitutive Models

In this section the main aspects of the selected constitutive models and their governing equations and representation in stress space is presented. A detailed analysis of the parameter determination methodology is discussed in Chapter 4.

3-2-1 Mohr - Coulomb model

The Linear Elastic Perfectly Plastic model, i.e. Mohr-Coulomb, is a simple model that combines Hooke's elastic law and the generalized form of Coulomb's failure criterion (Figure 3-7).

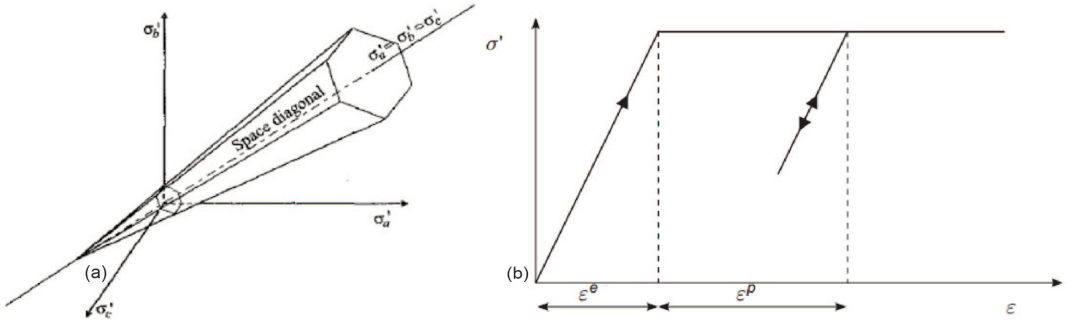

Figure 3-7: (a) Mohr-Coulomb yield surface in principal stress space (Potts & Zdravković, 1999) (b) Basic concept of an elastic perfectly plastic model (Plaxis, 2016a)

That means that the stiffness behavior below the failure line is assumed to be linear elastic and only when the failure envelope is reached plastic strains are generated. The model requires 5 parameters in total to describe a soil, two elastic parameters (Young's modulus, E and Poisson's ratio, v), two parameters for Mohr-Coulomb's failure criterion (friction angle, ϕ and cohesion, c) and the dilatancy angle, ψ.

As a result of the simplicity of the model and the incorporation of Mohr-Coulomb's failure envelope, the model is considered to predict well the failure of soils, mainly for drained stress paths (Brinkgreve, 2005), but in a deformation analysis the applicability of the model is poor. Therefore, Mohr-Coulomb can serve only as a first order model.

3-2-2 Hardening Soil model

The Hardening Soil (HS) model is an advanced constitutive model formulated by Schanz et al. (1999). It is capable to describe adequately the response of both cohesive and non-cohesive soils.

The most important features of the HS model that differentiates it from other advanced models are the introduction of a stress dependent stiffness for both loading and un-/reloading according to a power law, the use of the Mohr-Coulomb failure criterion to describe failure and the use of two yield surfaces, which are a yield cap and shear hardening surface, to account for development of plastic strains due to shearing and primary compression.

3-2-2-1 Shear hardening yield surface

The formulation of the yield function for the shear hardening surface is based on the hyperbolic stress-strain relationship originally developed by Kondner (1963) and was letter extended by Duncan & Chang (1970). The formulation of the shear hardening yield function (f_s) is given as (Schanz et al., 1999):

$$f_s = \bar{f} - \gamma^p \tag{3-2}$$

where subscript s is used to denote shearing and $\bar{f}$ and γ_p are calculated according to:

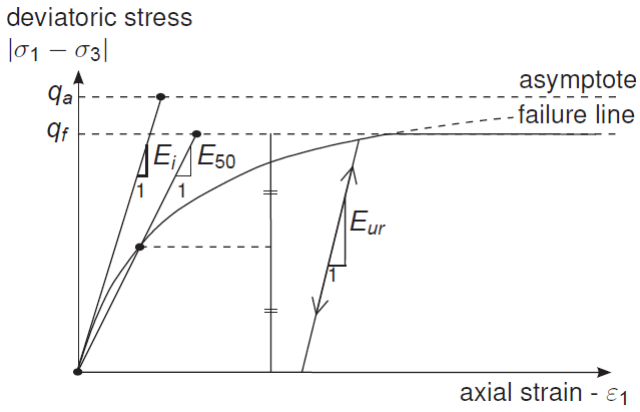

Figure 3-8: Hyperbolic stress-strain relationship in primary loading for a standard drained triaxial test (Plaxis, 2016a)

$$\bar{f} = \frac{2}{E_i} \frac{q}{1 - q/q_a} - \frac{2q}{E_{ur}} \qquad \gamma_p = (2\epsilon_1^p - \epsilon_v^p) \approx -2\epsilon_1^p \tag{3-3}$$

with E_i being the initial secant stiffness defined by Equation 3-4, q being the deviatoric stress and superscript p denoting plastic strains.

$$E_i = \frac{2E_{50}}{2 - R_f} \tag{3-4}$$

R_f is the failure stress ratio and is equal to q_f/q_a (Figure 3-8). q_f is determined by Equation 3-5. As soon as the $q = q_f$ the criterion is satisfied and perfect plastic yielding occurs. That ratio takes values equal or smaller than unity; in PLAXIS 0.9 is considered a suitable default value. Essentially failure ratio, R_f determined the strain level at failure, i.e. by decreasing the ratio the soil fails at lower strain level.

$$q_f = (c \cot \phi - \sigma_3') \frac{2 \sin \phi}{1 - \sin \phi} \tag{3-5}$$

Parameter E_{50} is the stress dependent secant stiffness for primary loading and is given by equation:

$$E_{50} = E_{50}^{ref} \left(\frac{c \cos \phi - \sigma_3' \sin \phi}{c \cos \phi + p_{ref} \sin \phi} \right)^m \tag{3-6}$$

where E_{50}^{ref} is the reference secant modulus (see Figure 3-8) corresponding to a reference confining pressure p_{ref}. The reference pressure is usually take equal to 100kPa.

The parameter E_{ur}, in Equation 3-3, is the un-/reloading modulus and is calculated as:

$$E_{ur} = E_{ur}^{ref} \left(\frac{c \cos \phi - \sigma_3' \sin \phi}{c \cos \phi + p_{ref} \sin \phi} \right)^m \tag{3-7}$$

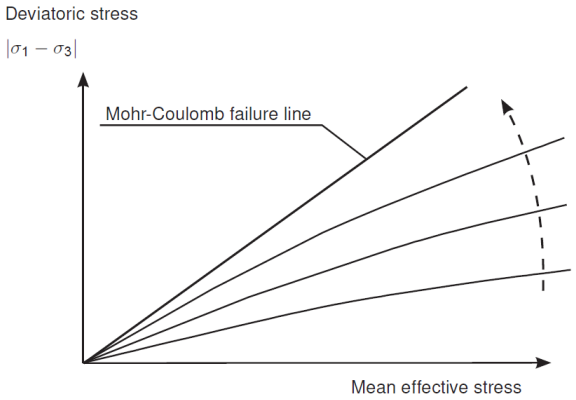

Figure 3-9: Evolution of shear hardening loci for different values of γ^p (Plaxis, 2016a)

where E_{ur}^{ref} is the inclination of the unloading-reloading path in a drained triaxial test performed at a p_{ref} confining pressure.

By setting $f_s = 0$ in Equation 3-2 it follows that:

$$\epsilon_1^p \approx \frac{1}{2}\bar{f} = \frac{1}{E_i}\frac{q}{1 - q/q_a} - \frac{q}{E_{ur}} \tag{3-8}$$

The elastic strains upon primary loading and un-/reloading are given by the equations:

$$\epsilon_1^e = \frac{q}{E_{ur}} \qquad \epsilon_2^e = \epsilon_2^e = \nu_{ur}\frac{q}{E_{ur}} \tag{3-9}$$

The total axial strain(sum of elastic and plastic components as described by Equations 3-9 and 3-8, respectively) is calculated by the equation:

$$\epsilon_1 = \epsilon_1^e + \epsilon_1^p \approx \frac{1}{E_i}\frac{q}{1 - q/q_a} \tag{3-10}$$

The evolution of the shape of shear hardening loci for increasing values of γ^p is shown in Figure 3-9.

Regarding the flow rule that controls the development of plastic volumetric strains in relationship to plastic shear strains, it is given by:

$$\dot{\epsilon}_v^p = \sin\psi_m \dot{\gamma}^p \tag{3-11}$$

where $\dot{\epsilon}_v^p$ is the rate of plastic volumetric stains and $\dot{\gamma}^p$ the rate of plastic deviatoric strains. The value of mobilized dilatancy angle, ψ_m varies according to the level of the mobilized friction angle.

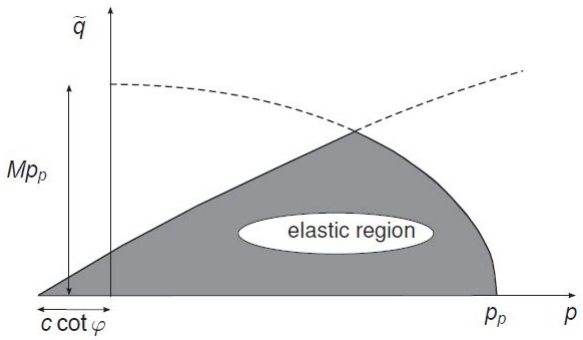

Figure 3-10: Cap and shear hardening surfaces of the HS model in $p - \tilde{q}$ space (Plaxis, 2016a)

3-2-2-2 Cap yield surface

The yield function for the cap is:

$$f^c = \frac{\tilde{q}^2}{M^2} + p'^2 - p_p^2 \tag{3-12}$$

where p_p is the pre-consolidation pressure and controls the magnitude of the yield cap, $p = (\sigma_1 + \sigma_2 + \sigma_3)/3$ and $\tilde{q}$ is a special stress measure of the deviatoric stresses calculated by Equation 3-13.

$$\tilde{q} = \sigma_1' + (\alpha - 1)\sigma_2' - \alpha\sigma_3' \qquad \text{with} \qquad \alpha = \frac{3 + \sin\phi}{3 - \sin\phi} \tag{3-13}$$

The value of parameters M is determined automatically by PLAXIS, based on K_0^{nc} and it controls the steepness of the cap, which in turn affects the orientation of the rate of plastic strains vector. The value of coefficient of earth pressure for normal consolidation is calculated by default as $K_0^{nc} = 1 - \sin\phi$ (Jaky, 1944). In case of triaxial compression ($\sigma_1' > \sigma_2' = \sigma_3'$) Equation 3-13 reduces to $\tilde{q} = \sigma_1 - \sigma_3$, while for triaxial extension ($\sigma_1' = \sigma_2' > \sigma_3'$) reduces to $\tilde{q} = \alpha(\sigma_1' - \sigma_3')$.

The hardening law that describes the evolution of the cap due to generation of plastic volumetric strains can be expressed as:

$$\epsilon_\nu^{pc} = \frac{K_s/K_c - 1}{K_s^{ref}} \left[\left(\frac{p_p + c\cot\phi}{p^{ref} + c\cot\phi} \right)^{-m} \right] \dot{p_p} \tag{3-14}$$

where K_s^{ref} is the reference bulk modulus for un-/reloading:

$$K_s^{ref} = \frac{E_{ur}^{ref}}{3(1 - 2\nu_{ur})} \tag{3-15}$$

and K_s/K_c is:

$$K_s/K_c \approx \frac{E_{ur}^{ref}}{E_{oed}^{ref}} \frac{K_0^{nc}}{(1+2K_0^{nc})(1-2\nu_{ur})} \tag{3-16}$$

Parameter E_{oed}^{ref} is the reference oedometer stiffness and determines the value of the stress-dependent oedometer modulus:

$$E_{oed} = E_{oed}^{ref} \left(\frac{c\cos\phi - \frac{\sigma_3'}{K_0^{nc}}\sin\phi}{c\cos\phi + p_{ref}\sin\phi} \right)^m \tag{3-17}$$

E_{oed}^{ref} is a tangent stiffness obtained from a ϵ_1 - σ_v' plot of an oedometer test at a reference pressure p^{ref} (Figure 3-11).

Figure 3-10 depicts the two yield surfaces of the model and the influence of parameters M and p_p on the steepness and size of the cap surface, respectively.

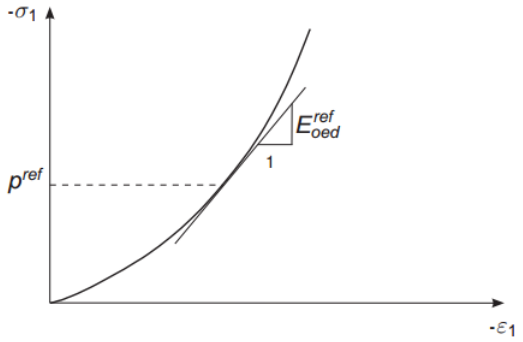

Figure 3-11: Determination of reference oedometer modulus (E_{oed}^{ref}) from an oedometer test (Plaxis, 2016a)

3-2-2-3 Initialization of the HS model

In PLAXIS the initial stresses are determined by a procedure, which is based on either the value of the Pre-Overburden Pressure (POP) or the value of the Over-Consolidation Ratio (OCR) (Figure 3-12). These parameters are defined as (Plaxis, 2016a):

$$POP = |\sigma_p' - \sigma_{yy}'^0| \qquad OCR = \frac{\sigma_p}{\sigma_{yy}'^0} \tag{3-18}$$

Then, the initial horizontal effective stresses will be:

$$\sigma_{xx}'^0 = K_0 \sigma_{yy}'^0 \tag{3-19}$$

with:

$$K_0 = \frac{K_0^{nc}(|\sigma_{yy}'^0|) - \frac{\nu_{ur}}{1-\nu_{ur}} POP}{|\sigma_{yy}'^0|} \qquad \text{or} \qquad K_0 = OCR K_0^{nc} - \frac{\nu_{ur}}{1-\nu_{ur}}(OCR - 1) \tag{3-20}$$

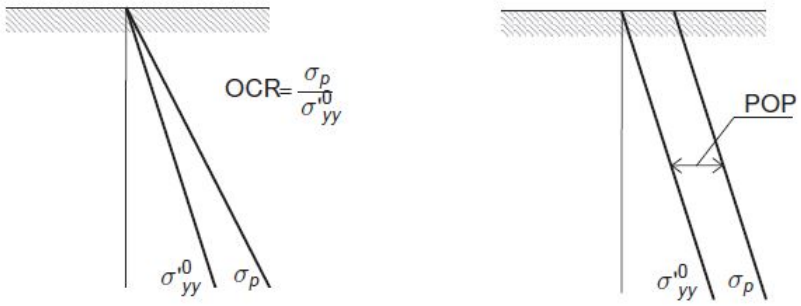

Figure 3-12: Illustration of the vertical pre-consolidation stress in relation to the in situ vertical stress. $\sigma_{yy}'^0$ is the insitu effective vertical stress and σ_p is the vertical pre-consolidation stress (Plaxis, 2016a)

3-2-2-4 HS model input parameters

The input parameters, that the HS model requires are listed in Table 3-1.

Table 3-1: Input parameters for HS model (Plaxis, 2016a)

Definition	Symbol	Unit
(Effective) friction angle	ϕ	[°]
(Effective) cohesion	c	[kPa]
Dilatancy angle	ψ	[°]
Reference secant stiffness	E_{50}^{ref}	[kPa]
Reference oedometer stiffness	E_{oed}^{ref}	[kPa]
Reference un-/reloading stiffness	E_{ur}^{ref}	[kPa]
Power of stress-level dependency of stiffness	m	[-]
Poisson's ratio in un-/reloading	ν_{ur}	[-]
Reference stress for stiffness	p^{ref}	[kPa]
K_0-value for normal consolidation	K_0^{nc} [-]	[-]
Failure stress ratio	R_f	[-]
Tensile strength	σ_t	[kPa]
Increase of cohesion per unit depth	c_{inc}	[kN/m^3]

3-2-3 Soft Soil model

The Soft Soil (SS) model is an advanced constitutive model that can simulate the behaviour of normally consolidated soft soils, such as peat and clay. The model is based on the Critical State theory and Modified Cam Clay (MCC) model (Roscoe & Burland, 1968). The great advantage of SS over HS is that the former is suitable for highly compressible soils (Plaxis, 2016a). Further advanced characteristics of the model are a stress dependent stiffness, distinction between primary loading and un-/reloading, consideration of OCR and failure accroding to Mohr-Coulomb criterion.

In order to simulate the extreme compressibility of soft soils, the model assumes that there is a logarithmic relation between changes in volumetric strain, ϵ_v, and changes in mean effective stress, p'. This logarithmic relation is formulated as:

$$\epsilon_v - \epsilon_v^0 = -\lambda^* \ln\left(\frac{p' + c\cot\phi}{p^0 + c\cot\phi}\right) \tag{3-21}$$

where λ^* is the modified compression index.

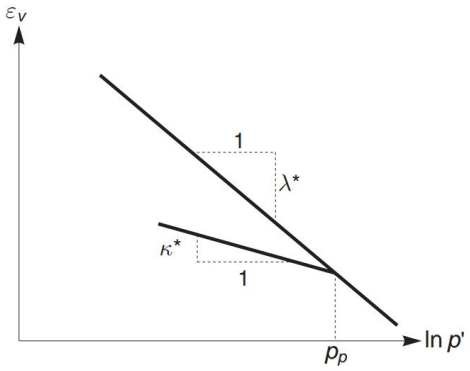

Figure 3-13: Logarithmic relation between volumetric strains (ϵ_v) and mean effective stress (p') (Plaxis, 2016a)

The plot of Equation 3-21 is a straight line as depicted in Figure 3-13. The path that is followed in isotropic un-/reloading is also depicted in the same figure. Both loading and unloading lines depend primarily on the pre-consolidation stress, p_p. The un-/reloading path is given by Equation 3-22.

$$\epsilon_v^e - \epsilon_v^{e0} = -\kappa^* \ln\left(\frac{p' + c\cot\phi}{p^0 + c\cot\phi}\right) \tag{3-22}$$

where κ^* is the modified swelling index. The superscript e denotes that soil response during unloading and reloading is elastic. The elastic behaviour is described by Hooke's law. Equation 3-23 implies that there is a linear stress dependency between the bulk modulus and the stiffness. Both the bulk modulus for un-/reloading, K_{ur} and the Young's modulus for un-/reloading, E_{ur} are determined by input parameters κ^* and ν_{ur}.

$$K_{ur} = \frac{E_{ur}}{3(1-2\nu_{ur})} = \frac{p'_{ref} + c\cot\phi}{\kappa^*} \tag{3-23}$$

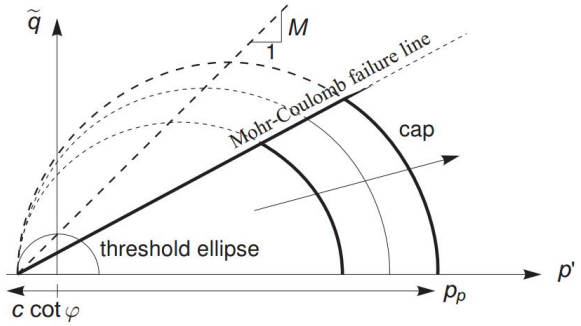

Figure 3-14: Representation of the yield surface of Soft Soil model in the p'-q plane (p') (Plaxis, 2016a)

The cap yield surface of the Soft Soil model is similar to the Modified Cam-Clay. It is formulated as:

$$f_c = \frac{q^2}{M^2} + p'(p' - p_c) \tag{3-24}$$

During loading, and when applied pressure exceeds the pre-consolidation pressure, the cap expands and plastic volumetric strains are accumulated. The hardening rule defining evolution of plastic strains is:

$$d\epsilon_v^p = (\lambda^* - \kappa^*)\frac{dp_p}{|p_p|} \tag{3-25}$$

What distinguishes Soft Soil from Modified Cam Clay is how failure is defined. In SS an additional Mohr-Coulomb yield function is introduced to describe failure. In p' - q plane is represented by a straight line (Figure 3-14) and is described by Equation 3-26.Thus, the model is not a true critical state model.

$$f_f = \frac{1}{3}(\sigma_3' - \sigma_1') + \frac{1}{2}(\sigma_3' + \sigma_1')\sin\phi' - c\cos\phi' \tag{3-26}$$

A further differentiation between SS and MCC is how parameter M is defined. It should be noted that parameter M does not control failure, as this is described by Mohr-Coulomb failure criterion, but it controls the shape and steepness of the cap and to a great extent the effective stress path during undrained loading. In MCC parameter M is determined as $M = 6\sin\phi_{cv}/3 + \sin\phi_{cv}$ (Wood, 1990). However, in the Soft Soil the parameter M is automatically calculated based on K_o^{nc} by Equation 3-27 (Brinkgreve, 1994).

$$M = 3\sqrt{\frac{(1 - K_0^{nc})^2}{(1 + 2K_0^{nc})^2} + \frac{(1 - K_0^{nc})(1 - 2\nu_{ur})(\lambda^*/\kappa^* - 1)}{(1 + 2K_0^{nc})(1 - 2\nu_{ur})\lambda^*/\kappa^* - (1 - K_0^{nc})(1 + \nu_{ur})}} \tag{3-27}$$

The input parameters of the Soft Soil model are summarized in Table 3-2.

Table 3-2: Input parameters for the SS model (Plaxis, 2016a)

Definition	Symbol	Unit
Modified compression index	λ^*	[-]
Modified swelling index	κ^*	[-]
K_0-value for normal consolidation	K_0^{nc}	[-]
Poisson's ratio in un-/reloading	ν_{ur}	[-]
K_0^{nc}-parameter	M	[-]
(Effective) friction angle	ϕ	[°]
(Effective) cohesion	c	[kPa]
Dilatancy angle	ψ	[°]

Chapter 4

Parameter determination and calibration

In this chapter, the determination and calibration of all necessary model parameters for the MC model, the SS model and the HS model is described. The parameters were initially realized by utilizing theoretical and empirical expressions and methods as described in Section 4-1. Then, having obtained a preliminary set of parameters, the laboratory tests were simulated as soil element tests with the PLAXIS SoilTest facility, as discussed in Section 4-2. Through the simulation of the laboratory tests an initial assessment of the performance of the soil models was done.

It is important to mention that (a) in the simulation stress test the dyke material and deep silty clay are modeled only with the Mohr-Coulomb model, as peat and organic clay are regarded to be the soil layers with the highest effect on the response of the system and (b) input parameters for these materials were provided, hence, the focus is on peat and organic clay. The decision to simulate with advanced soil models only the layers of peat and organic clay arise from the fact that they were the soil layers controlling the response of the system. Furthermore, these two materials, found frequently in the Netherlands, pose a challenge in modelling their behavior due to their atypical characteristics as discussed in Section 3-1.

4-1 Estimation of model input parameters

4-1-1 Strength parameters for Mohr-Coulomb model

According to the Mohr-Coulomb criterion strength is defined by parameters c' and ϕ', which are the apparent effective cohesion and friction angle, respectively. Both parameters can be determined through the representation of stresses in MIT stress plot or Cambridge stress plot. In this section the use of MIT plot will be discussed as it was the one used to analyze the triaxial tests.

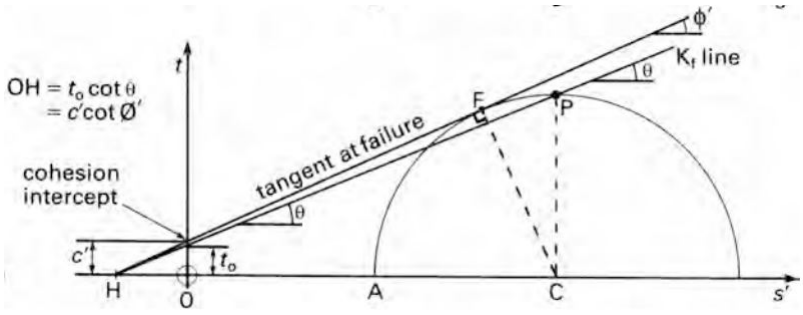

Figure 4-1: Mohr circle in s' - t plot and derivation of shear strength parameters for a CU triaxial test. K_f line indicates the equivalent failure envelope on the MIT stress plot (Head, 1986)

A depiction of a Mohr circle representing failure of a specimen in undrained triaxial compression test is shown in Figure 4-1. Parameters s' and t are defined as:

$$s' = \frac{\sigma'_1 + \sigma'_3}{2} \tag{4-1}$$

$$t = \frac{\sigma_1 - \sigma_3}{2} = \frac{\sigma'_1 + \sigma'_3}{2} \tag{4-2}$$

where σ'_1 and σ'_3 are the major and minor effective stress, respectively. The deviatoric stress t is the same for both total and effective stresses as the pore water pressure cancels out.

In Figure 4-1, lines PC and FC are radii of the circle, hence they are equal. Therefore:

$$\tan\theta = \sin\phi' \tag{4-3}$$

where θ is the angle of the K_f line (Figure 4-1. Also,

$$OH = c' \cot\phi' \tag{4-4}$$

Hence, by substituting from Equation 4-3:

$$c' = \frac{t_0 \cot\theta}{cot\phi} = \frac{t_0}{\cos\phi} \tag{4-5}$$

The elastic stiffness is described by Young's modulus . It is determined as a secant modulus at 50% stress (E_{50}) in $q - \epsilon$ plot (see Figure 3-8).

The MC strength parameters for peat were estimated with τ_{max} criterion, proposed by Khattak & Das (1985) and further developed and validated by Muraro (2018). Measured stresses are plotted in shear stress against normal stress plot. Then, a line is fitted through the points that correspond to maximum shear stress (Figure 4-2), representing the Mohr-Coulomb failure envelope. The slope of this line is equal to the frictions angle (ϕ), while the y-intercept is equal to cohesion (c). Young's modulus is determined as a secant modulus at 50% strain of the maximum shear stress.

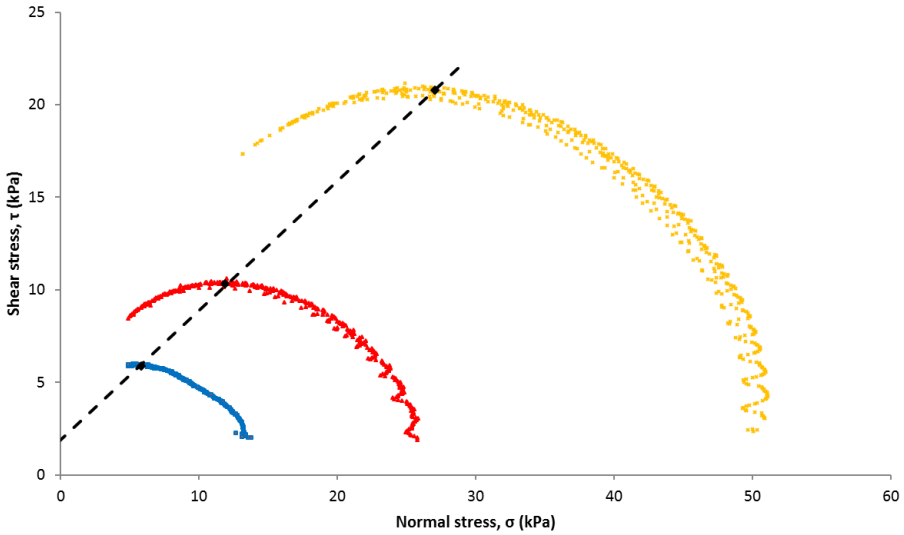

Figure 4-2: $\sigma - \tau$ plot for triaxial test B003. The dashed line indicates the MC failure envelope

4-1-2 Stiffness parameters for the Hardening Soil model

The Hardening Soil model requires in total three reference stiffness moduli. These are: the reference triaxial (secant) stiffness E_{50}^{ref}, the unload-reload triaxial (secant) stiffness E_{ur}^{ref} and finally the reference oedometric stiffness E_{oed}^{ref}. Graphic definition of reference moduli is shown in Figures 3-8 and 3-11, respectively.

For the reference oedometric stiffness E_{oed}^{ref} Plaxis manual (Plaxis, 2016a) suggests that:

$$E_{oed}^{ref} = \frac{p_{ref}}{\lambda^*} \tag{4-6}$$

where p_{ref} is the reference pressure, and λ^* is modified compression index (see Equation 4-11). Similarly, the unloading-reloading modulus relates to the modified swelling index κ^* by Equation 4-7.

$$E_{ur}^{ref} = \frac{2p_{ref}}{\kappa^*} \tag{4-7}$$

Both equations 4-6 and 4-7 apply only when parameter m is equal to 1, hence the user should pay appropriate attention when these equations are used to evaluate the moduli.

Regarding E_{50}^{ref} and E_{ur}^{ref} it is important to emphasize that they are defined for a drained triaxial test, which in engineering practise is not as common as undrained triaxial test. For an elastic material it is possible to convert an undrained modulus to the drained equivalent by Equation (Wood, 2003):

$$E' = \frac{2E_u(1-\nu')}{3} \tag{4-8}$$

However, HS moduli are elasto-plastic, therefore it is not possible to easily convert them to an equivalent drained modulus.

Another way to determine parameters E_{oed}^{ref}, E_{50}^{ref} and E_{ue}^{ref} is though the compression and the swelling indices, determined from an oedometer or isotropic compression test. In such case PLAXIS calculates automatically the moduli according to Equations:

$$C_c = \frac{2.3(1+e_0)p_{ref}}{E_{oed}^{ref}} \qquad \text{and} \qquad C_s \approx \frac{2.3(1+e_0)(1+\nu)(1-2\nu)p_{ref}}{(1-\nu)E_{ur}^{ref}K_0} \tag{4-9}$$

The value of reference secant modulus is automatically set to $E_{50}^{ref} = 1.25E_{oed}^{ref}$. Moreover, a value of $m = 1$ is automatically used by the program.

A further complication in determining input values for the HS model, is that PLAXIS performs an internal check every time an input parameter of the HS model is modified. If the combination of moduli does not satisfy the internal check that is performed, input values are rejected. Therefore a compromise between different stiffnesses should be made.

The conclusion of the above observations is that input parameters for the HS model should always be verified and calibrated by simulating laboratory tests either by finite elements or as a single element.

4-1-3 Stiffness parameters for Soft Soil model

Soil stiffness in the Soft Soil model is described by modified compression index, λ^* and modified swelling index, κ^*. The derivation of these parameters is a straight forward procedure as they are essentially the slope of normal consolidation line and unload-reload line in ϵ_v-$\ln \sigma'_p$ plot, as shown in Figure 3-13, by plotting oedometer or CRS test results.

Alternatively, they can be derived from void ratio, e versus logarithmic mean effective stress ($\ln \sigma'_v$) plot (Figure 4-3). In that case, compression index, C_c and swelling index, C_s are determined, as shown in Equation 4-10. Subsequently, parameters λ^* and κ^* can be determined by Equation 4-11.

$$C_c = \frac{\Delta e}{\Delta \log \sigma'_v} \qquad\qquad C_s = \frac{\Delta e}{\Delta \log \sigma'_v} \tag{4-10}$$

$$\lambda^* = \frac{\lambda}{1+e} = \frac{C_c}{2.3(1+e)} \qquad\qquad \kappa^* = \frac{\kappa}{1+e} \approx \frac{2C_s}{2.3(1+e)} \tag{4-11}$$

As indicated in Equation 4-11, there is not an exact relation between modified swelling index and one-dimensional compression index; that is because during unloading the ratio between horizontal and vertical stresses changes.

It is noted that for Dutch peat the typical range for ratio λ^*/κ^* is 2 to 10 (Servais, 2010).

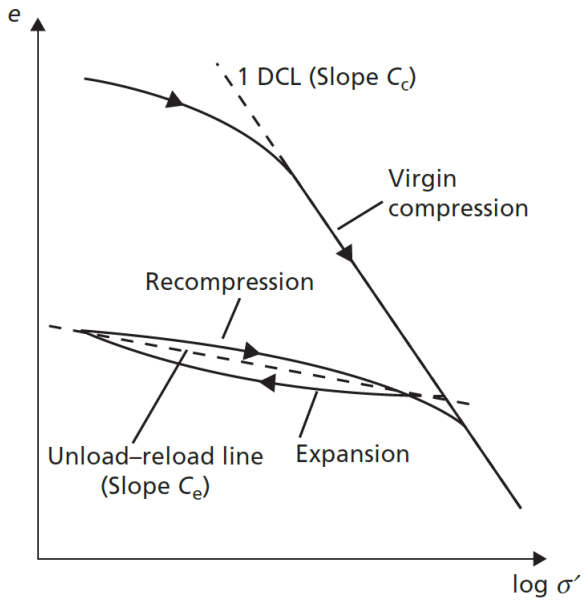

Figure 4-3: Determination of compression and swelling indices from $e - \log \sigma'$ plot (Knappett & Craig, 2012)

4-2 Evaluation of constitutive models with PLAXIS SoilTest facility

In this section the calibration of input parameters for the three soil models is presented. As discussed in previous sections input parameters should always be calibrated and evaluated before used in an actual analysis, especially for the HS model. The calibration was performed "by hand", in order to get a better feeling of model response, until the best possible fit between experimental and simulated results was achieved. First, the set up of the laboratory test simulations is described. Then, the assessment of the simulations for peat and organic clay follows. The results of the simulations of the triaxial tests were evaluated by means of $\epsilon_a - q$, $\epsilon_a - u$ and $p' - q$ (Figures 4-6, 4-7 and 4-8). The outcome of the simulation of the CRS tests is represented by a $\sigma'_v - \epsilon_a$ plot (Figure 4-12).

4-2-1 Set up of the laboratory test simulations

The laboratory tests used are two triaxial test on peat and two on the organic clay. For peat one test was on a sample retrieved from the toe while the other one was on a sample retrieved from the crest, i.e. below the body of the dyke. For the organic clay tested sample where from the slope of the dyke and crest. The calibration of parameters was conducted with consideration to the in situ stress level.

In addition, one K_0-CRS for the organic clay and 8 for peat were used. However, for illustrative purposes only selected results are presented here since the result was similar for all K_0-CRS tests.

Set up of the triaxial test

Figure 4-4 shows the set up for the simulation of the triaxial test B007 in peat. Since all tests are undrained, the test type was set to undrained conditions. The consolidation was not isotropic, hence a proper value for the ratio K_0 was selected. When an advanced constitutive models is used, a proper value of pre-consolidation stress was introduced, which is 15-18 kPa for peat and 35 kPa for organic clay. All the simulations stop at 15% axial strain.

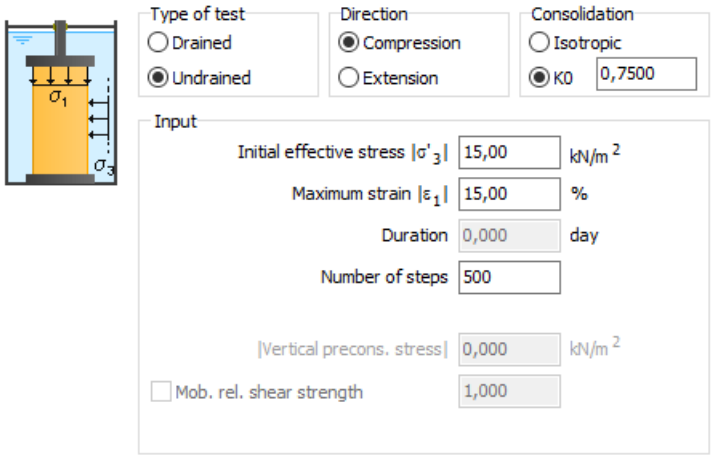

Figure 4-4: Example of input in PLAXIS SoilTest facility for the triaxial test B007 in peat

Set up of the K_0-CRS test

Figure 4-4 shows the set up for the simulation of a K_0-CRS test. As an example test B103-8 on peat is used. In total 5 stages were used in each simulation representing the different phases of the test, i.e. loading and un-/reloading. Since the considered models do not include time-dependency time is not really relevant. Moreover, similarly to triaxial test, a proper value of pre-consolidation stress was introduced when an advanced constitutive model was used.

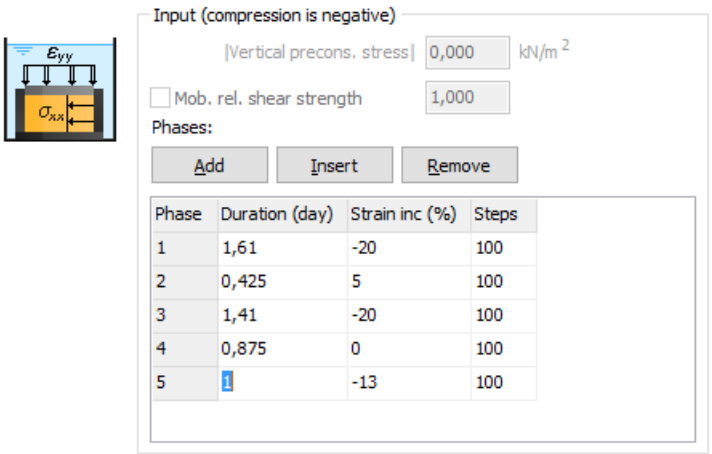

Figure 4-5: Example of input in PLAXIS SoilTest facility for the K_0-CRS test B103-8 in peat

4-2-2 Preliminary model parameters

Utilizing the relations and methodology described in Section 4-1 a preliminary set of parameters was determined. These parameters are presented in Tables 4-1 and 4-2, respectively for peat and organic clay. Values presented in these tables represent a cautious selected average of the available laboratory tests.

Table 4-1: Pre-calibration input parameters for peat. Set 1 describes peat at the toe and Set 2 describes peat located below the dyke

Model	Parameter	Unit	Set 1	Set 2
MC	Young's modulus (E)	[kPa]	900	700
	Friction angle (ϕ') [1]	[°]	33	36
	Cohesion (c') [1]	[kPa]	2	2.5
	Poisson's ratio (ν)	[-]	0.3	0.3
HS	Reference secant stiffness (E_{50}^{ref})	[kPa]	2200	3000
	Reference oedometer stiffness (E_{oed}^{ref})	[kPa]	450	450
	Reference un-/reloading stiffness (E_{ur}^{ref})	[kPa]	1500	1800
	Power of stress-level dependency of stiffness (m)	[-]	1	1
	K_0 value for normal consolidation (K_0^{nc})	[-]	0.3	0.3
	Reference pressure (p_{ref})	[kPa]	100	100
	Failure stress ratio R_f	[-]	0.9	0.9
SS	Modified compression index (λ^*)	[-]	0.25	0.22
	Modified swelling index (κ^*)	[-]	0.07	0.08
	K_0-value for normal consolidation (K_0^{nc})	[-]	0.3	0.3

[1] Common parameter for MC model, HS model and SS model

The MC stiffness was pre-determined considering the in-situ effective stresses, something that was also considered during the calibration. The preliminary HS and SS model parameters were determined from empirical correlation as presented in previous section. The advanced parameter Rf was kept equal to the default value of 0.9, as based on the literature the reported value for soils soils ranges from 0.7 to 0.95. It is worth citing the work of Surarak et al. (2012) who determined and calibrated parameters for soft and stiff Bangkok clays in the context of the HS model. Regarding peat, it is worth mentioning the work of Przystański (1994), who in the framework of Kondner's (1963) nonlinear stress-strain model, proposed empirical relationships for parameter Rf which in general yield values higher than 0.65. Similarly, for the advanced parameter m of the HS model the default value of 1 was maintained as it is a common value for soft clay soils (Janbu, 1963; Surarak et al., 2012; Plaxis, 2016a). Similar values are reported for silty clays (Stark et al., 1994). To the knowledge of the author there are no data available in the literature about parameters R_f and m for peats.

Table 4-2: Pre-calibration input parameters for organic clay

Model	Parameter	Unit	Value
MC	Young's modulus (E)	[kPa]	4000
	Friction angle (ϕ') [1]	[°]	31
	Cohesion (c') [1]	[kPa]	5.5
	Poisson's ratio (ν)	[-]	0.3
HS	Reference secant stiffness (E_{50}^{ref})	[kPa]	11000
	Reference oedometer stiffness (E_{oed}^{ref})	[kPa]	700
	Reference un-/reloading stiffness (E_{ur}^{ref})	[kPa]	30000
	Power of stress-level dependency of stiffness (m)	[-]	1
	K_0 value for normal consolidation (K_0^{nc})	[-]	0.4
	Reference pressure (p_{ref})	[kPa]	100
	Failure stress ratio R_f	[-]	0.9
SS	Modified compression index (λ^*)	[-]	0.14
	Modified swelling index (κ^*)	[-]	0.006
	K_0-value for normal consolidation (K_0^{nc})	[-]	0.4

[1] Common parameter for MC model, HS model and SS model

4-2-3 Simulation of triaxial and CRS tests on peat

In Table 4-3, the values of the input parameters of the three evaluated soil models, which gave the best fit with the laboratory data of peat, are shown.

The prediction of the models with regards to stress-strain response is shown in Figure 4-6. In general, the HS model appears to be the most capable in predicting the stress-strain behaviour of peat. Having reduced the failure stress ratio,R_f to 0.1 and 0.2 for test B007 and B003, respectively, a very good pre-failure prediction was achieved up to 10% and 4%, respectively for test B003 and B007. On the other hand, in test B007, SS predicts a reasonable response similar to the HS, however in test B003 the response is dominated by elastic strains, therefore overestimating pre-failure stiffness response. Moreover, the non-linearity is not captured well. The MC model, being a simple linear elastic - perfectly plastic model, it it not able to reproduce the non-linear response however, the initial stiffness is captured very good.

Evaluating the predicted stress paths (Figure 4-7), both the HS and the SS model give a good prediction accounting for effects such as ovesonsolidation in test B007. On the contrary, the MC model, being a linear elastic - perfectly plastic model, predicts only elastic deformation until the failure envelope is reached, hence the stress path is a straight line deviating to the right with an inclination 1:6.

The performance of the soil models in terms of excess pore pressure is shown in Figure 4-8. The SS model for both B003 and B007 triaxial tests is able to satisfactory predict the response even through initially the excess pore pressure is underestimated. Similar to the SS is also the performance of the MC model. However, since the failure envelope is reached at lower strain level, the prediction is acceptable only up to 2% strain. Predictions of both SS model and MC model are dominated by an elastic response. Regarding the performance of the HS

Table 4-3: Input parameters that provided the best fit with the laboratory data of peat. Set 1 describes peat at the toe and Set 2 describes peat located below the dyke

Model	Parameter	Unit	Set 1	Set 2
MC	Young's modulus (E)	[kPa]	1100	1100
	Friction angle (ϕ') [1]	[°]	33	36
	Cohesion (c') [1]	[kPa]	2	2
	Poisson's ratio (ν)	[-]	0.3	0.3
HS	Reference secant stiffness (E_{50}^{ref})	[kPa]	2000	1300
	Reference oedometer stiffness (E_{oed}^{ref})	[kPa]	500	420
	Reference un-/reloading stiffness (E_{ur}^{ref})	[kPa]	4000	4000
	Power of stress-level dependency of stiffness (m)	[-]	1	1
	K_0 value for normal consolidation (K_0^{nc})	[-]	0.35	0.35
	Reference pressure (p_{ref})	[kPa]	100	100
	Failure stress ratio (R_f)	[-]	0.1	0.2
SS	Modified compression index (λ^*)	[-]	0.22	0.21
	Modified swelling index (κ^*)	[-]	0.08	0.08
	K_0-value for normal consolidation (K_0^{nc})	[-]	0.4	0.4
	Poisson's ratio in un-/reloading (ν_{ur})	[-]	0.2	0.2

[1] Common parameter for MC model, HS model and SS model

model there is a distinctive difference in the response between the two tests. In the case of B003 test the excess pore pressure is underestimated, while with respect to B007 triaxial test the predictions is good.

Considering the response of models in oedometer stress conditions, i.e. in CRS tests, shown in Figure 4-12a, both advanced models (HS and SS) give a very good fit to the measured data; the slope of the virgin compression line and un-/reloading predicted by the models are close to those of the tested samples. On the other hand, MC model due to the non-stress dependent stiffness, i.e. constant stiffness, is not able to predict the response under one-dimensional compression.

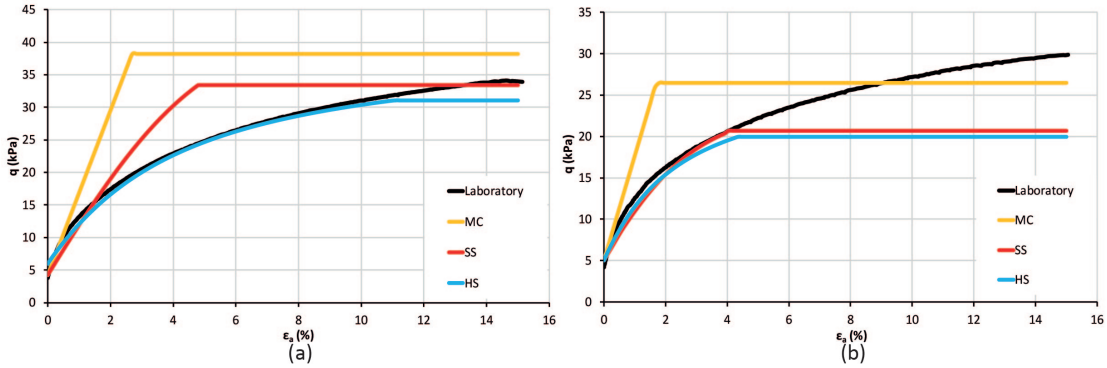

Figure 4-6: Deviatoric stress (q) versus axial strain (ϵ_a) for the triaxial tests (a) B003 and (b) B007 on peat

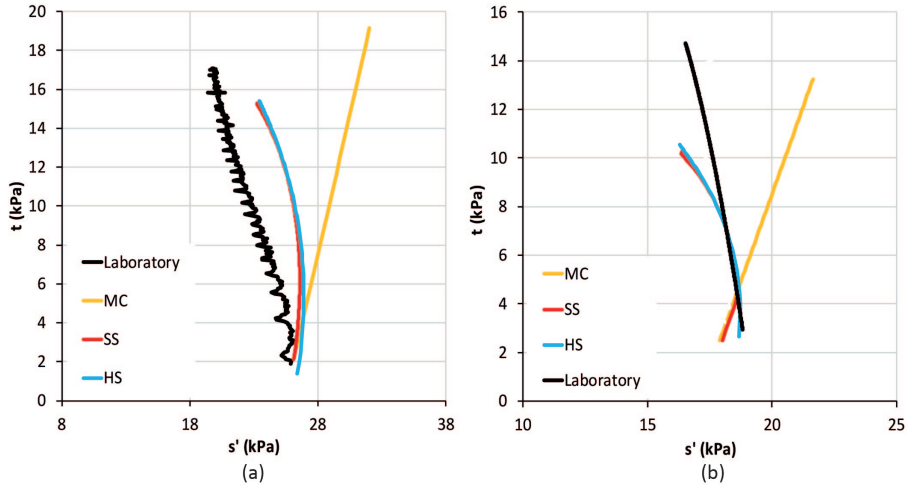

Figure 4-7: Stress path in s' -t plot for the triaxial tests (a) B003 and (b) B007 on peat

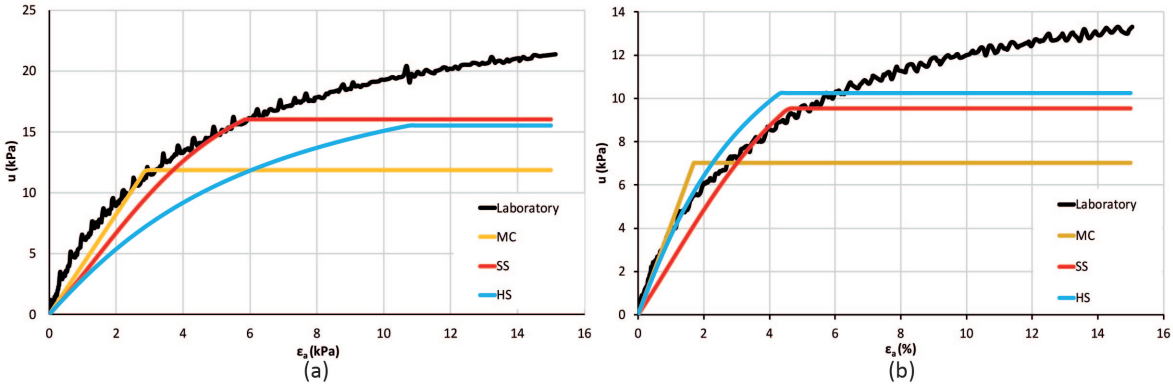

Figure 4-8: Excess pore pressure (u) versus axial strain (ϵ_a) for the triaxial tests (a) B003 and (b) B007 on peat

4-2-4 Evaluation of triaxial and CRS tests on organic clay

The values of the input parameters of the three evaluated soil models, which gave the best fit with the laboratory data, are shown in Table 4-4. In contrast to the peat, where different parameters were determined for the material located at the toe and that located at the crest of the dyke, only one set of parameters was calibrated for the whole layer of organic clay since the available laboratory suggested similar mechanical characteristics for all constitutive models.

Table 4-4: Input parameters that provided the best fit with the laboratory data of organic clay

Model	Parameter	Unit	Value
MC	Young's modulus (E)	[kPa]	4800
	Friction angle (ϕ') [1]	[°]	31
	Cohesion (c') [1]	[kPa]	4
	Poisson's ratio (ν)	[-]	0.3
HS	Reference secant stiffness (E_{50}^{ref})	[kPa]	2200
	Reference oedometer stiffness (E_{oed}^{ref})	[kPa]	900
	Reference un-/reloading stiffness (E_{ur}^{ref})	[kPa]	10000
	Power of stress-level dependency of stiffness (m)	[-]	1
	K_0 value for normal consolidation (K_0^{nc})	[-]	0.45
	Reference pressure (p_{ref})	[kPa]	100
	Failure stress ratio (R_f)	[-]	0.9
SS	Modified compression index (λ^*)	[-]	0.125
	Modified swelling index (κ^*)	[-]	0.018
	K_0-value for normal consolidation (K_0^{nc})	[-]	0.4
	Poisson's ratio in un-/reloading (ν_{ur})	[-]	0.2

[1] Common parameter for MC model, HS model and SS model

The prediction of the models with regards to stress-strain response is shown in Figure 4-9. For both tests the HS model appears to perform very good. The hardening behaviour that organic clay exhibits is captured very good, even though for the triaxial test B002, the mobilized shear strength and stiffness is initially slightly underestimated. Considering the SS model, it captures the maximum deviatoric stress satisfactory, however it mainly predicts an elastic response due to a confining pressure lower that the pre-consolidation pressure, hence the stiffness is over-predicted. Considering the MC model, it captures the value of q for the low confining pressure, but it overestimates it for higher confining pressure indicating that is not able to account for the stress dependency of the peak shear strength of the material. Moreover, the initial stiffness is predicted satisfactory.

The prediction of the constitutive models in terms of excess pore pressure is presented in Figure 4-11. The HS model seems to perform reasonably well but in general it underestimates the amount of excess pore pressure, especially for the test B002 where as the confining pressure increases the prediction is becoming less acceptable. On the other hand, the prediction of SS and MC model is dominated by linearity, therefore their response is deemed to be poor.

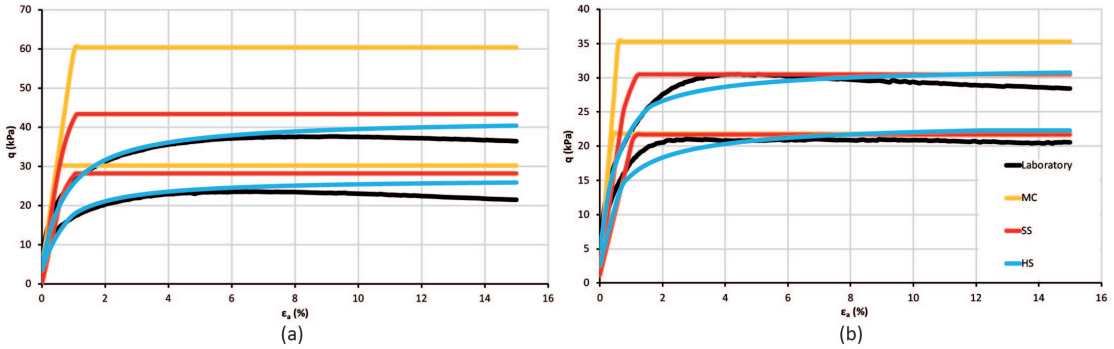

Figure 4-9: Deviatoric stress (q) versus axial strain (ϵ_a) for the triaxial tests (a) B003 and (b) B002 on organic clay

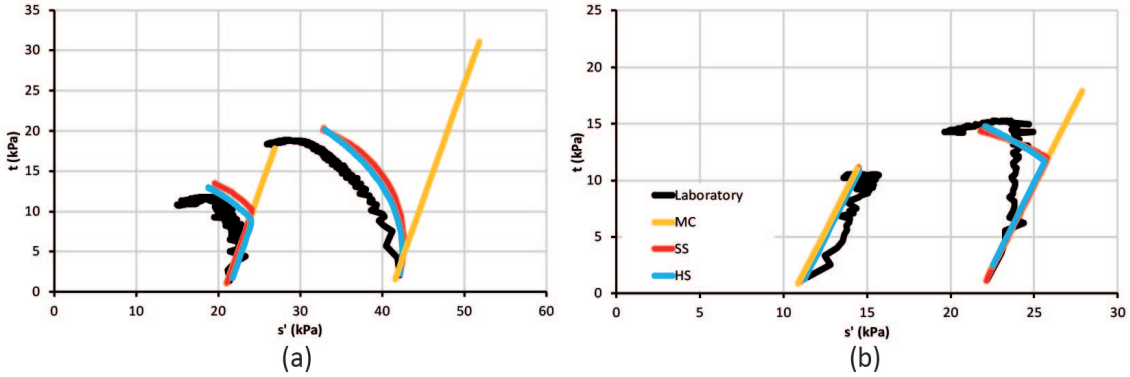

Figure 4-10: Stress path in s'-t plot for the triaxial tests (a) B003 and (b) B002 on organic clay

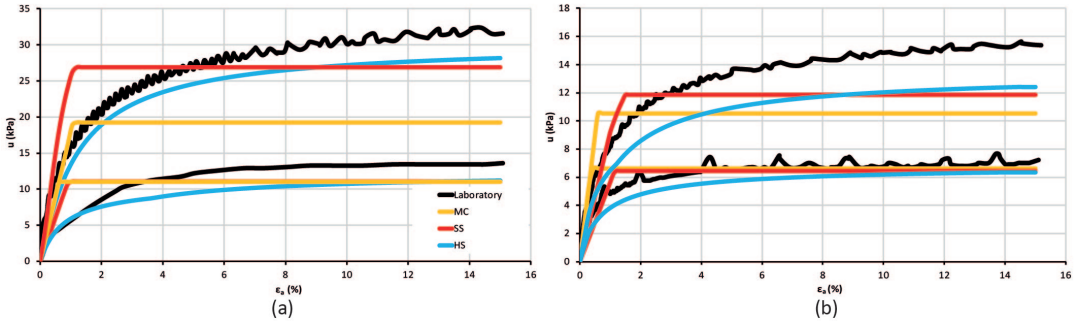

Figure 4-11: Excess pore pressure (u) versus axial strain (ϵ_a) for the triaxial tests (a) B003 and (b) B002 on organic clay

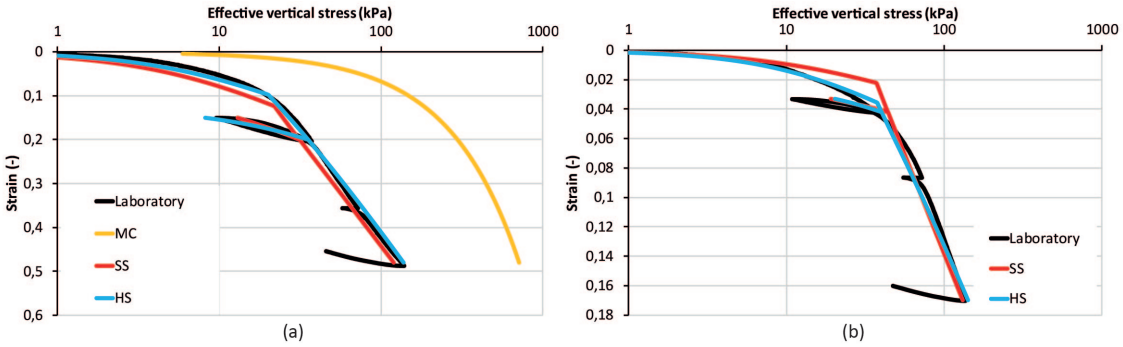

Figure 4-12: Axial strain (ϵ_a) versus effective vertical stress for K_0-CRS tests on (a) peat and (b) organic clay

The predicted stress paths shown in Figure 4-10 clearly indicate that HS and SS are equally capable in predicting a good response compared to the measured. The MC model predicts an elastic stress path that deviates to the right with an inclination 1:6.

Finally, regarding the performance of the SS and HS model in terms of one-dimensional loading, as shown in Figure 4-12b, the prediction is very close to that of the real data.

4-3 Discussion

In this chapter parameters for three constitutive models were estimated and calibrated for two different materials, i.e. peat and organic clay. Consequently, the model predictions were evaluated against measured response in terms of $q - \epsilon_a$, $t - s'$ and $u - \epsilon_a$ for triaxial tests and $\epsilon_a - \sigma'_v$ for K_0-CRS tests.

The HS model is considered to have performed the best in the simulation of both undrained compression triaxial and K_0-CRS tests for both materials especially with respect to mobilized shear strength, non-linear stiffness response and stress path. The implementation of two yield surfaces, where the shear yield surface is defined in the framework of Duncan and Chang model is clearly beneficial in describing the peat. Hence, the HS model can simulate the response in both one-dimensional loading and triaxial conditions, as well as under unloading. However, the excess pore water pressure response of peat is underestimated in the case of B003 test. For the organic clay the prediction in terms of excess pore pressure is deemed to be good for both tests. It is important to note that in order to capture the stress-strain response of peat the failure stress ratio (R_f) had to be dramatically reduced to an average value of 0.15. Than contradicts the values reported in the literature. Furthermore, by reducing parameter R_f the Mohr-Coulomb failure is reached at a lower strain level than in reality, hence the stress-strain behaviour of peat is described up to a point.

The MC model, due to the assumption of linear elasticity - perfect plasticity, is not capable to capture the typical elastoplastic response of an organic or inorganic soil. Hence, in terms of stiffness MC is reliable only for very low strain level. Similarly the prediction of excess pore pressure is pure. Furthermore, the stress path in $s' - t$ space is a straight line with a slope 1:6. Calibration of the model for the K_0-CRS tests was not possible due to its inability to capture the un-/reloading response as well as the use of a constant stress-independent stiffness.

The SS model appears to show the best performance in terms of excess pore pressure for both peat and organic clay. However, in terms of stress - strain response, the performance is good only for test B007 peat. In general, the prediction of the model is dominated by an elastic response for both materials. A likely explanation is the implementation of a single cap yield surface in contrast to the HS. Under an oedometric loading stress path the prediction is very good. Regarding the organic clay, in terms of ultimate q all models are considered to predict it adequately.

Based on the aforementioned, the HS model seems to perform better in describing the stress-strain behaviour of peat in both triaxial and oedometric conditions. Regarding excess pore pressures prediction it could be argued that the SS performs better than the HS. With regards to stress-strain response the SS is deems to reasonably well. As for the organic clay the performance of the HS model is deemed to be better than the SS and MC model with regards to all aspects.

As for the difficulty in parameter determination and calibration, even though the procedure for the MC and SS model is rather straightforward that is not the case for the HS model. That is because it required three reference stiffness in total that (a) have to be corrected for a reference stress-level, (b) triaxial secant stiffness E_{50} cannot be derived directly from undrained triaxial tests, therefore should be calibrated with simulations of the tests and (c) with regards to soft soils a compromise between triaxial and oedometer stiffnesses, i.e. E_{50} and E_{eod} should be made due to model restrictions (see Section 4-1-2).

Finally, it is important to note that limitations are imposed by the use of PLAXIS SoilTest facility and the available triaxial tests themselves. Since the simulations are done at a single element level, i.e. no finite element mesh is generated, effects that arise from the boundaries of the test, such as non-uniformities in stress, strain and excess pore pressure are not taken into account. That complicates the interpretation of the tests. Furthermore, a limitation related to the available triaxial tests in peat emerges. As discussed in Chapter 2 peat located in the polder and dyke toe is characterized by (a) an OCR equal to 3 and (b) very low effective stresses (lower than 10 kPa). Execution of laboratory tests at that low effective stress is challenging, therefore the available triaxial test for the specific peat is at a confining pressure of 15 kPa resulting in an OCR around 1.5.

Chapter 5

Modelling of the Leendert de Boerspolder stress test

5-1 Introduction

The scope of this chapter is to present the simulation of the stress test of the Leendert de Boerspolder dyke, with the use finite element program PLAXIS 2D 2016.01.

The chapter is structured in two main sections. In Section 5-2 the set up of the model is discussed. That is all the important aspects that were taken into consideration such as boundary conditions, hydraulic parameters etc. In Section 5-3 the outcome of the analysis is presented. Displacement and pore pressure results are presented and compared with the data measured from the monitoring equipment. Finally, conclusions about the soil models are drawn.

5-2 Set up of the model

5-2-1 Model geometry, boundary conditions and FE mesh

The model used in the analysis is 60 meters wide and 12 meters high (Table 5-1). The width was set to a high value to ensure that the lateral boundaries of the model will have no influence on the results. The bottom boundary of the model corresponds to the interface of the silty clay and the Pleistocenic sand that is assumed to be rigid. The simulated geometry represents the cross-section of the Central section of the dyke.

As shown in Figure 5-1, the domain is divided in four main layers; from top to bottom these are: (a) dyke material, (b) peat, (c) organic clay and (d) silty clay. An additional layer is introduced at the bottom of the dyke, denoted in yellow color in Figure 5-1, to account for a more impermeable layer that was identified (see Section 2-3-1). The assumption of that layer at that location is based on the interpretation of the recorded hydraulic response as well

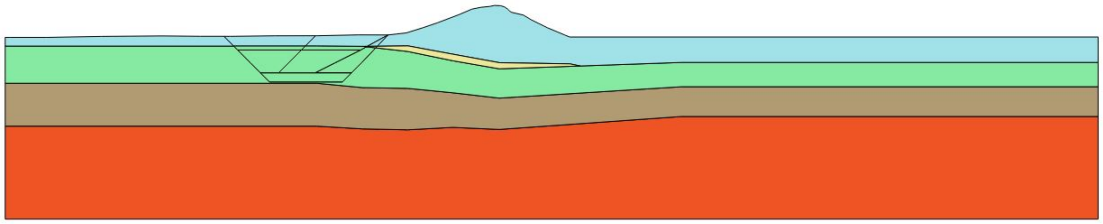

Figure 5-1: Simulated geometry in PLAXIS 2D

as the analysis of some of the CPTs. The assumption is reasonable considering the variable nature of the dyke soil, as revealed by sampling boreholes, and the consolidation process that lasted a few centuries resulting in a lower permeability at the bottom compared to the upper part of the dyke.

A very fine mesh consisting of ∼3000 15-Noded elements (Figure 5-2) was implemented aiming to minimize oscillations in predicted hydraulic head and their influence on the overall response. To achieve that, the soil clusters that correspond to the soil layers of interest were further refined, resulting in an average element size of 0.1 m^2. The appropriateness of the generated mesh was verified by performing a mesh sensitivity analysis.

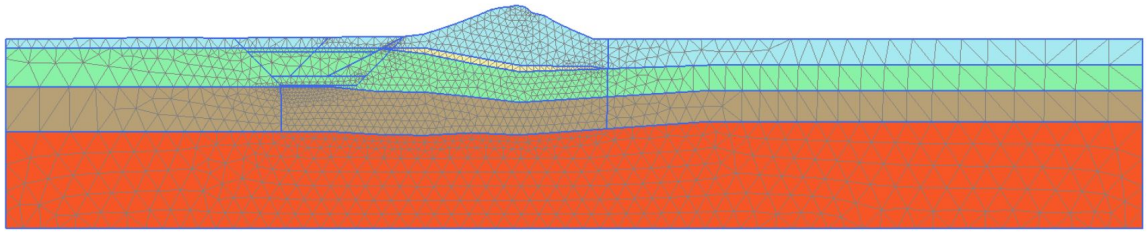

Figure 5-2: FE discretization of the model

Regarding mechanical boundary conditions, for the lower boundary of the domain full fixities were imposed, whereas the lateral boundaries were free to move in the vertical direction (horizontal fixities). No fixities were imposed on the top boundary. The lower hydraulic boundary on the model was kept closed, while the other three boundaries (top and lateral boundaries) were open, allowing free flow of water. A hydraulic boundary condition was introduced at the polder side to keep the groundwater level at -2.4 m NAP, as shown in Figure 5-3. This hydraulic boundary was deactivated after the first excavation.

Table 5-1: Dimensions of the model in PLAXIS 2D

Boundary	Value (m)
x_{min}	-15
x_{max}	45
y_{min}	-12
y_{max}	0

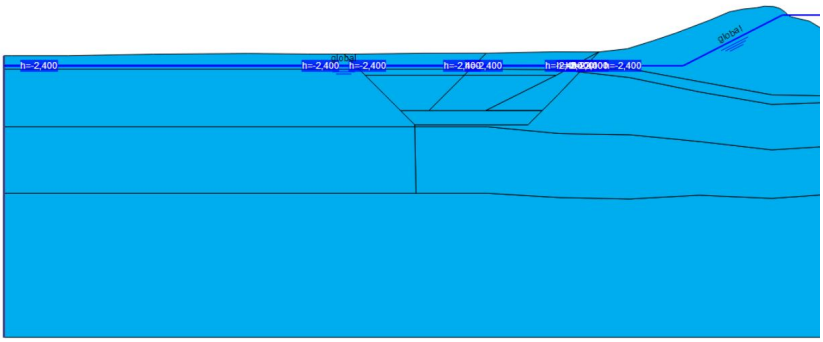

Figure 5-3: Imposed hydraulic boundary condition at the polder

5-2-2 Calculation phases

The backbone of the simulation includes 14 phases in total, each one of them representing a step of the stress test (see Chapter 2-1). In detail, these are:

1. Initial Phase
   Initial stress field is generated through the *Gravity loading* procedure. A steady state groundwater flow calculation is used to initialize the hydraulic conditions.
2. Nil-Step Phase
   This phase is essentially a plastic calculation where no additional loading is applied. It is used to restore equilibrium and solve large out-of-balance forces. Such a problem may occur if the initial stress field is generated through *K0 procedure* or *Gravity loading* predecure. For further information the reader is referred to Plaxis (2016b).
3. Phase 1: Excavation I
4. Phase 2: Consolidation
5. Phase 3: Drawdown I
6. Phase 4: Consolidation
7. Phase 5: Filling I
8. Phase 6: Consolidation
9. Phase 7 to 12
   These phases represent the second stage of the stress test. The sequence of phases is similar to Phases 1 to 6.
10. Phase 13: Excavation III

The wetting, both prior to the stress test as well as the continuous wetting during the stress test were not modeled in order to simplify the simulation. Instead, it was ensured that the dyke is fully saturated by setting properly the water retention properties of soil. The effect

of not modelling the continuous saturation is deemed to be insignificant on the results of the simulation.

The calculation type that is used for Phases 1 to 13 is the *fully coupled flow-deformation* analysis, i.e. the hydraulic and deformational calculations are executed in parallel. The choice is based on the fact that drawdown and filling impose a change in the hydraulic regime on the dyke. In this case, the response of the soil depends on a number of factors, such as soil permeability, constitutive behaviour, rate of water level lowering, imposed boundary conditions etc. As discussed by Pinyol et al. (2008), a fully coupled flow-mechanical analysis is the only way to properly consider all these aspects when a change in hydraulic regime can be dominant on the response of the system, as is the drawdown.

5-2-3 Initialization of the pre-consolidation stress

When an advanced model is used a pre-consolidation stress has to be determined. PLAXIS uses an equivalent pre-consolidation stress (p_p^{eq}) to determine the initial position of the cap, which is computed by vertical pre-consolidation stress, σ_p. The parameter σ_p is determined by the input parameters POP or OCR (see Figure 3-12 and Equation 3-18).

The equivalent pre-consolidation pressure is determined in a different way for each advanced model.

In the Hardening Soil model, p_p^{eq} is calculated as (Plaxis, 2016b):

$$p_p^{eq} = \sqrt{(p')^2 + \frac{q^2}{\alpha^2}} \tag{5-1}$$

where α is an internal model parameter (see Section 3-2-2-2) and parameters p' and q are:

$$p' = -\frac{1}{3}(1 + 2K_0^{nc})\sigma_p \qquad \text{and} \qquad q = (1 - K_0^{nc}\sigma_p) \tag{5-2}$$

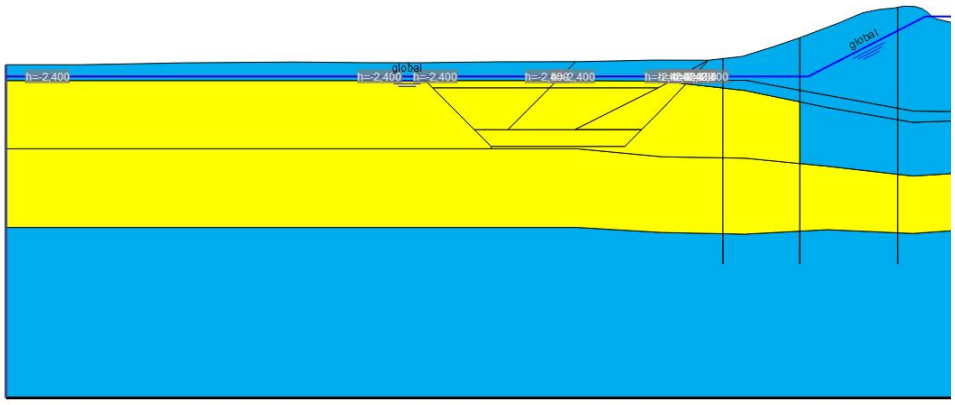

Figure 5-4: Soil clusters, where the degree of saturation is set to a value lower than unity

where K_0^{nc} is the coefficient of earth pressure for normal consolidation.

In the Soft Soil model, p_p^{eq} is calculated as:

$$p_p^{eq} = p' + \frac{q^2}{M^2(p' + c\cot\phi)} \tag{5-3}$$

where M is an internal model parameter (see Section 3-2-3) .

The ratio of p_p^{eq} and p_p determines the initial OCR in PLAXIS.

However, input parameters OCR and POP are automatically taken into account when a model is initialized with K_0 *procedure*. When a soil cluster is activated later or the initial stress field is generated through *Gravity loading*, then the stress state of that soil is assumed to be normally-consolidated. In this case, the over-consolidated stress state has to be simulated. That can be done in one of the following ways:

- apply a surface line load and remove it at the beginning of the next phase, or
- for one phase, set a saturation ratio lower than unity, or
- lower the level of the groundwater and then set it back to the proper level.

From the above methods, the second one was selected for the initialization of the preconsolidation stress although this gives an isotropic preconsolidation. For that reason, after the nil-step two extra phases were introduced. At the first phase, suction is induced at specific soil clusters, that correspond to the overconsolidated soil of the dyke toe and polder (Figure 5-4), by setting a saturation ratio lower than unity. In the phase that follows, the saturation ratio is set back to its default value, i.e. 0.99, and the groundwater regime is initialized.

5-2-4 Permeability

Permeability is one of two parameters that control the soil response in a coupled analysis. Therefore, it is important to use values that correspond to the field situation.

To derive the permeability of different soil layers, the K_0-CRS test, hydraulic head measurements during the stress test (see Section 2-3-3) and characteristic values mentioned in literature were used. Under the assumption that the ratio of horizontal to vertical permeability (k_h/k_v) is equal to unity, the possible range of permeability for soils was determined as: 10^{-5} to 10^{-8} m/s for peat, 10^{-6} to 10^{-9} m/s for dyke and 10^{-8} to 10^{-9} m/s for the organic clay. Through an iterative procedure that involved modifying the permeability of the three layers, the values presented in Table 5-2 were found to give qualitatively reasonable results for the majority of the piezometers. It is important to note that the values determined for peat from K_0-CRS tests is in the range of 1.3e-8, about one to two orders of magnitude lower than the estimated values.

Table 5-2: Determined values of permeability, k that were used in the simulations

Material	Permeability, k (m/s)
Dyke	10^{-7}
Dyke bottom [1]	10^{-8}
Peat toe	10^{-7}
Peat crest	5×10^{-8}
Organic clay	10^{-9}
Silty Clay	4.9×10^{-9}

[1] Refers to the impermeable layer at the bottom of the dyke

During consolidation the void ratio decreases resulting in a lower permeability. This change in permeability can be modelled with parameter C_k (Section 3-1-3). Using the K_0-CRS tests the change of permeability index was calculated with two different methods: (a) graphically from axial strain (ϵ_a) versus logarithm of permeability ($\log k$) plot by fitting a line through the data (Figure 5-5) and (b) using Equation 3-1. The calculated values are shown in Table 5-3. However, all values are one order of magnitude higher that these reported in the literature (e.g. den Haan et al., 2012; Hayashi et al., 2012). Hence, the calibration of parameter C_k by modeling the K_0-CRS tests with finite elements is considered necessary. In the framework of this research work all laboratory tests where simulated with PLAXIS SoilTest facility, thus it was not possible to calibrate parameter C_k. Subsequently the default value, which is 10^{15}, was used, resulting in a constant value of permeability throughout the simulation of the stress test.

Table 5-3: Determined values of permeability change index (C_k) for peat

MC	B103-8-3	B101-3-3	B101-3-6	B104-3-2	B102-5-3	B102-5-4	B105-3-2	B105-5-2	B105-5-3
Equation 3-1 Mesri & Ajlouni (2007)	1.65	2.3	2.02	1.75	2.04	1.71	1.65	1.7	1.41
Graphical determination	2.06	1.06	1.88	1.75	2.41	1.96	-	1.61	1.08

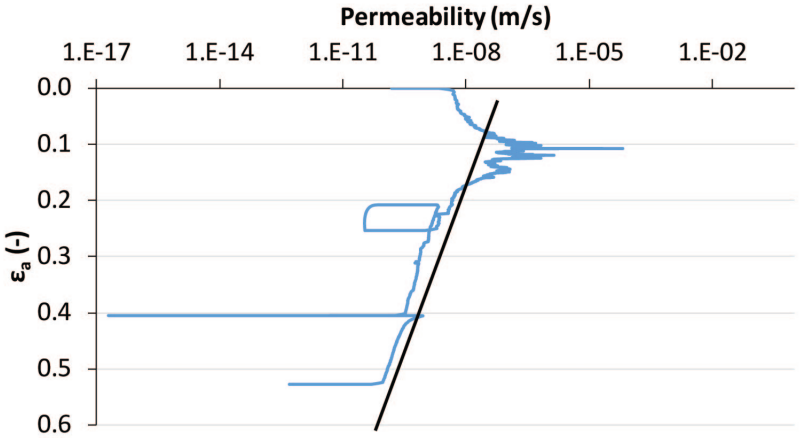

Figure 5-5: Graphical determination of permeability change index (C_k) from axial strain (ϵ_a) versus logarithm of permeability ($\log k$) plot for K_0-CRS test B105-5-2

5-2-5 Soil model input parameters

The adopted model parameters for peat and organic clay have been introduced in Chapter 4 in Tables 4-3 and 4-4, respectively. The Mohr-Coulomb parameters used for dyke and deep silty clay are shown in Table 5-4.

Table 5-4: MC input parameters for dyke and silty clay

Soil	E (kPa)	ν'	ϕ' (°)	c' (kPa)
Dyke	5600	0.3	33	5
Silty clay	5300	0.35	30	1.9

5-2-6 Combination of constitutive models

In total three finite element calculations with different combination of soil models were conducted. The combination of constitutive models is presented in Table 5-5.

Table 5-5: Combinations of constitutive models

Combination	Dyke	Peat	Org. clay	Silty clay
Combination 1 (MC)	MC	MC	MC	MC
Combination 2 (HS)	MC	HS	HS	MC
Combination 3 (SS)	MC	SS	SS	MC

5-3 Results

The purpose of this section is to present and discuss the results of the stress test simulation in PLAXIS 2D. The horizontal displacements are presented in Figures 5-6 and 5-8. The predicted hydraulic head over time for the first and second stage is depicted in Figures 5-9 and 5-10, respectively. These plots focus on the response of piezometers located in peat and organic clay as the response of the dyke was not possible to predicted satisfactory. The most probable reason for that is the high variability of the dyke.

5-3-1 Displacements

Figure 5-6 depicts the predicted response in terms horizontal displacements during excavation and drawdown steps. The depiction of these specific steps is because are the main events when horizontal strains occurred. All models overpredict the amount of horizontal displacements with MC being the closest to measured response and HS being the most conservative overestimating displacements by a factor of 2 to 3.

More precisely, the prediction of HS is the "softest" compared to the MC and SS calculations, even though it appeared to be the most capable soil model in describing the behaviour of both soils at an element level (see Section 4-2). The interpretation of displacement measurements suggests that the use of a second yield surface in the HS model, i.e. shear hardening yield surface, is activated prematurely leading to stiffness degradation and therefore predicting unrealistic high horizontal displacements for the organic clay. That is also supported by the projection of plastic points during the second drawdown, shown in Figure 5-7. In the HS calculation the dominant plastic points are hardening points while in MC and SS failure points dominate, i.e. the failure envelope is activated. Therefore, it appears that a deviatoric mechanism is not that relevant for the organic clay. With regards to peat results suggest that a higher secant stiffness is be necessary. That would be justifiable due ot the tensioning of the fibers. It is reminded that in order to use higher secant stiffness, E_{50} would be necessary to also increase the oedometric stiffness, E_{oed} due to the limitations that the HS imposes regarding the difference between the different stiffnesses, resulting in a compromise of the behaviour in oedometric conditions.

On the other hand, the fact that the SS model uses only a cap yield surface leads to a "stiffer" prediction. Furthermore, it is surprising the fact that MC prediction is quantitatively the best compared to the HS and SS calculations. However, qualitatively cannot account for the displacements and it measured by the inclinometers.

A further implication is the kinematic compatibility between the layers of peat and organic clay. That is that due to the different stress-strain response of peat and organic clay, where

the ultimate shear strength of peat cannot be mobilized because it is attained at such a high strain level that the organic clay has already reached failure. Therefore, the necessary strain level to induce failure in the peat is not reached. So, the overall displacement and the mechanism of the interface is ruled by the organic clay.

Motivated by the results of these three calculations a fourth analysis was conducted where the peat and the organic clay are modelled with the HS model and the SS model, respectively. The outcome of this analysis in terms of displacements during the second stage is shown in Figure 5-8. The projected results of this calculation are denoted as HS-SS and are compared to SS and HS calculations. It can be seen that in terms of lateral displacements the response of the organic clay is stiffer resulting in an overall better result. That is also supported by the projection of plastic points (Figure 5-7d).

With regards to the vertical displacements it is noted that are dramatically underestimated by about 4 to 5 times compared to the measured displacements. Therefore, it is believed that the overestimation of the lateral displacements is compensated by the vertical displacements response. A plot of the predicted and measured vertical displacements was not possible due to scale issues.

Finally, it is important to highlight the fact that the constitutive models considered in this research assume an isotropic soil. However, all soils and especially peats as discussed in Section 3-1, are anisotropic. it has been outlined that ignoring the anisotropy leads to underestimation of the vertical displacements and overestimation of horizontal displacements. It is worth citing the work of Karstunen et al. (2005) and Yildiz et al. (2009) who studied the influence that anisotropy has in displacements for two different embankments pointing out the importance of it.

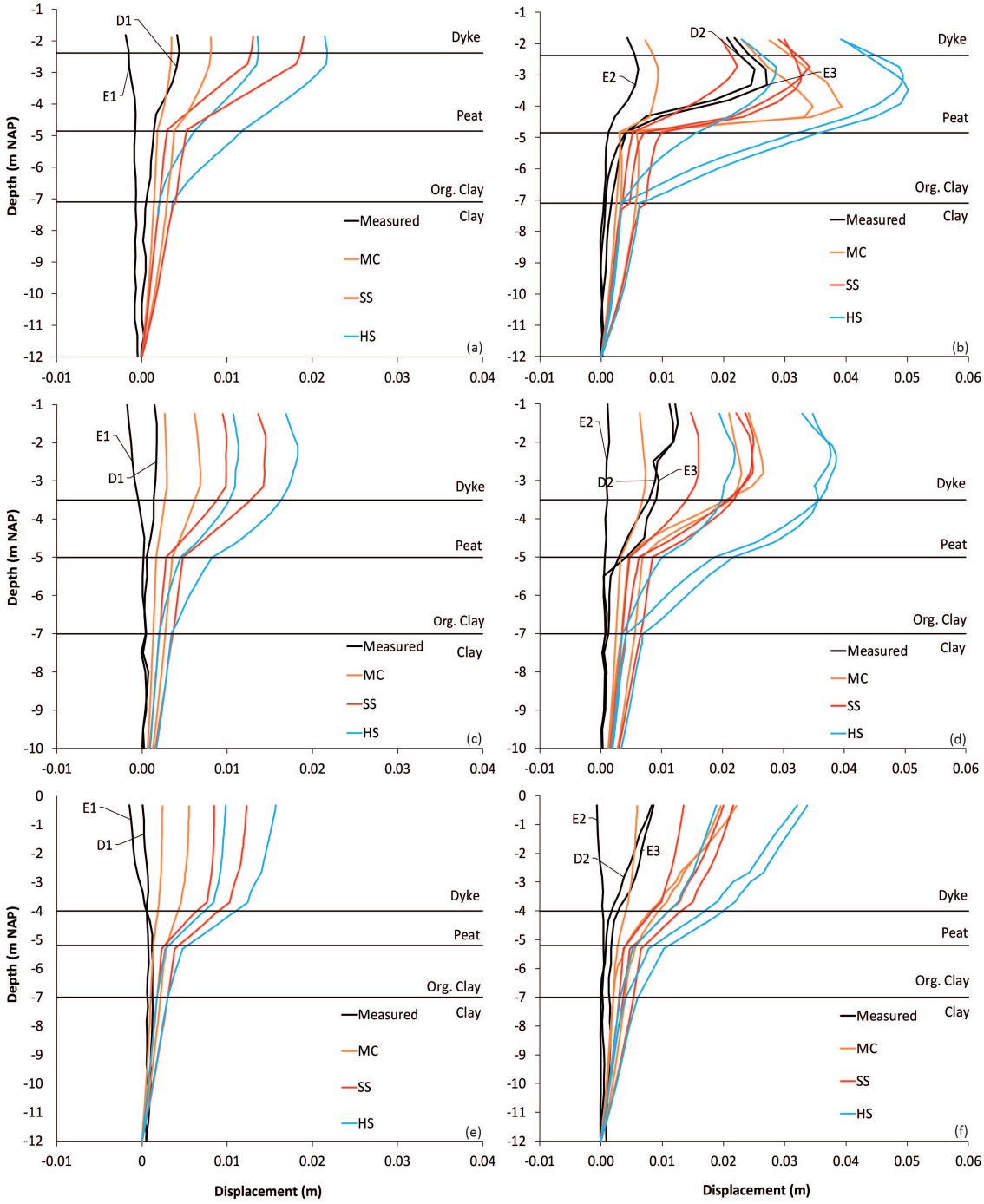

Figure 5-6: Comparison of measured to predicted horizontal displacements for model combinations MC, SS and HS for inclinometers (a,b) StC, (c,d) SmC and (e,f) ScC during excavation (E) and drawdown (D) steps. The location of the sensors in shown in Figure 2-4. Left column (a,c,e) correspond to the 1^{st} stage whereas the right column (b,d,f) corresponds to the 2^{nd} stage

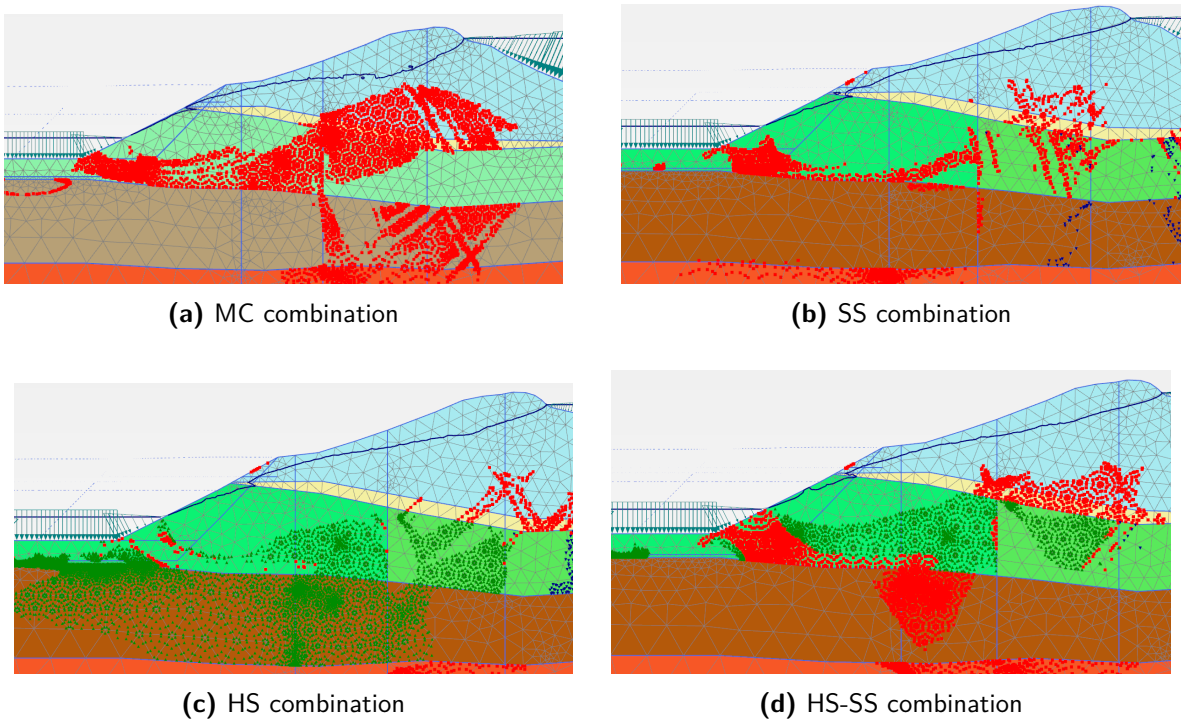

(a) MC combination

(b) SS combination

(c) HS combination

(d) HS-SS combination

Figure 5-7: Plastic points (failure points, hardening points and cap points) for four model combinations

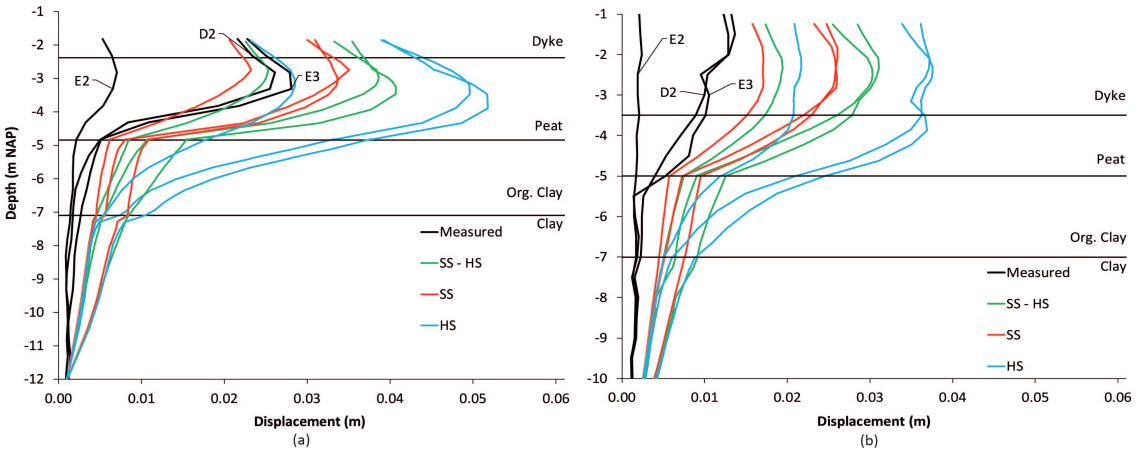

Figure 5-8: Comparison of measured to predicted horizontal displacements for model combinations HS-SS, SS and HS for inclinometers (a) StC and (b) SmC at excavation (E) and drawdown (D) steps during the 2^{nd} stage

5-3-2 Hydraulic head

This sections focuses on the hydraulic head results for the four calculations conducted with different constitutive model combinations as presented in Table 5-5 and discussed in the previous section. Figure 5-9 shows the predicted hydraulic head response for piezometers located in peat and organic clay during the first stage. i.e. first excavation, drawdown and filling, while Figure 5-10 shows the response during the second stage of the stress test.

Regarding the SS and the HS calculations, both perform similarly during the first phase. However, the HS performs overall "softer" than the SS model. This is for example observable after the excavations where the HS predicts a higher drop compared to other models, as well as during the second stage of the stress test.

Interesting is the fact that MC model seems to perform quantitatively better than the advanced models, especially at the toe of the dyke. A likely interpretation is that the subsoil is in an overconsolidated state, hence initially the elastic strains are relevant. But, when relevant plastic strains start to accumulate changing the deformational behavior of the soil, while the load remains below the failure load, the performance of the MC constitutive model becomes poor. Hence, during the second stage stage of the stress test it found that in general the opposite trend of what was measured by the sensors is predicted. Therefore, the performance of the model is poor.

This observation also suggests that it is possible the OCR to have been slightly underestimated. As a consequence, when the advanced models were used, plastic strains are generated prematurely.

It is noted that qualitatively the best results were achieved when the SS model was used for organic clay and the HS model for peat for similar reasons as explained in the previous section.

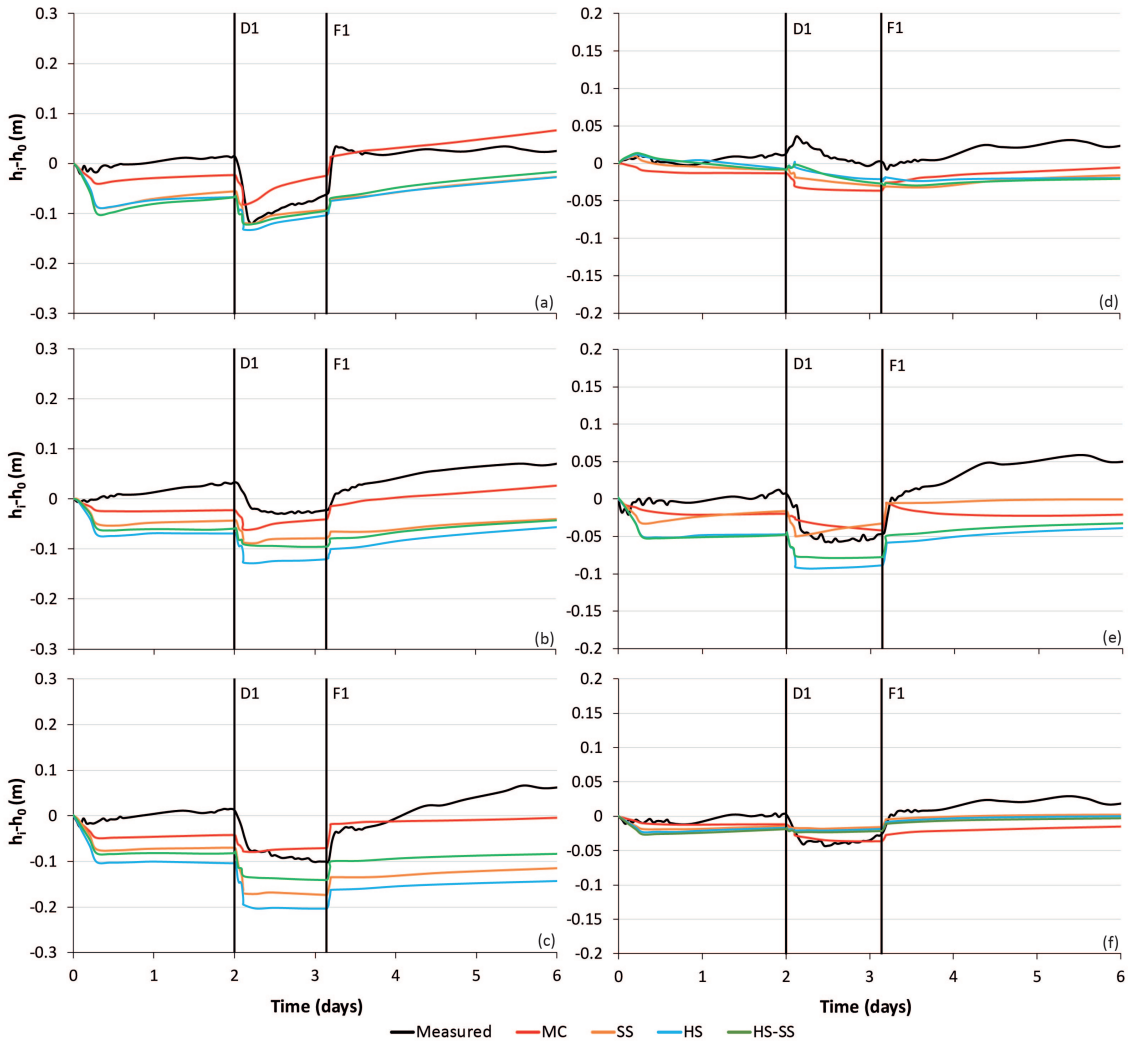

Figure 5-9: Comparison of measured hydraulic head to predicted hydraulic head with MC, SS HS and HS-SS model combinations for piezometers (a) PtC1, (b) PtC2, (c) PtC3, (d) PmC5, (e) PcC7 and (f) PwC8 during the 1^{st} stage of the stress test. The location of the sensors in shown in Figure 2-4. Black lines indicate different steps of the stress test, i.e. drawdown (D) and filling (F). Time origin is the 1^{st} excavation. y-axis is offset to 0

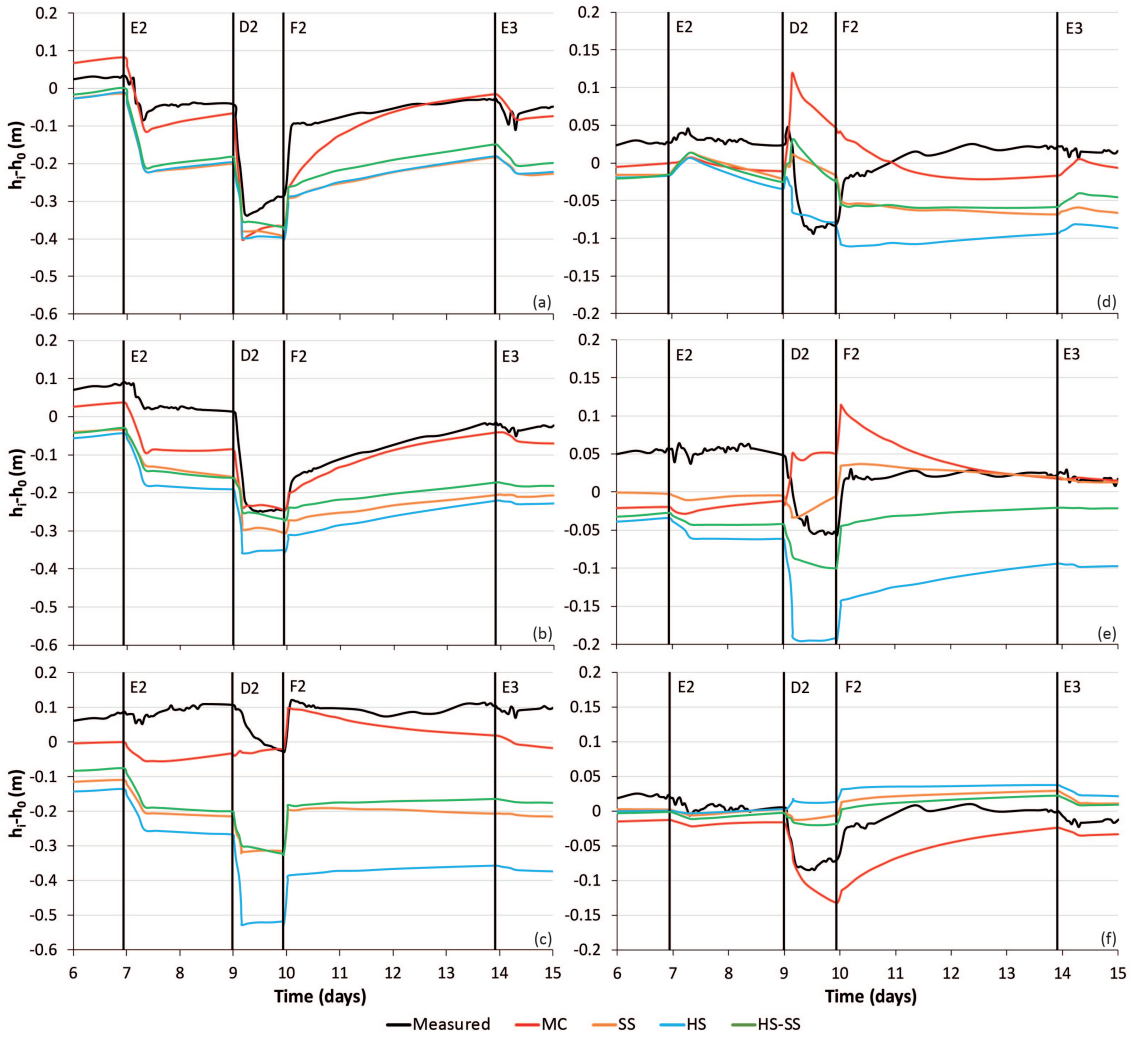

Figure 5-10: Comparison of measured hydraulic head to predicted hydraulic head with MC, SS HS and HS-SS model combinations for piezometers (a) PtC1, (b) PtC2, (c) PtC3, (d) PmC5, (e) PcC7 and (f) PwC8 during the 2^{nd} stage of the stress test. The location of the sensors in shown in Figure 2-4. Black lines indicate different steps of the stress test, i.e. excavation (E), drawdown (D) and filling (F). Time origin is the 1^{st} excavation. y-axis is offset to 0

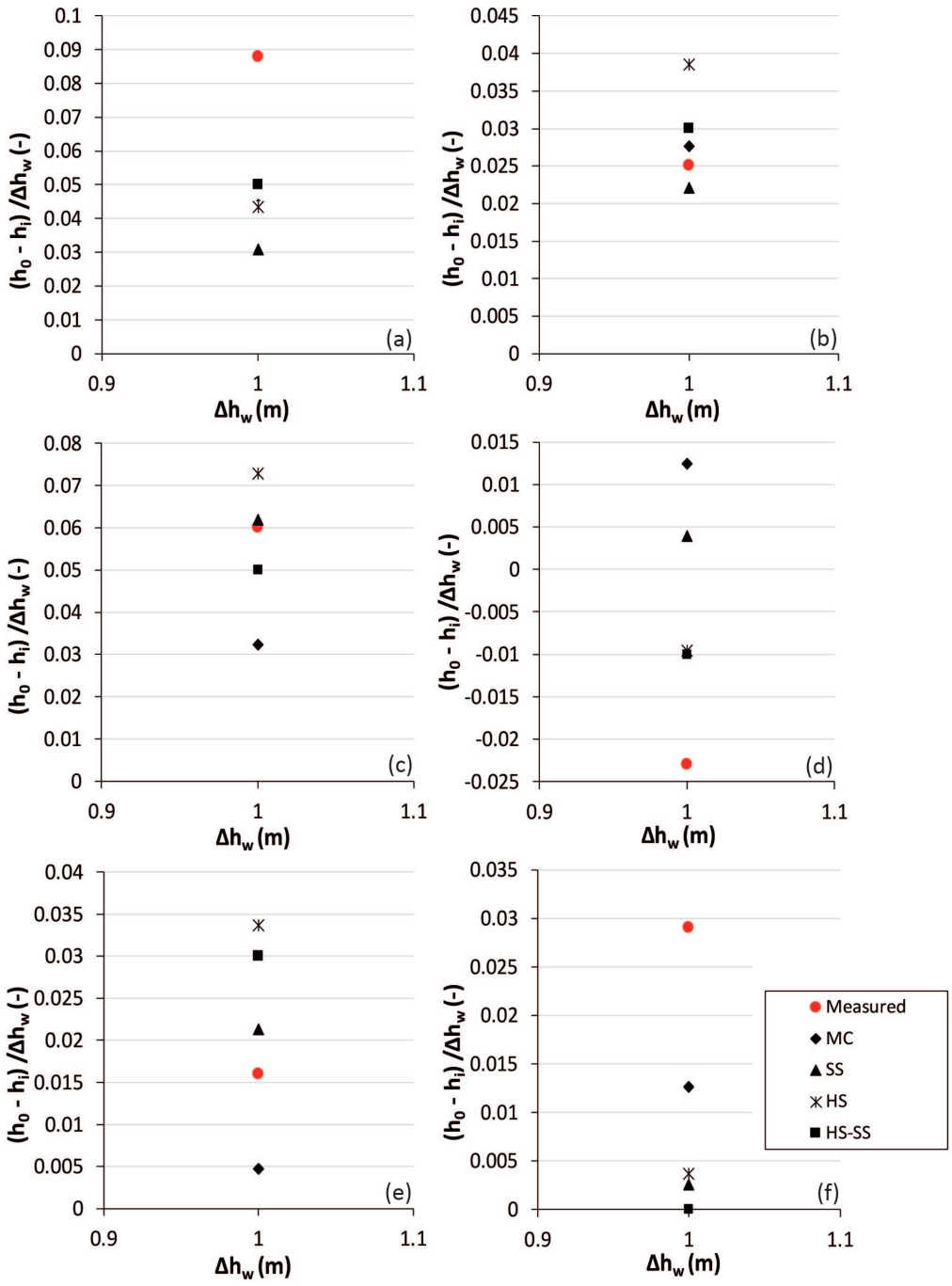

Figure 5-11: Observed and computed normalized change in groundwater head versus change of water level in the trench (Δh_w) during the first drawdown for piezometers (a) PtC1, (b) PtC2, (c) PtC3, (d) PmC5, (e) PcC7 and (f) PwC8. The location of the sensors in shown in Figure 2-4

Figure 5-11 illustrates the change in hydraulic head during the first drawdown between different calculation schemes and the measured. It is clear that the change is influenced by the calculation model. Generally speaking, a clear conclusion can not be drown as the the performance is inconsistent between the sensors. However, it is worth mentioning that the

advanced models in general predict a more realistic response.

Finally, it is important to mention that there are some considerable limitations that hinder a better prediction of the hydraulic head response. First of all, under Biot's consolidation theory (Biot, 1941) water contained in the pores is assumed to be incompressible. Under this assumption in general higher pore excess pore pressures are predicted. Secondly, there is some uncertainties regarding the exact location of the piezometers; a small change in the coordinates could yield a different response. Finally, considering that there is a direct coupling between displacements and pore water pressures, the use of isotropic soil models affects the outcome of the analysis as discussed in the previous section.

5-4 Discussion

In this chapter the Leendert de Boerspolder stress test was numerically simulated in a fully-coupled calculation in PLAXIS 2D. The aim was to evaluate the soil models in the context of the stress test. Therefore, the displacement and pore water pressure predictions were compared to the measured.

It was found that the HS model, even though performed the best in the simulation of the laboratory tests, in the context of the stress test its performance if too "soft" with regards to lateral displacements. With regards to the organic clay, results suggest that the reason for that could be the premature activation of the deviatoric yield surface resulting in stiffness degradation and therefore excessive lateral displacements. For peat it is believed that this attributed to the implemented secant stiffness; a higher stiffness seems to justifiable due to the tensioning of the fibers under a deviatoric loading.

The MC model was found to perform quantitatively reasonably well especially during the first stage of the stress test. That is due to the overconsolidated state of the soil. When plastic strains become relevant changing the deformational behavior of the soil, while the stresses remain below the failure load, the performance of the MC quantitatively is getting worse. Hence, the performance of the model is poor. It should be mentioned that the performance of the MC in terms of displacements during the first stage suggests that the OCR of the organic clay and peat was probably underestimated.

The aforementioned constitutive models represent the two extremes. The performance of the SS lies between these two. With regards to that it is noted that the best results were obtained by combining the SS model for the organic clay and the HS model for peat. However, it can be argued that the improvement does not justify the extra work that is needed in determining parameters for the HS model.

Finally, it is argued that the differences between the observed response and the results obtained by FE analysis are explained by complexities not considered in this work such as: (a) anisotropy, (b) 3d effects and (c) the behavior of the interfaces.

Chapter 6

Conclusions and recommendations

6-1 Concluding remarks

In this study the capabilities of three constitutive models, i.e. Mohr-Coulomb, Hardening Soil and Soft Soil were examined in terms of reproducing the coupled hydro-mechanical responses of peat and organic clay in comparison with data measured on site during the Leendert de Boerspolder stress test. The soil models evaluation was done in two steps: (a) simulation of the laboratory tests as single soil element tests and (b) evaluation of the soil models by conducting a fully coupled simulation of the Leendert de Boerspolder stress test. The conclusions of this work with reference to the questions presented in Section 1-2 are presented below.

Which one of the considered constitutive models can simulate better the behaviour of peat and organic clay in triaxial and oedometric laboratory testing?

The constitutive models were evaluated in oedometric and triaxial stress paths through the simulation of the laboratory tests as single element tests with the SoilTest facility in PLAXIS. From a calibration point of view, the Hardening Soil model performed the best for both CRS and triaxial tests resulting in a very good fit to experimental data. For the case of peat in order to achieve that, the failure stress ratio R_f had to be reduced to an average value of 0.15, in contrast to what is mentioned in the literature.

The Soft Soil model performed good in the simulation of the CRS tests for both materials. In the simulation of the undrained triaxial tests, for what concerns the peat, the performance of the model was found to be too stiff in terms of stress-strain response. Regarding the organic clay the mechanical behavior is sufficiently described by the model. It is noted that for both materials in order to achieve good performance with regards to the stress path the K_0^{nc} value had to be increased.

Finally, the performance of the Mohr-Coulomb model is deemed to be poor due to the fact that it is a simple linear elastic perfectly plastic model. Hence, the mechanical behavior of peats and organic clays is not described sufficiently.

How do these soil models perform in the simulation of a real dyke with complex hydraulic and stress conditions as is case of the Leendert de Boerspolder dyke

Undertaking the analysis of a complex geotechnical problem, as the stress test of the Leendert de Boerspolder, the best qualitative results in terms of displacements and pore pressure response were obtained by combining the SS model for the organic clay and the HS model for peat.

Overall, the Hardening Soil seems to perform too "soft" even though the fit to laboratory data was very good. It is believed that with regards to the organic clay the reason for that is the premature activation of the shear yield surface resulting in stiffness degradation and excessive displacements. Hence, the model seems to describe poorly the behavior of organic clays. For the peat it is believed that a higher secant stiffness is necessary in order to describe properly its behaviour due to the extra strength and stiffness that fibers provide under tensioning. However, due to the HS model constraints related to input stiffnesses that is not possible, unless the oedometric stiffness is compromised.

The Mohr-Coulomb model quantitatively performed reasonably well with regards to both displacements and pore water pressure. But to evaluate a constitutive model it is of primary importance to also judge the qualitative response. Considering that the MC model performed good only up to the point. When relevant plastic strains started to accumulate changing the deformational response, while the stresses remained below the overall failure load, the performance of the model is poor. That can be seen in the pore water pressure results after the second excavation but also the displacements.

Finally, it is important to note that the discrepancies between the observed displacements and the results obtained by FE analysis are partially affected by complexities which are not considered in this research work, such as (a) the anisotropy, (b) 3d effects and (c) the local behaviour of the interface between the peat and the organic clay.

Which soil model is currently recommended for the simulation of these soils?

Having assessed the models in standard laboratory stress paths and in a complex geotechnical problem, i.e. the Leendert de Boerspolder stress test, the following comments can be made about the considered models.

- The Soft Soil model appears to overall preform better than the Mohr-Coulomb and the Hardening Soil in terms of pore water pressure and displacements in the complex stress path and hydraulic regime of the considered test case. Furthermore, the derivation and calibration of parameters is a straightforward, relatively simple procedure. Therefore, at this stage it is recommended for use for both considered soils.
- With reference to the peat, the Hardening Soil model should be used with caution and when the deviatoric yield mechanism is regarded to be the dominant type of deformation for the considered engineering problem. In that case, the calibration should be done focusing on triaxial tests, therefore compromising the oedometric stiffness. Moreover, the use of a high secant stiffness should be used, even if it appears to be unrealistic for a soft soil. That might be justified by the tensioning of the fibers under deviatoric loading

resulting in a high stiffness. Moreover, the failure ratio R_f should be carefully evaluated during calibration as in the case of peat a reduction may be necessary. Regarding the organic clay the use of the HS model shall be avoided as the results of the simulations suggest that the deviatoric yield mechanism is not relevant for that soil.

- The Mohr-Coulomb model, because of the assumption of linear elasticity - perfect plasticity can serve only as a rough approximation.

6-2 Recommendations for further research

Based on the conclusions of this thesis and the limitations discussed in section 1-4, in order to have a more complete picture, the following suggestions for further research arise.

- In Chapter 3-1 the highly anisotropic nature of peat was highlighted. Furthermore, in literature the importance of considering soil anisotropy for capturing the lateral displacements is emphasized (e.g. Karstunen et al., 2005). Therefore, the simulation of peat and organic clay with an anisotropic constitutive model is considered to be important, as it is likely to provide a better prediction of the pre-failure response.
- The stress test should be simulated with a three-dimensional model. That is important because the overestimation of the displacements is partly attributed to the absence of constraining effects of the "shoulders" which in reality are present in a three-dimensional problem providing additional constraint.
- The focus of this research was the pre-failure behaviour; the study of the failure of the dyke would be necessary for a complete evaluation of the soil models and the stress test. This is suggested to be investigated in a 3D model as the failure of the dyke was observed to be three-dimensional.
- The role of interfaces between the different layers should be carefully evaluated especially regarding the interface between peat and organic clay, where the kinematic compatibility may play an important role in governing the overall behaviour of the system.

References

ASTM D5715-00. (2006). Standard test method for estimating the degree of humification of peat and other organic soils (visual/manual method).

Beckwith, C. W., Baird, A. J., & Heathwaite, A. L. (2003). Anisotropy and depth-related heterogeneity of hydraulic conductivity in a bog peat. I: laboratory measurements. *Hydrological processes*, *17*(1), 89–101.

Biot, M. A. (1941). General theory of three-dimensional consolidation. *Journal of applied physics*, *12*(2), 155–164.

Brinkgreve, R. B. J. (1994). *Geomaterial models and numerical analysis of softening* (PhD Thesis). Delft University of Technology, Delft, the Netherlands.

Brinkgreve, R. B. J. (2005). Selection of soil models and parameters for geotechnical engineering application. In *Soil constitutive models: Evaluation, selection, and calibration* (pp. 69–98). ASCE, Austin, Texas, USA.

Cola, S., & Cortellazzo, G. (2005). The shear strength behavior of two peaty soils. *Geotechnical and Geological Engineering*, *23*(6), 679–695.

de Jong, A. (2007). *Modelling peat dike stability: back analysis of direct simple shear test results* (MSc Thesis). Delft University of Technology, Delft, the Netherlands.

den Haan, E., & Feddema, A. (2012). Deformation and strength of embankments on soft Dutch soil. *Proceedings of the ICE - Geotechnical Engineering*, *166*(3), 239 – 252.

den Haan, E., & Kruse, G. (2007). Characterisation and engineering properties of dutch peats. *Characterisation and Engineering Properties of Natural Soils*, *3*, 2101–2133.

den Haan, E., Kruse, G., Koelewijn, A., & Zwanenburg, C. (2012). Failure of a trial embankment on peat in Booneschans, the Netherlands. *Géotechnique*, *62*(6), 479–490.

Dhowian, A. W., & Edil, T. B. (1980). Consolidation behavior of peats. *Geotechnical Testing Journal*, *3*(3), 105–114.

Duncan, J. M., & Chang, C. Y. (1970). Nonlinear analysis of stress and strain in soils. *Journal of the Soil Mechanics and Foundation Division*, *96*(5), 1629–1653.

Edil, T. B., & Wang, X. (2000). Shear strength and K_0 of peats and organic soils. In *Geotechnics of high water content materials.* ASTM International.

Farrell, E. R. (2012). Organics/peat soils. In *ICE Manual of Geotechnical Engineering: Volume 1* (pp. 463–479). Thomas Telford Ltd.

Gras, J. P., Sivasithamparam, N., Karstunen, M., & Dijkstra, J. (2017). Permissible range of model parameters for natural fine-grained materials. *Acta Geotechnica*, 1–12.

Grimstad, G., Degago, S. A., Nordal, S., & Karstunen, M. (2010). Modeling creep and rate effects in structured anisotropic soft clays. *Acta Geotechnica*, *5*(1), 69–81.

Hayashi, H., Yamazoe, N., Mitachi, T., Tanaka, H., & Nishimoto, S. (2012). Coefficient of earth pressure at rest for normally and overconsolidated peat ground in Hokkaido area. *Soils and Foundations*, *52*(2), 299–311.

Hayward, P., & Clymo, R. (1982). Profiles of water content and pore size in sphagnum and peat, and their relation to peat bog ecology. *Proceedings of the Royal Society of London B: Biological Sciences*, *215*(1200), 299–325.

Head, K. (1986). *Manual of soil laboratory testing, volume 3: Effective stress tests.* Pentech Press, London.

Hendry, M. T. (2012). *The geomechanical behaviour of peat foundations below rail-track structures* (PhD Thesis). University of Saskatchewan, Saskatchewan, Canada.

Hendry, M. T., Barbour, S. L., & Martin, C. D. (2014). Evaluating the effect of fiber reinforcement on the anisotropic undrained stiffness and strength of peat. *Journal of Geotechnical and Geoenvironmental Engineering*, *140*(9), 04014054.

Hendry, M. T., Sharma, J. S., Martin, C. D., & Barbour, S. L. (2012). Effect of fibre content and structure on anisotropic elastic stiffness and shear strength of peat. *Canadian Geotechnical Journal*, *49*(4), 403–415.

Hobbs, N. B. (1986). Mire morphology and the properties and behaviour of some British and foreign peats. *Quarterly Journal of Engineering Geology and Hydrogeology*, *19*(1), 7–80.

Jaky, J. (1944). The coefficient of earth pressure at rest. *Journal of the society of Hungarian Architects and Engineers*, 355–388.

Janbu, N. (1963). Soil compressibility as determined by oedometer and triaxial tests. In *Proceedings of the european conference on soil mechanics and foundation engineering* (Vol. 1, pp. 19–25).

Karstunen, M., Krenn, H., Wheeler, S. J., Koskinen, M., & Zentar, R. (2005). Effect of anisotropy and destructuration on the behavior of Murro test embankment. *International Journal of Geomechanics*, *5*(2), 87–97.

Khattak, A., & Das, B. (1985). Effect of high excess pore pressure on strength parameters of organic soil. *Soils and Foundations*, *25*(1), 99–104.

Knappett, J. A., & Craig, R. F. (2012). *Craig's soil mechanics.* Spon Press.

Kondner, R. (1963). *A hyperbolic stress-strain formulation for sands* (PhD Thesis). Northwestern University, Evanston, USA.

Landva, A., Korpijaakko, E., & Pheeney, P. (1983). Geotechnical classification of peats and organic soils. In *Testing of peats and organic soils.* ASTM International.

Landva, A., & Pheeney, P. E. (1980). Peat fabric and structure. *Canadian Geotechnical Journal*, *17*(3), 416–435.

Leoni, M., Karstunen, M., & Vermeer, P. A. (2008). Anisotropic creep model for soft soils. *Géotechnique*, *58*(3), 215–226.

Leroueil, S., & Vaughan, P. R. (1990). The general and congruent effects of structure in natural soil and weak rock. *Géotechnique*, *40*(3), 467–488.

Matsuoka, H., & Nakai, T. (1974). Stress-deformation and strength characteristics of soil under three different principal stresses. In *Proceedings of the Japan Society of Civil Engineers* (Vol. 232, pp. 59–70).

Mayne, P., & Kulhawy, F. H. (1982). Ko- OCR Relationships in Soil. *Journal of the Soil Mechanics and Foundations Division*, *108*(6), 851–872.

Mesri, G., & Ajlouni, M. (2007). Engineering properties of fibous peat. *Journal of Geotechnical and Geoenvironmental Engineering*, *133*(7), 850–866.

Muraro, S. (2018). *Hydromechanical behaviour of peat* (Unpublished PhD Thesis). Delft University of Technology, Delft, the Netherlands.

NEN 5104. (1989). *Geotechniek, classificatie van onverharde grondmonsters.* Normalisatie-Instituut, Delft, the Netherlands.

O'Kelly, B. C. (2007). Compressibility and permeability anisotropy of some peat soils. In *Proceedings of the 60th canadian geotechnical conference, Ottawa, Ontario, Canada.*

O'Kelly, B. C. (2015a). Atterberg limits are not appropriate for peat soils. *Geotechnical Research*, *2*(3), 123–134.

O'Kelly, B. C. (2015b). Effective stress strength testing of peat. *Environmental Geotechnics*, *2*(1), 34–44.

Pinyol, N. M., Alonso, E. E., & Olivella, S. (2008). Rapid drawdown in slopes and embankments. *Water resources research*, *44*(5).

Plaxis. (2016a). *Plaxis 2d 2016 - Material models manual* (R. B. J. Brinkgreve, S. Kumarswamy, & W. Swolfs, Eds.). PLAXIS bv, Delft, the Netherlands.

Plaxis. (2016b). *Plaxis 2d 2016 - Reference manual* (R. B. J. Brinkgreve, S. Kumarswamy, & W. Swolfs, Eds.). PLAXIS bv, Delft, the Netherlands.

Potts, D. M., & Zdravković, L. (1999). *Finite element analysis in geotechnical engineering: theory.* Thomas Telford Publishing.

Przystański, J. (1994). Application of Kondner's nonlinear model in describing stress–strain relation in peat, considering consolidation. *Advances in the Understanding and Modelling the Mechanical Behaviour of Peat, De Haan et al.(eds.), Balkema, Rotterdam*, 203–209.

Radforth, N. (1969). Muskeg as an engineering problem. In *Muskeg engineering handbook* (pp. 3–30). Univ. of Toronto Press, Toronto.

Rodriguez Barragan, O. (2015). *Numerical model for the induced failure of the Leendert de Boerspolder embankment* (MSc Thesis). Delft University of Technology, Delft, the Netherlands.

Roscoe, K., & Burland, J. (1968). On the generalized stress-strain behaviour of wet clay. In *Engineering Plasticity* (pp. 535–609). Cambridge University.

Schanz, T., Vermeer, P., & Bonnier, P. (1999). The hardening soil model: formulation and verification. In *Beyond 2000 in computational geotechnics* (pp. 281–296). Taylor & Francis, Rotterdam, the Netherlands.

Servais, R. (2010). *Plaxis ssc: de toepassing van een isotroop kruipmodel op de anisotrope ondergrond* (MSc Thesis). Delft University of Technology, Delft, the Netherlands.

Sexton, B. G., McCabe, B. A., Karstunen, M., & Sivasithamparam, N. (2016). Stone column settlement performance in structured anisotropic clays: the influence of creep. *Journal of Rock Mechanics and Geotechnical Engineering*, *8*(5), 672–688.

Sivasithamparam, N., Karstunen, M., & Bonnier, P. (2015). Modelling creep behaviour of anisotropic soft soils. *Computers and Geotechnics*, *69*, 46–57.

Stark, T. D., Ebeling, R. M., & Vettel, J. J. (1994). Hyperbolic stress-strain parameters for silts. *Journal of Geotechnical Engineering*, *120*(2), 420–441.

Surarak, C., Likitlersuang, S., Wanatowski, D., Balasubramaniam, A., Oh, E., & Guan, H. (2012). Stiffness and strength parameters for hardening soil model of soft and stiff bangkok clays. *Soils and Foundations*, *52*(4), 682–697.

Tavenas, F., Jean, P., Leblond, P., & Leroueil, S. (1983). The permeability of natural soft clays. Part II: Permeability characteristics. *Canadian Geotechnical Journal*, *20*(4), 645–660.

van Baars, S. (2005). The horizontal failure mechanism of the Wilnis peat dyke. *Géotechnique*, *55*(4), 319–323.

Waterman, D., & Broere, W. (2005). *Practical application of the soft soil creep–Part III. Plaxis Benchmarking.*

Wheeler, S. J., Näätänen, A., Karstunen, M., & Lojander, M. (2003). An anisotropic elastoplastic model for soft clays. *Canadian Geotechnical Journal*, *40*(2), 403–418.

Wood, D. M. (1990). *Soil Behavior and Critical State Soil Mechanics.* Cambridge university press.

Wood, D. M. (2003). *Geotechnical modelling* (Vol. 1). CRC Press.

Yamaguchi, H., Ohira, Y., Kogure, K., & Mori, S. (1985). Undrained shear characteristics of normally consolidated peat under triaxial compression and extension conditions. *Soils and Foundations*, *25*(3), 1–18.

Yildiz, A., Karstunen, M., & Krenn, H. (2009). Effect of anisotropy and destructuration on behavior of Haarajoki test embankment. *International Journal of Geomechanics*, *9*(4), 153–168.

Zentar, R., Karstunen, M., Wiltafsky, C., Schweiger, H., & Koskinen, M. (2002). Comparison of two approaches for modelling anisotropy of soft clays. In *Proceedings of the 8th international symposium on numerical models in geomechanics (numog viii)* (pp. 115–121). A.A. Balkema, Rotterdam.

Zwanenburg, C. (2005). *The influence of anisotropy on the consolidation behaviour of peat* (PhD thesis). Delft University of Technology, Delft, the Netherlands.

Zwanenburg, C., & Jardine, R. (2015). Laboratory, in situ and full-scale load tests to assess flood embankment stability on peat. *Géotechnique*, *65*(4), 309–326.

Appendix A

Site layout and monitoring equipment

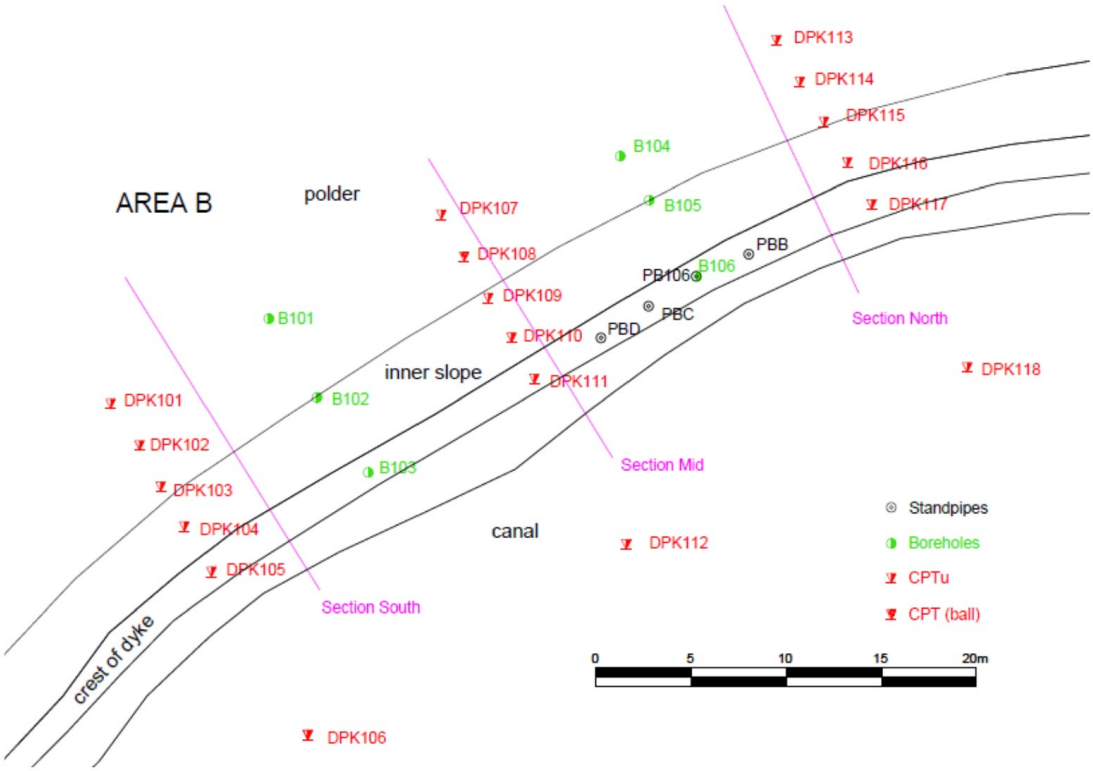

Figure A-1: Location of boreholes and CPTs. Samples retrieved from these boreholes were tested in K_0-CRS tests

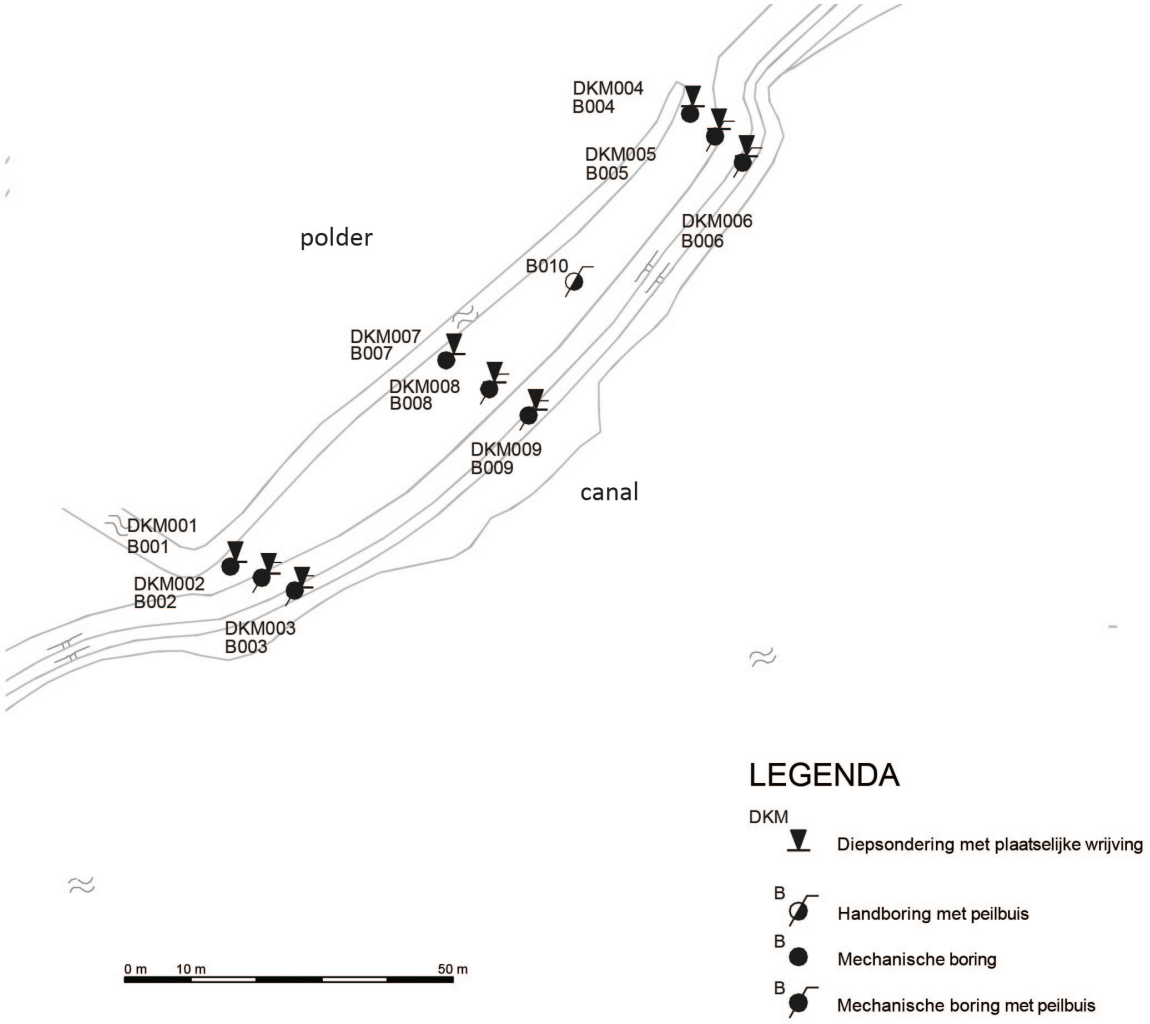

Figure A-2: Location of boreholes from where samples for undrained triaxial testing were retrieved

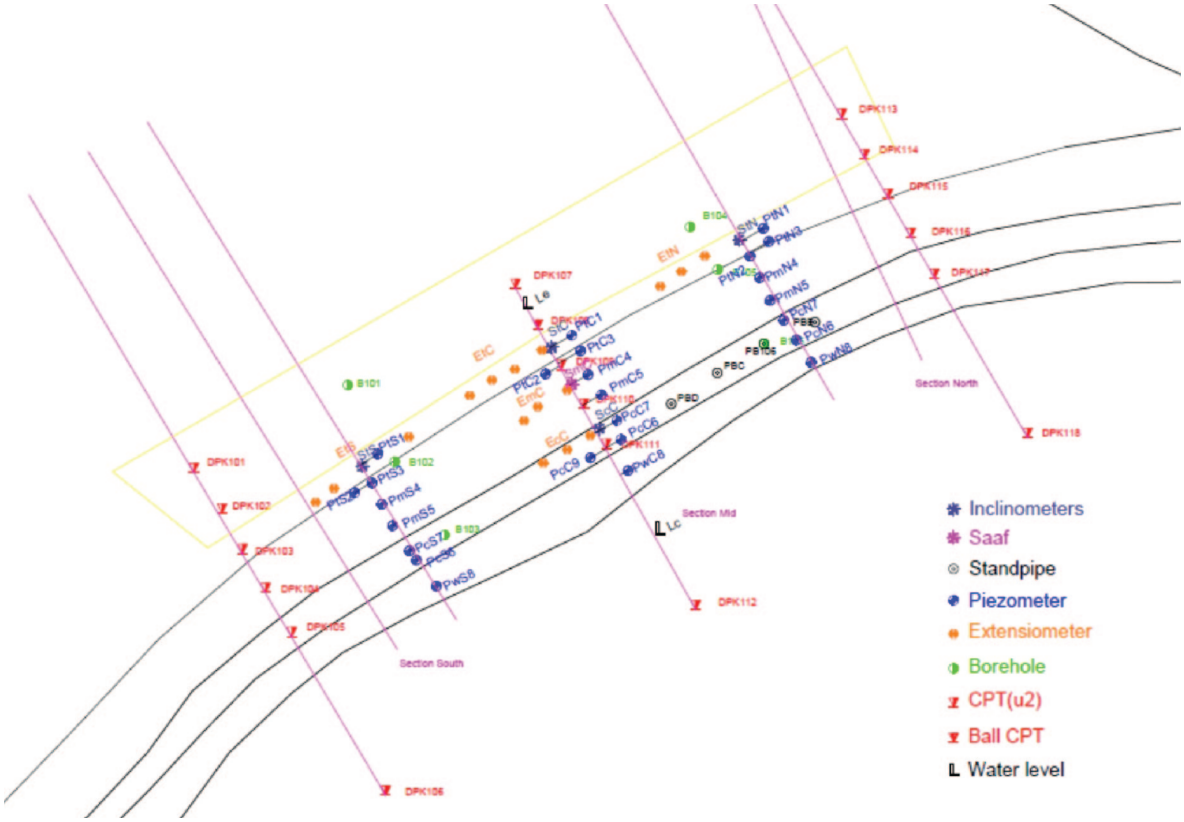

Figure A-3: Schematic of the monitoring equipment

Appendix B

Creep-SCLAY1S constitutive model

Within the context of this research work the anisotropic constitutive model Creep-SCLAY1S (Sivasithamparam et al., 2015) was considered for peat. It was not implemented in the simulation of the stress test due to the fact that in PLAXIS it is a user-defined soil model but a preliminary set of parameters for peat was determined and a sensitivity analysis was conducted. As a reference for future work the theory and constitutive relationships the model and the outcome of the sensitivity analysis are presented in Sections B-1 and B-2, respectively.

B-1 Mode description and constitutive equations

Yield surfaces

Creep-SCLAY1S is an advanced model that accounts for anisotropy, degradation of bonding (see Leroueil & Vaughan, 1990) and creep. The model is an extension of S-CLAY1S model (Karstunen et al., 2005) and Anisotropic creep model (Leoni et al., 2008).

It uses three surfaces to describe the state of the soil, as shown in Figure B-1. The outer surface is called Normal Consolidation Surface (NCS) and defines the boundary between small and large creep strains. The second surface is called Current Stress Surface (CSS) and as its name indicates, it describes the current state of effective stress in the soil. The third surface is thhe imaginary intrinsic compression surface (ICS) and relates to the bonding. The form of these yield surfaces is described by the Equation (Wheeler et al., 2003):

$$(q - ap')^2 - (M^2 - a^2)(p'_{\text{size}} - p')p' = 0 \tag{B-1}$$

where M is the critical state parameter, p'_{size} is the isotropic preconsolidation pressure defining the size of the curves and is equal to p'_p, p'_{eq} or p'_{mi} for the NCS, the CSS and the ICS respectively and α is a state variable that controls the inclination of the curves. The ratio p'_p/p'_{ep}, annotated as OCR*, is a measurement of the distance between the CSS and NCS, i.e. is a generalization of the OCR.

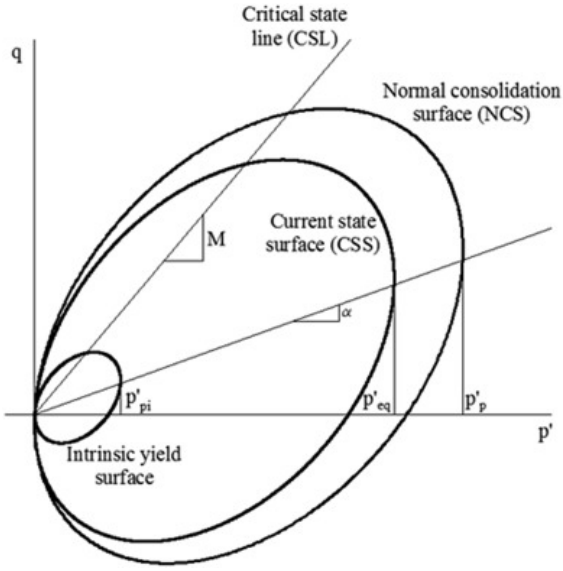

Figure B-1: Yield surfaces of the Creep-SCLAY1S model in triaxial stress space (Sexton et al., 2016)

The initial size of the CSS is derived based on the in situ vertical stress, the in situ K_0 value and α_0 (initial inclination of the surface). The initial size of the NCS is derived from in situ vertical effective stress, assumed value of K_0^{nc}, α_0 and the value of pre-overburden pressure, POP or over-consolidation ratio, OCR (Figure 3-12). OCR and POP are defined in Equation 3-18.

Hardening laws

The Creep-SCLAY1S incorporates different hardening rules to describes changes in the orientation and size of the three surfaces. The preconsolidation pressure p'_p evolves with volumetric creep strains according to the hardening law:

$$p'_{\mathrm{p}} = p'_{\mathrm{p0}} exp\Big(\frac{\epsilon^c_{\mathrm{v}}}{\lambda^*_i - \kappa^*_i}\Big) \tag{B-2}$$

where λ^*_i and κ^*_i are the modified intrinsic compression index and swelling index, respectively. The variation of the equivalent mean stress p'_{eq}, which determines the size of the CSS, is described by the law:

$$p'_{\mathrm{eq}} = p' + \frac{(q - \alpha p')^2}{(M^2(\theta) - \alpha^2)p'} \tag{B-3}$$

where $M(\theta)$ is the stress ratio at critical state dependent on Lode angle θ and α is a scalar quantity that describes the orientation of the surfaces. The evolution of the size of intrinsic yield surface p'_{mi} if described by equation B-4:

$$p'_{\mathrm{mi}} = \frac{p'_{\mathrm{mi}}}{\lambda^*_i - \kappa_i} \dot{\epsilon^c_v} \tag{B-4}$$

Moreover, the model includes a law to describe the change of inclination of the surfaces, i.e. the evolution of anisotropy due to generation of volumetric and deviatoric strains . In triaxial stress space the law can be expressed in the following form:

$$\dot{\alpha} = \omega\Big(\Big[\frac{3q}{4p'} - \alpha\Big]\langle\dot{\epsilon_v^c}\rangle + \omega_d\Big[\frac{q}{3p'} - \alpha\Big]|\dot{\epsilon_d^c}|\Big) \tag{B-5}$$

where η denotes the stress ratio, ω and ω_d are model parameters controlling the absolute rate of rotation and the relative effectiveness of deviatoric creep strains and volumetric creep strains, respectively. At a macroscopic level, these two parameters are related to changes in fabric anisotropy due to the creep strain rate.

The last law that the model includes is used to describe the degradation of bonding and is expressed by:

$$\dot{\chi} = -\alpha\chi\Big(|\dot{\epsilon_v^c}| + b|\dot{\epsilon_q^c}|\Big) \tag{B-6}$$

where α and b are parameters that describe the absolute and relative rate of destructuration, respectively.

Flow rule

The model assumes an associated flow rule as experimental data have showns that this is a reasonable assumption for clays when the evolution of anisotropy is considered (Gras et al., 2017).

The direction of the volumetric and deviatoric creep strains are defined as:

$$\dot{\epsilon_v^c} = \dot{\Lambda}\frac{\partial p'_{eq}}{\partial p'} \qquad \text{and} \qquad \dot{\epsilon_q^c} = \dot{\Lambda}\frac{\partial p'_{eq}}{\partial q} \tag{B-7}$$

where $\dot{\Lambda}$ is a viscoplastic multiplier proposed by Sivasithamparam et al. (2015), following the idea of Grimstad et al. (2010). It is defined as:

$$\dot{\Lambda} = \frac{\mu_i^*}{\tau}\left(\frac{p'_{eq}}{p'_m}\right)^{\beta}\left(\frac{M_c^2 - \alpha_{K_0^{nc}}^2}{M_c^2 - \eta_{K_0^{nc}}^2}\right) \tag{B-8}$$

where μ_i^* is he modified intrinsic creep index, $\beta = (\lambda_i^* - \kappa^*)/\mu_i^*$, $\eta_{K_0^{nc}}$ is defined as $3(1 - K_0^{nc})/(1 + 2K_0^{nc})$ and $\alpha_{K_0^{nc}}$ defines the initial inclination of the three ellipses. Since there is no consistency rule, the stress state can be outside the NCS surface Sivasithamparam et al. (2015).

Lode angle dependency

As mentioned in equation B-3, the critical state parameter M is incorporated as a function of Lode angle θ in order to achieve a smooth critical surface similar to the Matsuoka & Nakai (1974) failure surface. The formulation of lode angle dependency is given by Equation B-9.

$$M(\theta) = M_c\Big(\frac{2m^4}{1+m^4+(1-m^4)sin3\theta_\alpha}\Big)^{\frac{1}{4}} \tag{B-9}$$

where m is the ratio of the critical state parameter in extension to the critical state parameter in compression, $m = M_e/M_c$.

Model input parameters

The Creep-SCLAY1S model requires in total 14 input parameters to describe soil behavior as presented in Table B-1

Table B-1: Input parameters for the Creep-SCLAY1S model

Definition	Symbol	Unit
Modified compression index	λ^*	[-]
Modified swelling index	κ^*	[-]
Intrinsic modified creep index	μ_i^*	[-]
Poisson's ratio	ν'	[-]
Reference time	τ	[days]
Critical state parameter in compression	M_c	[-]
Critical state parameter in extension	M_e	[-]
Absolute effectiveness of rotational hardening	ω	[-]
Relative effectiveness of rotational hardening	ω_d	[-]
Absolute rate of destructuration	a	[-]
Relative rate of destructuration	b	[-]
Initial amount of bonding	χ_0	[-]
Initial inclination of the yield surfaces	α_0	[-]
Over-consolidation ratio or pre-overburden pressure	OCR / POP	[-/kPa]

B-2 Parameter determination and sensitivity analysis

B-2-1 Parameter determination

The input parameters of the Creep-SCLAY1S model can be divided into four categories: (a) isotropic parameters, which are similar to the Soft Soil model, (b) anisotropic parameters, (c)

structure parameters and (d) viscosity parameters. Given that the model has a hierarchical structure it is possible to switch off anisotropy and destructuration. By setting parameter χ to zero and using modified compression index, λ^* and modified swelling index, κ^* instead of the intrinsic parameters λ_i^* and κ_i^* the model reduces to Creep-SCLAY1. Furthermore, if the values of parameters α_0 and ω are set to zero the model will further reduce to a visco-plastic Modified Cam-Clay model. Strain-rate effects are not possible to be totally switched-off but the effect of rate-dependency can be reduced by reducing the value of the modified creep index.

Since structure is not considered relevant for the Leendert de Boerspolder stress test parameters a, b and χ_0 are set equal to 0. Moreover, due to the short duration of the stress test creep is not considered relevant. Thus, following the recommendation of Waterman & Broere (2005) with regards to the admissible values of creep index, parameter μ^* was set equal to $\mu^* = (\lambda^* - \kappa^*)/25$.

Isotropic parameters κ^* and λ^* (also used in other models such as MCC and SS) can be determined as described in Section 4-1-3.

Regarding the anisotropic parameters $\alpha_{K_0^{nc}}$ and ω_d they can be estimated with Equations B-10 and B-11, respectively.

$$\alpha_0 = \frac{\eta_{K_0^{nc}}^2 + 3\eta_{K_0^{nc}} - M_c^2}{3} \tag{B-10}$$

$$\omega_d = \frac{3(4M_c^2 - 4\eta_{K_0^{nc}}^2 - 3\eta_{K_0^{nc}})}{8(\eta_{K_0^{nc}}^2 - M_c^2 + 2\eta_{K_0^{nc}})} \tag{B-11}$$

where, $\eta_{K_0^{nc}} = 3(1 - K_0^{nc})/(1 + 2K_0^{nc})$.

Parameter ω, which controls the rate at which α tends toward its target value, i.e. controls the rate of rotation of the yield surface, it is difficult to be determined and it should be calibrated against triaxial tests, ideally both extension and compression tests. Gras et al. (2017) suggest that when structure of the soil in not considered parameter ω is in the range:

$$\frac{1.5}{\xi^*} \leq \omega \geq \frac{4.2}{\xi^*} \tag{B-12}$$

where ξ^* is equal to $\lambda^* - \kappa^*$. Furthermore, Zentar et al. (2002) suggest that parameter ω usually lies in the range $10/\lambda$ to $15/\lambda$.

Finally, critical state parameter in compression (M_c) and extension (M_e) can be estimated with Equations B-13 and B-14 (Wood, 1990), respectively.

$$M_c = \frac{6\sin\phi'_{cv}}{3 - \sin\phi'_{cv}} \tag{B-13}$$

$$M_e = \frac{6\sin\phi'_{cv}}{3 + \sin\phi'_{cv}} \tag{B-14}$$

B-2-2 Sensitivity analysis

A sensitivity analysis was performed aiming to show the influence of anisotropy parameters on the model behaviour with regards to peat. The response has been evaluated for undrained triaxial test.

Using the formulas described in the previous section a set parameters for peat was determined, presented in Table B-2. These parameters are adopted as starting values in the sensitivity analysis presented in the following section. It is worth of noting that the parameter K_0^{nc} was determined based on CRS tests and not Jaky's formula. The parameter M_c was determined from triaxial tests performed in reconstituted material yielding a friction angle ϕ'_{cv} of 42 °and K_0^{nc} equal to 0.33. Hence, the values of ω and α_0 are consistent with the critical state friction angle.

The simulations were performed with finite element calculations in PLAXIS 2D 2016.01. An axisymmetric model representing an undrained triaxial test was designed.

Table B-2: Creep-SCLAY1S input parameters for peat

Parameter	Value	Unit
Modified compression index (λ^*)	0.22	[-]
Modified swelling index (κ^*)	0.08	[-]
Modified creep index (μ^*)	0.05	[-]
Poisson's ratio (ν')	0.3	[-]
Reference time (τ)	1	[day]
Critical state parameter in compression (M_c)	1.72	[-]
Critical state parameter in extension (M_e)	1.1	[-]
Absolute effectiveness of rotational hardening (ω)	10-28	[-]
Relative effectiveness of rotational hardening (ω_d)	0.3	[-]
Initial inclination of the yield surfaces (α_0)	0.9	[-]
Pre-overburden pressure (POP)	10	[kPa]

Figures B-2 and B-3 show the influence of the absolute and relative rate of rotation on the stress path and stress-strain response. As parameter ω increases there is a great effect on both stress path and stress-strain prediction. With regards to the stress path there is a clear deviation towards the right as ω increases. Regarding the stress-strain response, as ω increases the ultimate deviatoric stress, q_{ult} increases. Furthermore, for high values of absolute rotation softening is observed with regards to the post-peak behavior. On the other hand the sensitivity of the model to the relative rate of rotation ω_d seems to be very low and the response barely changes. Regarding the proposed range by Gras et al. (2017) (Equation B-12) the value is dramatically underestimated for peats.

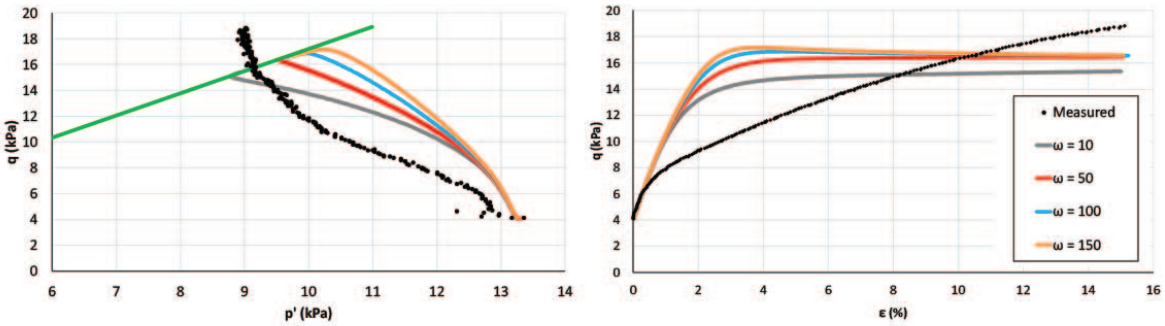

Figure B-2: Absolute rotation rate ω influence on the stress path in p'-q plane and stress-strain response during undrained triaxial test. In figure (a) the critical state line is annotated in green

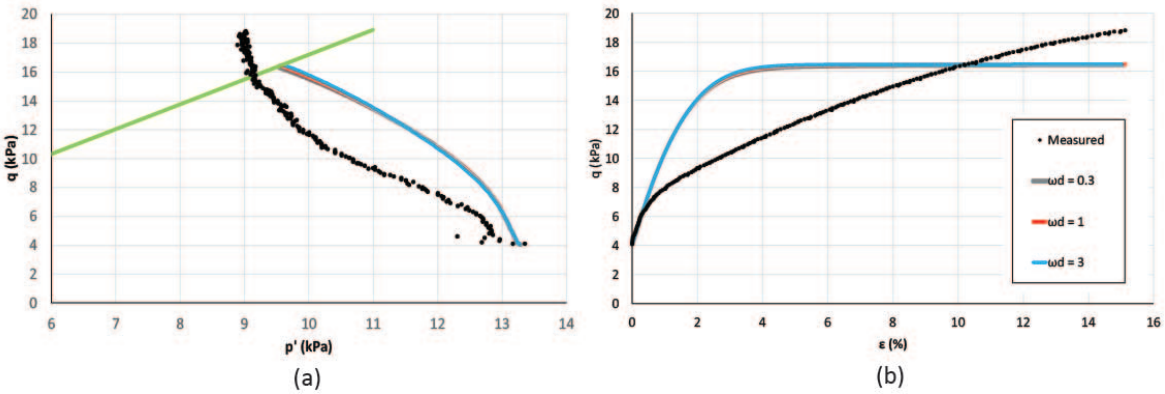

Figure B-3: Relative rotation rate ω_d influence on the stress path in p'-q plane and stress-strain response during undrained triaxial test. In figure (a) the critical state line is annotated in green

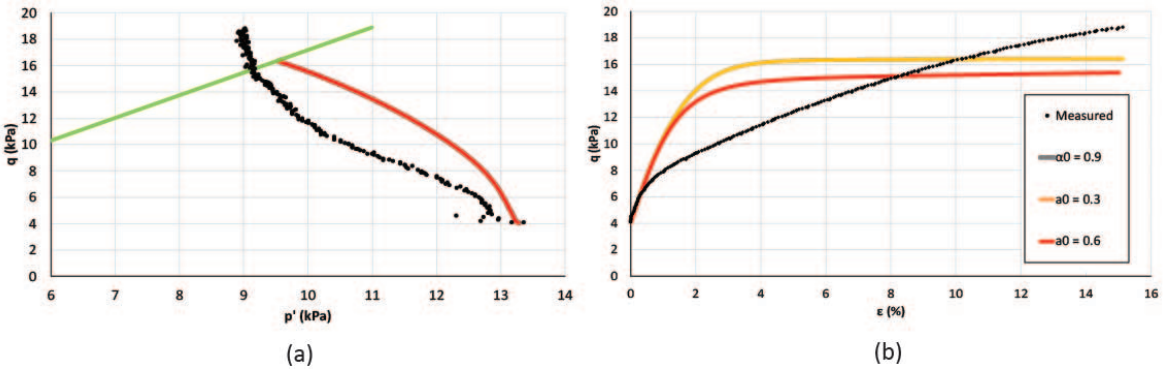

Figure B-4: Influence of initial anisotropy α_0 on the stress path in p'-q plane and stress-strain response during undrained triaxial test. In figure (a) the critical state line is annotated in green

The sensitivity of the model to the initial anisotropy α_0 is shown in Figure B-4. As the value increases no effect is observed even though a change in the hardening behavior was expected. It is worth noting that with regard to the initial anisotropy α_0 values lower than unity are regarded as realistic for soils, hence values $0 < \alpha_0 \leq 1$ should be used (Wheeler et al., 2003).

B-3 Conclusions

A sensitivity analysis was performed aiming in (a) understanding the influence of anisotropic parameters α_0, ω and ω_d in undrained triaxial test and (b) assessing the applicability of the model in describing peat.

It appears that the model can describe reasonably well the behavior of peat in undrained triaxial test. A limitation is with regards to the stress-strain performance where the response is too stiff and subsequently the deviatoric stress is overestimated. That could be due to the very low effective stress under which the samples were consolidated. An improved response could be possible achieved through the change of other parameter. However, this parametric analysis focused only on parameters α_0, ω and ω_d.

In regards to the considered parameters, the model is not very sensitive for parameters α_0 and ω_d. That is for the chosen values that where selected to be close to what the authors believes to be realistic for peats. Regarding parameter ω it was shown that the proposed ranges are not applicable for peats as values close to 100 seem to result in a realistic behavior.